Tampere University

ILKKA RUOKOSENMÄKI

Real Time Path Integral Simulation Methods for Quantum Particles

Tampere University Dissertations 184

Tampere University Dissertations 184

ILKKA RUOKOSENMÄKI

Real Time Path Integral Simulation Methods for Quantum Particles

ACADEMIC DISSERTATION
To be presented, with the permission of
the Faculty of Engineering and Natural Sciences
of Tampere University,
for public discussion in the auditorium SA203 (S2)
of Sähkötalo building, Korkeakoulunkatu 3, 33720 Tampere,
on 29 November 2019, at 12 o'clock.

ACADEMIC DISSERTATION
Tampere University, Faculty of Engineering and Natural Sciences
Finland

Responsible supervisor and Custos
Professor Tapio Rantala
Tampere University
Finland

Pre-examiners
Professor Martti Puska
Aalto University
Finland

Senior Scientist Sara Bonella
Ecole polytechnique fédérale de Lausanne
Switzerland

Opponent
Professor Kari Rummukainen
University of Helsinki
Finland

Cover design: Roihu Inc.

ISBN 978-952-03-1370-8 (print)
ISBN 978-952-03-1371-5 (pdf)
ISSN 2489-9860 (print)
ISSN 2490-0028 (pdf)
http://urn.fi/URN:ISBN:978-952-03-1371-5

PunaMusta Oy – Yliopistopaino
Tampere 2019

PREFACE

What is the wave function? That was the question on my mind when I started this journey all those years ago. I still cannot say that I know the answer to that one, but during the pursuit I have learned a lot about the strange world we actually live in. It is a world where particles take all the paths when we do not look and sometimes even go backwards in time. It is a world that can be modelled with surprisingly few equations and assumptions and yet from those emerges the rich and chaotic environment we see around us, that almost seems to obey different rules than the underlying Nature. Even though the equations are few, they are by no means easy to solve and it is a small slice of those problems that are the focus of this work.

I want to thank all the friendly people at the Physics Unit for answering my stupid and sometimes even not so stupid questions and making it possible for me to work here, so I could complete this journey. Especially, I thank Juha Tiihonen for physics related discussions and helping me out with all the things computer related. I thank Matti Lindroos for those great lectures of quantum mechanics that were the highlights of the day and really solidified my interest in this topic during the early days of my studies. I thank my colleagues and co-authors Ilkka Kylänpää and Hossein Gholizadehkalkhoran, for their contributions to this work. I thank my pre-examiners, professor Martti Puska and Dr. Sara Bonella, for their constructive feedback.

Most of all, I would like to thank my supervisor, professor Tapio Rantala, for allowing me this possibility, for all the great and inspiring discussions during the years and for having continual faith in this project.

None of this would have been possible without my parents who always let me choose my own paths.

ABSTRACT

Quantum mechanics represents our current best knowledge of how Nature works. It is especially important for the electronic structure calculations, where classical mechanics breaks down. Even though the theory is well known, only handful of problems can be solved exactly, so approximations and numerical methods are required.

Feynman path integral approach offers an intuitively welcome description of nonrelativistic quantum mechanics, rooted in space and time, where quantum many-body effects are included transparently. The formalism based on multidimensional integrals naturally calls for the powerful Monte Carlo techniques to be applied when numerical calculations are performed. In this thesis we present a new approach how real time path integral formalism can be applied to simulate dynamics and states of quantum particles, even electrons.

We first give a brief introduction to the theory of path integrals and Monte Carlo simulations. Much of this theory can be found in textbooks of quantum mechanics but it is included here for completeness, so that this work could serve as a self-contained introduction to anyone interested in path integral simulations. Second, we discuss the imaginary time methods which have proven to be successful in simulations of statistical physics description of the quantum many-particle systems. Finally, we delve into the challenges of the path integrals in real time domain and present the novel methods from the four original papers with demonstrations.

The challenges associated with the real time path integral methods are discussed and we present approaches for solving some of these, such as the wave function guided sampling and "widening" of walkers to improve the propagator. We also introduce a novel method for finding stationary eigenstates of quantum systems, called "incoherent propagation". This approach can be used to find the excited states, unlike the conventional Quantum Monte Carlo methods. Presented techniques are then applied to the Hooke's atom, a system of strong correlation, that is challeng-

ing for conventional approaches. Simulations of the ground state and lowest excited states of Hooke's atom give excellent results for energetics. We also demonstrate simulation of coherent quantum dynamics at the presence of an external transient electric field. We also introduce how conventional diffusion Monte Carlo (DMC) method can be combined with incoherent propagation.

Not having a positive sampling distribution is a problem that plagues real time path integral calculations. To alleviate this problem, we introduce a novel probabilistic interpretation of the real time propagator and an approach called "real time diffusion Monte Carlo method". This method is demonstrated in simulation of the time evolution of one dimensional harmonic oscillator and in finding eigenstates of the system using it in conjunction with incoherent propagation.

TIIVISTELMÄ

Kvanttimekaniikka edustaa tämänhetkistä parasta tietoa siitä, kuinka luonto toimii. Se on erityisen tärkeää elektronirakennelaskennassa, jossa klassinen mekaniikka ei enää toimi. Vaikka teoria on hyvin tunnettu, ainoastaan pieni joukko ongelmia voidaan ratkaista eksaktisti, minkä vuoksi joudutaan turvautumaan approksimaatioihin ja numeerisiin menetelmiin.

Feymanin polkuintegraalimuotoilu tarjoaa intuitiivisen lähestymistavan epärelativistiseen kvanttimekaniikkaan. Sen pohjana ovat paikka ja aika, ja siihen monen kappaleen kvantti-ilmiöt sisältyvät läpinäkyvästi. Kun kyseessä on formalismi, joka perustuu moniulotteisiin integraaleihin, tehokkaat Monte Carlo tekniikat tarjoavat luonnollisen keinon numeeriseen laskentaan. Tässä väitöskirjassa esitetään uusi menetelmä siihen, kuinka polkuintegraaliformalismia voidaan käyttää kvanttihiukkasten dynamiikan ja tilojen simulointiin, jopa elektroneille.

Ensiksi annetaan lyhyt johdanto polkuintegraaleihin ja Monte Carlo -simulointeihin. Suuri osa tästä teoriasta löytyy kvanttimekaniikan oppikirjoista, mutta se on sisällytetty tähän, jotta tämä työ voisi toimia itsenäisenä alustuksena kenelle tahansa, joka on kiinnostunut polkuintegraalisimuloinneista. Seuraavaksi tarkastellaan imaginääriajan menetelmiä, jotka ovat osoittautuneet menestyksellisiksi tehtäessä statistisen fysiikan simulaatioita monen kappaleen kvanttisysteemille. Sitten paneudutaan reaaliajan polkuintegraalien haasteisiin ja esitellään uudet menetelmät neljästä alkuperaisestä julkaisusta ja demonstroidaan niiden käyttöä.

Seuraavaksi tarkastellaan reaaliajan polkuintegraalimenetelmiin liittyviä ongelmia ja esitetään joitakin keinoja näiden ratkaisemiseksi, sellaisia kuten aaltofunktion ohjaama otanta ja "levennetty walker" propagaattorin parantamiseksi. "Epäkoherentti propagaatio" esitellään uudenlaisena menetelmänä stationääristen ominaistilojen etsimiseksi. Tämän avulla voidaan etsiä myös viritystiloja, toisin kuin tavanomaisilla kvantti-Monte Carlo -menetelmillä. Esiteltyjä tekniikoita sovelletaan Hooken atomiin, vahvan korrelaation systeemin, joka on haastava perinteisille lähestymis-

tavoille. Perustilan ja alimpien viritystilojen simuloinnit antavat erinomaiset tulokset tilojen energioille. Myös koherenttia dynamiikkaa simuloidaan ajasta riippuvassa sähkökentässä. Sitten esitellään kuinka perinteinen diffuusio-Monte Carlo -menetelmä ja epäkoherentti propagaatio voidaan yhdistää.

Reaaliajan polkuintegraalilaskuja vaivaa positiivisen jakautumafunktion puuttuminen. Tämän ongelman lieventämiseksi esitellään uudenlainen reaaliajan propagaattorin todennäköisyystulkinta ja menetelmä, jota kutsutaan "reaaliajan diffuusio-Monte Carlo -menetelmäksi". Tätä menetelmää demonstroidaan simuloimalla yksiulotteisen harmonisen oskillaattorin aikaevoluutiolla ja etsitään viritystiloja käyttäen epäkoherenttia propagaatiota.

CONTENTS

LIST OF SYMBOLS AND ABBREVIATIONS

E_n	n^{th} energy eigenvalue
G	Green's function
K	time evolution amplitude, kernel, propagator
L	Lagrangian
M	Trotter number, number of walkers
N	number of particles
R	center of mass coordinate
S	action
T	kinetic energy
$T(x \to x')$	transition probability
V	potential energy
Z	partition function
Δt	real time difference, time step
β	inverse temperature
$\hat{H}$	Hamilton operator
$\hat{T}_t$	time ordering operator
$\hat{T}$	kinetic energy operator
$\hat{U}$	time evolution operator
$\hat{V}$	potential energy operator
$\hat{p}$	momentum operator
$\hat{x}$	position operator

$\hbar$	reduced Planck's constant
ω	angular frequency
ϕ_n	n^{th} energy eigenstate wave function
ψ	generic wave function
ρ	density matrix
σ	standard deviation
τ	imaginary time
d	number of dimensions
k	Boltzmann constant
p	momentum variable in one or more dimensions
r	relative motion coordinate
t_n	real time variable
x	position variable in one or more dimensions
DFT	density functional theory
DMC	diffusion Monte Carlo method
iRTPI	incoherent real time path integral method
ODHO	one dimensional harmonic oscillator
PIMC	path integral Monte Carlo method
QMC	quantum Monte Carlo
RTPI	real time path integral method
WKB	Wentzel–Kramers–Brillouin

ORIGINAL PUBLICATIONS

Publication I — I. Ruokosenmäki and T. T. Rantala. Numerical Path Integral Approach to Quantum Dynamics and Stationary Quantum States. *Communications in Computational Physics* 18 (2015), 91–103. DOI: 10.4208/cicp.180914.161214a.

Publication II — I. Ruokosenmäki, H. Gholizade, I. Kylänpää and T. T. Rantala. Numerical Path Integral Solution to Strong Coulomb Correlation in One Dimensional Hooke's Atom. *Computer Physics Communications* 210 (2017), 45–53. DOI: 10.1016/j.cpc.2016.09.012.

Publication III — H. Gholizadehkalkhoran, I. Ruokosenmäki and T. T. Rantala. Eigenstates and Dynamics of Hooke's Atom: Exact Results and Path Integral Simulations. *Journal of Mathematical Physics* 59 (2018). DOI: 10.1063/1.5028503.

Publication IV — I. Ruokosenmäki and T. T. Rantala. Real-Time Diffusion Monte Carlo Method. *Communications in Computational Physics* 25 (2019), 347–360. DOI: 10.4208/cicp.OA-2018-0048.

For the included papers the author has written the software, carried out all the path integral simulations and done the writing of the first draft of the articles, except for the perturbation theory parts. The perturbation theory analyses in papers II and III have been carried out by Hossein Gholizadehkalkhoran. Assistance in result analysis and writing has been provided by the co-authors.

1 INTRODUCTION

People have always been curious about surrounding Nature. We want to know why things happen the way they do. Early attempts to explain the phenomena in nature were solely based on philosophical discussions, but gradually they evolved towards the scientific method we know today. The scientific method is the process where we start from making observations, next we formulate a hypothesis that explains these observations, and then, that can be used to predict the outcome of relevant natural processes. Finally, we test the hypothesis by making observations on these predicted processes, thus closing the circle. There are more refined definitions of scientific method with more steps, but following the same general principle.

1.1 Quantum Mechanics

Following the scientific method has deepened our understanding of the nature and given rise to the technologically advanced society we live in. The "crown jewel" of this understanding, at the moment, is called quantum mechanics, the playground of this thesis [1, 2, 3, 4]. We can say this, because quantum mechanics makes predictions about certain physical phenomena and quantities that can be measured at very high precision. For example, the electron anomalous magnetic moment can be measured and compared with theory and the agreement is found to be within one part in trillion (10^{-12}) [5, 6]. This is comparable to the case where classical physics could predict, and we could measure, the distance in a javelin throw to the size of an atom.

Rigorous mathematical formulation of quantum mechanics is generally credited to John von Neumann [7]. We can compare this formulation with classical mechanics. For example, let us assume a system where one particle with mass m is moving in a potential field U. In classical mechanics the particle starts from some initial position $\mathbf{x}$ with some initial momentum $\mathbf{p}$, *i.e.*, the initial state of the system is a point in a phase space $(\mathbf{x}, \mathbf{p})$. From the potential field we can extract a conservative force

$\mathbf{F} = -\nabla U$ and use Newton's second law $\mathbf{F} = \dot{\mathbf{p}}$ and the fact that $\mathbf{p} = m\dot{\mathbf{x}}$ to determine how the momentum and position change from the initial time t_a to the final time t_b. Even though the concepts of potential and force might be a bit mysterious it is not hard to visualize how this formulation describes, for example, a falling body in Earth's gravitational field.

In the conventional quantum mechanical description of the same system the initial state is $|\,\psi(t_a)\rangle$, which is a vector in an infinite-dimensional complex vector space called Hilbert space. When we operate on this state with a time-evolution operator $\hat{U}(t_b, t_a)$, we get the final state $|\,\psi(t_b)\rangle$. For each physically observable quantity we can assign a Hermitian operator $\hat{O}$ and the eigenvalues of that operator correspond to actual quantities we can measure. There is only little or no doubt that this works as was emphasized before, but we have lost the intuition inherent in a classical mechanics. However, there is another, equivalent approach to quantum mechanics that avoids the use of operators and retains the particle picture, called path integral formalism [8, 9].

1.2 Scope and Aims

In this study we show how this formalism and Monte Carlo techniques can be used in real time simulations of quantum particles, such as electrons. Unlike in the more conventional approaches such as Hartree–Fock [10], Density Functional Theory (DFT) [11, 12] and basically all the methods that use finite basis sets [13], the Quantum Monte Carlo (QMC) methods and path integral formalism includes correlations between particles transparently and exactly within the numerical accuracy. The conventional imaginary time approaches diffusion Monte Carlo (DMC) [14] and path integral Monte Carlo (PIMC) [15] are efficient methods of calculating equilibrium properties of quantum systems. They both become more laborious and inefficient when applied on a fermion system or when excited states are considered.

The aim of our studies is to develop new real time path integral (RTPI) methods that can be used even for electrons. Our novel "incoherent propagation" does not have the restrictions of PIMC and DMC and can be used to calculate both fermion systems and excited states. We show how the "incoherent propagation" in real time and conventional imaginary time methods yield comparable accuracy with the same number of walkers, though the former is computationally more demanding. With

our real time diffusion Monte Carlo method, we demonstrate how the complex propagator can be used as a probability, similarly to the conventional DMC method.

Thus, we aim at paving the way for new methods in electronic structure calculations, although these approaches are not without their own challenges discussed in this thesis.

2 QUANTUM THEORY OF PATH INTEGRALS

This chapter gives the background theory of path integrals starting from the more commonly known Schrödinger formalism. The following derivation follows that in *Path Integrals in Quantum Mechanics, Statistics, Polymer Physics, and Financial Markets* [16].

2.1 Time evolution operator

The basis independent non-relativistic Schrödinger equation can be written as an operator equation

$$\hat{H}(t)\,|\,\psi(t)\rangle = \mathrm{i}\hbar\partial_t\,|\,\psi(t)\rangle. \tag{2.1}$$

For time-independent Hamiltonians $\hat{H}(t) = \hat{H}(t_a)$ the solution is

$$|\,\psi(t_b)\rangle = \exp\Big(-\frac{\mathrm{i}}{\hbar}\hat{H}(t_a)(t_b - t_a)\Big)\,|\,\psi(t_a)\rangle. \tag{2.2}$$

The operator

$$\hat{U}(t_b, t_a) = \exp\Big(-\frac{\mathrm{i}}{\hbar}\hat{H}(t_a)(t_b - t_a)\Big) \tag{2.3}$$

is called the time evolution operator.

We are interested in causal time evolution, so, from now on, we shall always assume $t_b > t_a$.

For more general case, where the Hamiltonian $\hat{H}(t)$ is time dependent, we divide the time interval $t_b - t_a$ into N small pieces of thickness $\epsilon = (t_b - t_a)/N = t_n - t_{n-1}$. If N is large enough we can approximate that the Hamiltonian is piecewise constant, *i.e.*, $\hat{H}(t) \approx \hat{H}(t+\epsilon)$ and write

$$|\psi(t_b)\rangle \approx \exp(-\frac{\mathrm{i}}{\hbar}\hat{H}(t_b)(t_b - t_{N-1}) \ldots \exp(-\frac{\mathrm{i}}{\hbar}\hat{H}(t_n)(t_n - t_{n-1})) \ldots \times \exp(-\frac{\mathrm{i}}{\hbar}\hat{H}(t_1)(t_1 - t_a))\,|\,\psi(t_a)\rangle. \quad (2.4)$$

where $n = 1, 2, \ldots N$, $t_a \equiv t_0$ and $t_b \equiv t_N$. This approximation will converge to the exact one when $N \to \infty$, so we can write

$$\hat{U}(t_b, t_a) = \lim_{N\to\infty} \hat{T}_t \left\{ \prod_{n=1}^{N} \exp(-\frac{\mathrm{i}}{\hbar}\hat{H}(t_n)\epsilon) \right\} \quad (2.5)$$

where $\hat{T}_t$ is the chronological time ordering operator which rearranges the product according to the "two ls rule": later times go to the left.

The time evolution amplitude is defined as the representation of time evolution operator in localized basis states

$$K(\mathbf{x}_b, t_b; \mathbf{x}_a, t_a) \equiv \langle \mathbf{x}_b \,|\, \hat{U}(t_b, t_a) \,|\, \mathbf{x}_a \rangle \quad (2.6)$$

This is also called the propagator, the kernel or the Green's function.

2.2 Path integral approach

2.2.1 Propagator

For simplicity we assume that the space is one-dimensional and discuss the systems with more dimensions later. We also assume that the continuum limit $N \to \infty (\epsilon \to 0)$ is taken as above. From Eqs. (2.3), (2.5) and (2.6) it follows that

$$K(x_b, t_b; x_a, t_a) = \langle x_b \,|\, \hat{U}(t_b, t_{N-1})\hat{U}(t_N, t_{N-2}) \ldots \hat{U}(t_n, t_{n-1}) \ldots \hat{U}(t_1, t_a) \,|\, x_a \rangle. \quad (2.7)$$

Inserting the identity operator in the form of completeness relation [16, 17]

$$\int_{-\infty}^{\infty} |\, x_n \rangle\langle x_n \,|\, \mathrm{d}x_n = 1, n = 1, \ldots, N-1 \quad (2.8)$$

between each $\hat{U}$ in Eq. (2.7) and using Eq. (2.3) the amplitude becomes

$$K(x_b,t_b;x_a,t_a)=\hat{T}_t\Big\{\int_{-\infty}^{\infty}...\int_{-\infty}^{\infty}\prod_{n=1}^{N}\Big[\langle x_n\,|\,\exp(-\frac{\mathrm{i}}{\hbar}\hat{H}(t_n)\epsilon)\,|\,x_{n-1}\rangle\Big]\mathrm{d}x_1...\mathrm{d}x_{N-1}\Big\} \tag{2.9}$$

where $t_a\equiv t_0$ and $t_b\equiv t_N$

Assuming that the Hamiltonian has the standard form, being the sum of the kinetic and potential energies

$$\hat{H}(t)=T(\hat{p},t)+V(\hat{x},t), \tag{2.10}$$

the exponential operator can be factorized using the Baker–Campbell–Hausdorff formula

$$\begin{aligned}\exp(-\frac{\mathrm{i}}{\hbar}(\hat{T}+\hat{V})\epsilon)=&\exp(-\frac{\mathrm{i}}{\hbar}\hat{T}\epsilon)\exp(-\frac{\mathrm{i}}{\hbar}\hat{V}\epsilon)\\&\times\exp\Big\{\frac{\mathrm{i}\epsilon^2}{\hbar^2}(\frac{\mathrm{i}}{2}[\hat{V},\hat{T}]-\frac{\epsilon}{\hbar}(\frac{1}{6}[\hat{V},[\hat{V},\hat{T}]]-\frac{1}{3}[[\hat{V},\hat{T}]],\hat{T}])+...)\Big\}\end{aligned} \tag{2.11}$$

where $[\hat{A},\hat{B}]$ is the commutator of $\hat{A}$ and $\hat{B}$. This can be written as

$$\exp(-\frac{\mathrm{i}}{\hbar}(\hat{T}+\hat{V})\epsilon)=\exp(-\frac{\mathrm{i}}{\hbar}\hat{T}\epsilon)\exp(-\frac{\mathrm{i}}{\hbar}\hat{V}\epsilon)+O(\frac{\epsilon^2}{\hbar^2}) \tag{2.12}$$

where at the limit $\epsilon\to 0$ the terms proportional to ϵ^2 do not contribute, when the operators are bound from below [16].

Keeping in mind that we take the limit $N\to\infty$ and $\epsilon\to 0$ and inserting the completeness relation we can write

$$\begin{aligned}\langle x_n\,|\,\exp(-\frac{\mathrm{i}}{\hbar}\hat{H}(t_n)\epsilon)\,|\,x_{n-1}\rangle=&\\&\int_{-\infty}^{\infty}\langle x_n\,|\,\exp(-\frac{\mathrm{i}}{\hbar}\hat{V}\epsilon)\,|\,x_n'\rangle\langle x_n'\,|\,\exp(-\frac{\mathrm{i}}{\hbar}\hat{T}\epsilon)\,|\,x_{n-1}\rangle\mathrm{d}x_n'\end{aligned} \tag{2.13}$$

Since we assume $\hat{V}(t)=V(\hat{x},t)$ and $\hat{x}$ has a simple multiplicative form in position

space $\langle x \mid \hat{x} \mid x' \rangle = \delta(x - x')x'$ [13]

$$\langle x_n \mid \exp(-\frac{\mathrm{i}}{\hbar}\hat{H}(t_n)\epsilon) \mid x_{n-1} \rangle = \exp(-\frac{\mathrm{i}}{\hbar}V(x_n, t_n)\epsilon)\langle x_n \mid \exp(-\frac{\mathrm{i}}{\hbar}\hat{T}\epsilon) \mid x_{n-1} \rangle \quad (2.14)$$

Similarly $\hat{T}(t) = T(\hat{p}, t)$ and $\hat{p}$ has a simple multiplicative form in momentum space $\langle p \mid \hat{p} \mid p' \rangle = 2\pi\hbar\delta(p - p')p'$ [13, 16].
Since

$$\int_{-\infty}^{\infty} \frac{1}{2\pi\hbar} \mid p \rangle\langle p \mid \mathrm{d}p = 1 \quad (2.15)$$

and

$$\langle x \mid p \rangle = \exp(\frac{\mathrm{i}px}{\hbar}), \quad (2.16)$$

we get

$$\begin{aligned}
&\langle x_n \mid \exp(-\frac{\mathrm{i}}{\hbar}\hat{H}(t_n)\epsilon) \mid x_{n-1} \rangle \\
&= \exp\Big(-\frac{\mathrm{i}}{\hbar}V(x_n, t_n)\epsilon\Big)\int_{-\infty}^{\infty}\int_{-\infty}^{\infty} \frac{1}{(2\pi\hbar)^2}\langle x_n \mid p_n \rangle\langle p_n \mid \exp(-\frac{\mathrm{i}}{\hbar}\hat{T}\epsilon) \mid p_n' \rangle\langle p_n' \mid x_{n-1} \rangle \mathrm{d}p_n \mathrm{d}p_n' \\
&= \exp\Big(-\frac{\mathrm{i}}{\hbar}V(x_n, t_n)\epsilon\Big) \\
&\times \int_{-\infty}^{\infty}\int_{-\infty}^{\infty} \frac{1}{2\pi\hbar}\langle x_n \mid p_n \rangle\delta(p_n - p_n')\exp\Big(-\frac{\mathrm{i}}{\hbar}T(p_n', t_n)\epsilon\Big)\langle p_n' \mid x_{n-1} \rangle \mathrm{d}p_n \mathrm{d}p_n' \\
&= \exp\Big(-\frac{\mathrm{i}}{\hbar}V(x_n, t_n)\epsilon\Big)\int_{-\infty}^{\infty} \frac{1}{2\pi\hbar}\exp\Big(\frac{\mathrm{i}p_n}{\hbar}(x_n - x_{n-1}) - \frac{\mathrm{i}}{\hbar}T(p_n, t_n)\epsilon\Big)\mathrm{d}p_n \\
&= \int_{-\infty}^{\infty} \frac{1}{2\pi\hbar}\exp\Big(\frac{\mathrm{i}p_n}{\hbar}(x_n - x_{n-1}) - \frac{\mathrm{i}\epsilon}{\hbar}\Big(T(p_n, t_n) + V(x_n, t_n)\Big)\Big)\mathrm{d}p_n.
\end{aligned}$$

Inserting this into Eq. (2.9) we get

$$K(x_b, t_b; x_a, t_a) = \int_{-\infty}^{\infty} \ldots \int_{-\infty}^{\infty} \frac{1}{2\pi\hbar}\exp(\frac{\mathrm{i}}{\hbar}S_N)\mathrm{d}x_1 \ldots \mathrm{d}x_{N-1}\mathrm{d}p_1 \ldots \mathrm{d}p_N, \quad (2.17)$$

where S_N is

$$S_N = \sum_{n=1}^{N} [p_n(x_n - x_{n-1}) - \epsilon H(p_n, x_n, t_n)] \tag{2.18}$$

$$= \sum_{n=1}^{N} [p_n \frac{(x_n - x_{n-1})}{\epsilon} - H(p_n, x_n, t_n)]\epsilon \tag{2.19}$$

In the continuum limit $N \to \infty$ and $\epsilon \to 0$ this tends towards the integral

$$S[p,x] = \int_{t_a}^{t_b} [p(t)\dot{x}(t) - H(p(t), x(t), t)]\mathrm{d}t, \tag{2.20}$$

which is the classical action [18].

Note that the time ordering operator $\hat{T}_t$ is dropped since we do not have any other operators left, but work with complex numbers, which do commute.

This form is a bit more generic than usually needed and we can simplify it by assuming that we can write $T(p,t) = p^2/2m$ where m is the mass of the particle. Now Eq. (2.18) becomes

$$S_N = \sum_{n=1}^{N} [p_n(x_n - x_{n-1}) - \epsilon \frac{p_n^2}{2m} - \epsilon V(x_n, t_n)], \tag{2.21}$$

By using the integral formula [19]

$$\int_{-\infty}^{\infty} \exp(-ay^2 + by)\mathrm{d}y = \sqrt{\frac{\pi}{a}} \exp(\frac{b^2}{4a}) \tag{2.22}$$

the momentum integrals in Eq. (2.17) can be calculated

$$\int_{-\infty}^{\infty} \frac{1}{2\pi\hbar} \exp(\frac{\mathrm{i}}{\hbar}(p_n(x_n - x_{n-1}) - \epsilon \frac{p_n^2}{2m}))\mathrm{d}p_n = \sqrt{\frac{m}{2\pi\hbar \mathrm{i}\epsilon}} \exp\Big(\frac{\mathrm{i}}{\hbar} \frac{m}{2} \frac{(x_n - x_{n-1})^2}{\epsilon}\Big) \tag{2.23}$$

and the Kernel becomes

$$K(x_b, t_b; x_a, t_a) = \sqrt{\frac{m}{2\pi\hbar \mathrm{i}\epsilon}}^N \int_{-\infty}^{\infty} ... \int_{-\infty}^{\infty} \exp(\frac{\mathrm{i}}{\hbar} S_N)\mathrm{d}x_1 ... \mathrm{d}x_{N-1}, \tag{2.24}$$

where S_N is now

$$S_N = \epsilon \sum_{n=1}^{N} [\frac{m}{2}(\frac{x_n - x_{n-1}}{\epsilon})^2 - V(x_n, t_n)]. \tag{2.25}$$

In the continuum limit this takes the form

$$S[x] = \int_{t_a}^{t_b} [\frac{m}{2}\dot{x}^2 - V(x,t)]\mathrm{d}t \equiv \int_{t_a}^{t_b} L(x,\dot{x})\mathrm{d}t \tag{2.26}$$

where $L(x,\dot{x})$ is the Lagrangian of the system.

We have now arrived at the path integral formula for the propagator that we shall be using in most of this work

$$K(x_b,t_b;x_a,t_a) = \sqrt{\frac{m}{2\pi\hbar \mathrm{i}\epsilon}}^{N} \int_{-\infty}^{\infty} ... \int_{-\infty}^{\infty} \exp\Big(\frac{\mathrm{i}}{\hbar} S[x]\Big)\mathrm{d}x_1 ... \mathrm{d}x_{N-1}. \tag{2.27}$$

This formula has a very intuitive interpretation. The prefactor before the product is just a normalization constant, whose origin can be traced back to the momentum integrals. This may seem like a strange normalization constant especially in the limit $N \to \infty$ and $\epsilon \to 0$, but when we actually calculate the integrals (for those few cases we actually are able to) and substitute $\epsilon = (t_b - t_a)/N$, the N dependence vanishes and the limiting procedure is trivial [16, 19].

If we consider the integrals as infinite sums over all position coordinates then the first integral becomes a sum of the integrand where x_1 goes from $-\infty$ to ∞, the second integral then becomes a product of sums where x_1 goes from $-\infty$ to ∞ and x_2 goes from $-\infty$ to ∞, and so on, until all the integrals are done and we have a product of $N-1$ infinite sums. In other words the sum of all the possible zigzag paths, which exist from a fixed $x_a \equiv x_0$ to a fixed $x_b \equiv x_N$. See Fig. 2.1. The integrand tells us that for each of these paths we sum the exponential term whose argument is proportional to the classical action for that path.

Formally, we write the path integral formula as

$$K(x_b,t_b;x_a,t_a) = \int_{x_a}^{x_b} \exp(\frac{\mathrm{i}}{\hbar} S[x(t)])\mathscr{D}x(t). \tag{2.28}$$

The script $\mathscr{D}$ tells us that we need to sum over all $x(t)$ from x_a to x_b and taking into

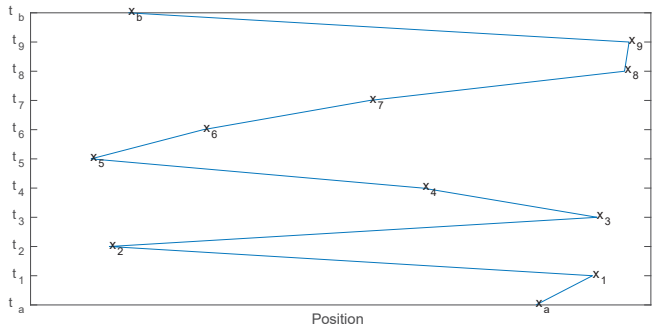

Figure 2.1 One of the zigzag paths a particle can move from x_a to x_b in time interval $t_b - t_a$. The total amplitude is gained by summing the phase factors of all the possible paths in the limit, where time axis is sliced into infinitely many and infinitely thin slices.

account the normalization constant.

To summarize, starting from the abstract operator equation Eq. (2.1) we find the time evolution amplitude from x_a to x_b in time $\Delta t = t_b - t_a$ by taking into account all the paths between those positions and summing exponential terms, whose arguments are proportional to the classical action for that path.

Note that "all the paths" include also paths that are classically forbidden, *e.g.*, paths that move through potential barriers higher than particle's energy and paths where the particle moves faster than light. One way of limiting the space of possible paths is by "measurement". For example, if we construct a two slit experiment for electron, then normally we will calculate all the paths through both slits and arrive at the expected interference pattern. However if we have some apparatus that detects, which slit the electron goes through, then only those paths that pass through that slit will contribute and the interference pattern disappears. Also, like in the two slit experiment we do not include the paths through the screen, except from where the slits are located. This is because the screen acts as infinite potential and the propagator of Eq. (2.28) vanishes for all paths that cross it. Mathematically this can be seen from the Riemann-Lebesgue lemma [20] which states that the integral of highly oscillatory function approach zero

$$\lim_{z\to\infty} \int f(x)\exp(-\mathrm{i}zx)\mathrm{d}x = 0. \tag{2.29}$$

We have now regained the classical-like picture, where particle propagates from

a to b, but instead of following a single path, it follows all the possible paths! Even if it is tempting to think of these exponentials as probabilities, they are not. Instead of probability we have a phase factor assigned to each possible path and the total probability amplitude is gained by summing all these phase factors.

The above derivation of path integrals was done to show that it is equivalent to the more common formalism starting from the postulated Schrödinger's equation Eq. (2.1). We can also take the reverse view and postulate path integrals as the starting point and derive the whole quantum mechanics, as it is presented in Feynman's book *Quantum Mechanics and Path Integrals* [8].

2.2.2 Interpretation of propagator

The wave function

$$\psi(x,t) \equiv \langle x \mid \psi \rangle \tag{2.30}$$

evolves in time according to Eq. (2.2)

$$\mid \psi_b \rangle = \hat{U}(t_b, t_a) \mid \psi_a \rangle \tag{2.31}$$

$\Rightarrow$

$$\langle x_b \mid \psi_b \rangle = \langle x_b \mid \hat{U}(t_b, t_a) \mid \psi_a \rangle \tag{2.32}$$

$$= \int_{-\infty}^{\infty} \langle x_b \mid \hat{U}(t_b, t_a) \mid x_a \rangle \langle x_a \mid \psi_a \rangle \mathrm{d}x_a \tag{2.33}$$

$\Rightarrow$

$$\psi(x_b, t_b) = \int_{-\infty}^{\infty} K(x_b, t_b; x_a, t_a) \psi(x_a, t_a) \mathrm{d}x_a. \tag{2.34}$$

If $\psi(x'_a, t_a) = \delta(x_a - x'_a)$, then

$$\psi(x_b, t_b) = \int_{-\infty}^{\infty} K(x_b, t_b; x'_a, t_a) \delta(x_a - x'_a) \mathrm{d}x'_a \tag{2.35}$$

$$= K(x_b, t_b; x_a, t_a) \tag{2.36}$$

and so

$$|\psi(x_b,t_b)|^2=|K(x_b,t_b;x_a,t_a)|^2\,. \tag{2.37}$$

Following the probability interpretation of the wave function [17] we can assert, that when computing the absolute square of the amplitude, we get the classical probability for a particle to go from a fixed x_a to x_b in time t_b-t_a. In section 6.5 we will develop a similar interpretation for the contributing parts of the complex valued propagator.

2.2.3 Eigenfunction basis

Above, we used spatially localized basis states x_n to derive the propagator, but similar derivation can be done choosing other basis states, such as momentum states p_n to find the time evolution amplitude in that space [8, 16, 19].

Another interesting representation of the propagator that we will use later is the special case, where the Hamiltonian is time independent. Then, it is convenient to choose its orthonormal eigenstates ϕ_n as the basis, $\{\phi_n\}$,

$$\phi_n(x,t)=\exp(-\frac{\mathrm{i}}{\hbar}E_n t)\phi_n(x), \tag{2.38}$$

and then

$$\psi(x,t)=\sum_{n=1}^{\infty}c_n\exp(-\frac{\mathrm{i}}{\hbar}E_n t)\phi_n(x). \tag{2.39}$$

The coefficients c_n are easy to calculate by multiplying from the left by $\phi_m^*(x)\exp(\frac{\mathrm{i}}{\hbar}E_m t)$, integrating over all space and using the orthonormality of the basis functions

$$\psi(x_b,t_b)=\int_{-\infty}^{\infty}\sum_{n=1}^{\infty}\phi_n^*(x_a)\exp(\frac{\mathrm{i}}{\hbar}E_n t_a)\psi(x_a,t_a)\exp(-\frac{\mathrm{i}}{\hbar}E_n t_b)\phi_n(x_b)\mathrm{d}x_a. \tag{2.40}$$

By comparing this with Eq. (2.34) we see that the propagator in this basis is

$$K(x_b,t_b;x_a,t_a)=\sum_{n=1}^{\infty}\phi_n(x_b)\phi_n^*(x_a)\exp(-\frac{\mathrm{i}}{\hbar}E_n(t_b-t_a)). \tag{2.41}$$

In this work we will mostly use the coordinate space representation.

2.2.4 Multivariable systems in coordinate space

We have been considering one-dimensional one-particle system but the generalization to multivariable systems is easy. Note that the extra variables can be both spatial dimensions and extra particles, the formalism is still the same. By replacing $x(t)$ with $\mathbf{x}(t)$ where the symbol $\mathbf{x}(t)$ now represents all d coordinates where d is the dimensionality of our system the former derivation can be redone. Only difference is that we get d times as many momentum integrals, and so, the Eq. (2.27) becomes

$$K(\mathbf{x}_b,t_b;\mathbf{x}_a,t_a)=\sqrt{\frac{m}{2\pi\hbar\mathrm{i}\epsilon}}^{Nd}\int_{-\infty}^{\infty}...\int_{-\infty}^{\infty}\exp\Big(\frac{\mathrm{i}}{\hbar}S[\mathbf{x}]\Big)\mathrm{d}\mathbf{x}_1...\mathrm{d}\mathbf{x}_{N-1}. \tag{2.42}$$

and the Eq. (2.28) can be written simply as

$$K(\mathbf{x}_b,t_b;\mathbf{x}_a,t_a)=\int_{\mathbf{x}_a}^{\mathbf{x}_b}\exp(\frac{\mathrm{i}}{\hbar}S[\mathbf{x}(t)])\mathscr{D}\mathbf{x}(t). \tag{2.43}$$

The interpretation remains the same. We need to sum over all the paths one can go through this d dimensional space from x_a to x_b. For particles with different masses the normalization constant will be different but can still be written formally as Eq. (2.43).

For the rest of this work, unless otherwise noted, non-bold x_n stands for all coordinates of particles in one or more spatial dimensions. In case with multiple variables the products should be understood as inner products.

3 MONTE CARLO METHOD

This chapter gives the background theory of Monte Carlo integration and explains why it is needed.

3.1 Curse of dimensionality

In numerical simulations in space and time we need to span a grid that covers the whole allowed space and is dense enough so that the grid is sufficient for an accurate representation of the actual function. As the dimensionality of the system increases, conventional methods that use regular grids become untenable.

As an example we can consider calculation of the electronic structure of a Zinc atom by solving Schrödinger equation in 3-dimensional grid (spin and quantum effects of the nucleus are ignored). The wave function for the system of 30 electrons is then $\psi(x_1, y_1, z_1, ..., x_{30}, y_{30}, z_{30})$. Even if we use moderately sparse grid in spatial dimensions, like 20 grid points per dimension we still end up with 20^{90} total grid points! This is a huge number. If we assume that we can store the information of each grid point in a single atom we would then need 20^{90} atoms for the total memory. Comparing this with the number of atoms in the observable universe $\approx 10^{80}$, which can be estimated from the cosmological parameters [34], we see that modelling even this simple system of one atom in a relative small spatial grid would need storage capacity of at least billion times greater than the whole observable universe.

This sc. curse of dimensionality has limited the success of calculations of many-body wave functions and provoked statements such as: *In general the many-electron wavefunction $\psi(r_1, ..., r_N)$ for a system of N electrons is not a legitimate scientific concept, when $N \geq N_0$, where $N_0 \approx 10^3$* [35].

3.2 Monte Carlo integration

In path integral formalism we need to evaluate often multidimensional integrals such as Eq. (2.28) and Eq. (2.34). As was discussed above, using any regular grids, when the dimensionality grows, becomes unfeasible. Thus, the natural way to proceed is by using Monte Carlo integration. Monte Carlo integration is based on the law of large numbers which allows us to write

$$I \equiv \int_\Omega f(x)\mathrm{d}x = \lim_{M\to\infty} \frac{V}{M}\sum_{i=1}^{M} f(x_i), \tag{3.1}$$

where Ω is the domain of integration with volume $V = \int_\Omega dx$ and x_i are random points within the domain.

This integral can be approximated by

$$I \approx I_M = \frac{V}{M}\sum_{i=1}^{M} f(x_i). \tag{3.2}$$

Central limit theorem states that the sum of large number of independent random variables is normally distributed, provided they have finite expectations and variances even though the variables themselves are not normally distributed. This allows us to estimate the statistical error of I_M, and assuming that variables $f(x_i)$ are uncorrelated, we can write

$$\begin{aligned}
\mathrm{Var}(I_M) &= \langle I_M^2\rangle - \langle I_M\rangle^2 && (3.3)\\
&= \frac{V^2}{M^2}\Big[\langle\big(\sum_{i=1}^{M} f(x_i)\big)^2\rangle - \langle\big(\sum_{i=1}^{M} f(x_i)\big)\rangle^2\Big] && (3.4)\\
&= \frac{V^2}{M^2}\mathrm{Var}\big(\sum_{i=1}^{M} f(x_i)\big) && (3.5)\\
&= \frac{V^2}{M}\mathrm{Var}\big(f(x_i)\big) && (3.6)
\end{aligned}$$

where $\langle\ \rangle$ means the expectation value. Now the statistical error of the integral can

Table 3.1 Proportionality of uncertainty of the integral for Monte Carlo estimates and some quadrature rules [36].

Monte Carlo	$M^{-1/2}$
Trapezoidal rule	$M^{-2/d}$
Simpson's rule	$M^{-4/d}$
k-point Gauss rule	$M^{-(2k-1)/d}$

be estimated by the standard deviation $\sigma = \sqrt{Var}$

$$\sigma_{I_M} = V \frac{\sigma_f}{\sqrt{M}}. \tag{3.7}$$

It is interesting to note that the error does not depend on the dimensionality of the system, though it depends on the volume of the domain.

If we compare this with some other numerical integration methods that use multidimensional quadrature rules we see that those methods are much more efficient when the dimensionality d of the system is low, but as the Monte Carlo is independent of dimensionality there is always some d for which Monte Carlo converges faster than any fixed quadrature method, as shown in the table 3.1 [36, 37, 38].

It may seem strange that random distribution of points becomes superior to a regular grid when the dimensionality increases. We see that regular grid is more homogeneous in one dimension but the assumption that the same holds, when the dimensionality increases in wrong. Intuitively this can be understood by considering a d dimensional regular grid with M points in each dimension and projecting it onto one random axis. On that axis, there are only M spikes of d points on the location of the original grid points and nothing between them. If we consider the same projection using the same parameters but Monte Carlo grid we will end up with random distribution of M^d points along that one axis. In this way random distribution becomes more homogeneous when the dimensionality increases [36, 38]. This effect is illustrated in Fig. 3.1.

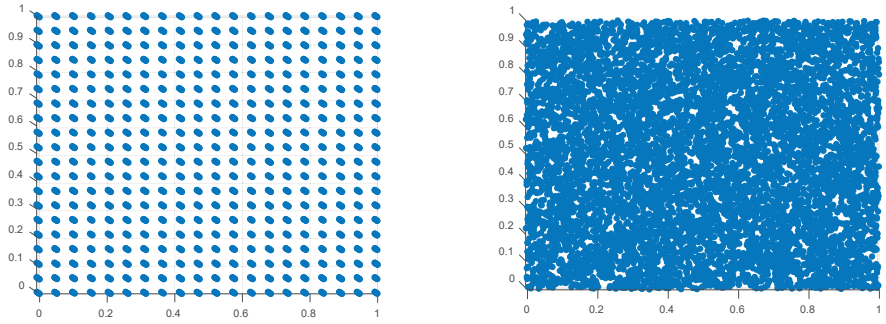

Figure 3.1 Comparison of a regular 3 dimensional grid with 8000 grid points and a Monte Carlo grid of the same size. In this 2D projection, most of the points on the regular grid are on top of each other making the grid look sparse, while Monte Carlo points fill the space "smoothly".

3.3 Importance sampling

In reality the crude Monte Carlo integral is not very efficient and one way to improve the convergence is the importance sampling method [14, 36, 37, 38]. Mathematically this corresponds to changing variable $f(x)\mathrm{d}x$ in Eq. (3.1) to $\frac{f(x)}{g(x)}g(x)\mathrm{d}x \equiv \frac{f(x)}{g(x)}\mathrm{d}G(x)$ where $g(x)$ is a probability density function and therefore it must be non-negative everywhere and normalized. $G(x)$ is the associated cumulative distribution function.

With this Monte Carlo estimate for the integral becomes

$$I_M = \frac{V'}{M}\sum_{i=1}^{M}\frac{f(X_i)}{g(X_i)}, \tag{3.8}$$

where the random variables X_i are now sampled according to the distribution $g(x)$ and $V' = \int_\Omega dG(x)$. In practice, we need either some way of producing $g(x)$ distributed random numbers or we need to be able to calculate the inverse of $G(x)$ analytically, because $G^{-1}(\mathrm{unif}(0,1)) = \mathrm{X_i}$, where unif$(0,1)$ is the uniform distribution on the interval $[0,1]$.

Choosing $g(X)$ so that it is close to $f(X)$ (*i.e.*, $f(X)/g(X) \approx$ constant) minimizes the fluctuations in the integrand and hence the variation in the Monte Carlo estimate

of the integral becomes

$$\mathrm{Var}(I_M) = \frac{V'^2}{M^2}\Big[\langle(\sum_{i=1}^{M}\frac{f(X_i)}{g(X_i)})^2\rangle - \langle(\sum_{i=1}^{M}\frac{f(X_i)}{g(X_i)})\rangle^2\Big]. \tag{3.9}$$

If we are able to choose $g(X) = f(X)$ then both the sums in the above equation are just M^2 and the variance will be zero.

Another advantage of writing the Monte Carlo estimate like this is that more points are concentrated on the region where $f(X)$ is large and little computation is used on points that give little or no contribution to the integral.

Writing the wave function as

$$\psi(x,t) = |\psi(x,t)|\exp\big(\mathrm{i}\phi(x,t)\big) \tag{3.10}$$

and choosing the sample points from distribution $|\psi(x,t)|$ we can use importance sampling method to evaluate Eq. (2.34)

$$\psi(x_b,t_b) = \int_{-\infty}^{\infty} K(x_b,t_b;x_a,t_a)\psi(x_a,t_a)\mathrm{d}x_a \tag{3.11}$$

$$\approx \frac{V'}{M}\sum_{a=1}^{M}\frac{K(x_b,t_b;X_a,t_a)}{|\,\psi(X_a,t_a)\,|}\,|\,\psi(X_a,t_a)\,|\exp\big(\mathrm{i}\phi(X_a,t)\big) \tag{3.12}$$

$$= \frac{V'}{M}\sum_{a=1}^{M}K(x_b,t_b;X_a,t_a)\exp\big(\mathrm{i}\phi(X_a,t)\big) \tag{3.13}$$

$$\equiv \psi_N(x_b,t_b). \tag{3.14}$$

3.4 Random walk, Markov chain and Metropolis Monte Carlo

The question how to produce $g(x)$ distributed random numbers was brought up, above. In practice, unless $g(x)$ is some standard function like normal distribution, we do not have an easy way of doing that, as the inverse cumulative distribution functions do not usually have closed-form expressions and they might be difficult to solve numerically [39]. We could always normalize $g(x)$ and use it as an acceptance probability for uniformly distributed x', but this method is obviously very ineffi-

cient, if $g(x)$ is small over large part of x space. This can be improved by choosing non-uniform distribution $h(x)$, for which random number generator exists, that is everywhere greater than, but is close to $g(x)$ and then use $\frac{g(x)}{h(x)}$ as the acceptance probability. In general, we cannot find such a function and this method also becomes inefficient.

Another approach to sampling any probability density function is sc. random walk method. In this method we do not form statistically uncorrelated points x_i, but instead, we define an object called a walker that moves through the space by a combination of deterministic transition probabilities and random displacements. The sequence of correlated steps is called a Markov chain, if the transition probabilities depend only on the current state of the system, not on how or when it got there [14]. Markov chain is called ergodic, if it is not periodic and every configuration can be reached from every other configuration with a finite number of steps [38].

To clarify the difference between Markov chain and truly random chain of events we consider the joint probability of N independent events occurring in succession

$$P(x_1, x_2, ..., x_N) = P(x_1)P(x_2)...P(x_N) \tag{3.15}$$

where $P(x_i)$ is the probability for an event x_i to occur. For Markov chain this same probability is instead

$$P(x_1, x_2, ..., x_N) = P(x_1)T(x_1 \to x_2)T(x_2 \to x_3)...T(x_{N-1} \to x_N) \tag{3.16}$$

where $T(x \to x')$ is the transition probability, *i.e.* the probability that the event x' follows x in the sequence. They are properly normalized, so that the probability of something to happen is 1:

$$\sum_{x'} T(x \to x') = 1. \tag{3.17}$$

With enough time, ergodic Markov chain can produce the desired invariant distribution[38]. We now need to choose the transition probabilities so that the random walk yields the desired distribution.

One approach to accomplish this is the Metropolis Monte Carlo method [40].

If $g(x,t)$ is defined as the probability for the configuration x at time t, then

$$g(x,t+1) = \sum_{x'} g(x',t)T(x' \to x). \tag{3.18}$$

Note that t is not a proper time in the physical sense, but the running index of Markov step. We are aiming at finding stationary distribution $g(x,t)$ so that

$$g(x,t+1) = g(x,t). \tag{3.19}$$

Using Eq. (3.18) and multiplying the right hand side by 1 in the form of Eq. (3.17) this becomes

$$\sum_{x'} g(x',t)T(x' \to x) = \sum_{x'} g(x,t)T(x \to x'). \tag{3.20}$$

The general solution to this equation is difficult to find [38], but one apparent solution is:

$$g(x',t)T(x' \to x) = g(x,t)T(x \to x') \tag{3.21}$$

for all pairs of configurations x and x'. This solution is called "principle of detailed balance" and it says that the total rate of transitions from x' to x is the same as the total rate of transitions from x to x'.

As the equation must hold for all t's we can omit them and write the transition probability as the product of an *a priori* sampling probability $p(x \to x')$ and an acceptance probability $a(x \to x')$:

$$T(x \to x') = p(x \to x')a(x \to x'). \tag{3.22}$$

Substituting this into Eq. (3.21) and requiring that the sampling probability is symmetric ($p(x \to x') = p(x' \to x)$) we get

$$\frac{a(x \to x')}{a(x' \to x)} = \frac{g(x')}{g(x)}. \tag{3.23}$$

This fraction does not determine the transition probability uniquely and we are allowed certain freedom in choosing it. The Metropolis choice is to take

$$\text{If } g(x') < g(x) : a(x \rightarrow x') = \frac{g(x')}{g(x)} \tag{3.24}$$

$$\text{If } g(x') \geq g(x) : a(x \rightarrow x') = 1. \tag{3.25}$$

We can now construct a simple algorithm that will produce any desired distribution $g(x)$. We start from any random configuration x and then make a trial move according to the sampling probability $p(x \rightarrow x')$ to produce new configuration x'. We then calculate $g(x')/g(x)$. If this is less than 1 the move is accepted with this probability and if it is equal to or greater than 1 the move is always accepted. If the move is accepted the configuration x' replaces x and if it is rejected the system stays in configuration x. If given enough time this algorithm will find equilibrium and then x will be distributed according to the $g(x)$.

Ergodicity will ensure that the time average will be the same as ensemble average so usually in practice it is faster to sample an ensemble of walkers over shorter time than follow only one walker over longer time. In both cases the simulation should be run long enough for the system to find equilibrium, after which the distribution can be used in importance sampling techniques.

The points in Metropolis Monte Carlo simulations are correlated and the Eq. (3.7) needs to be modified to account for this. This can be done by introducing a measure of autocorrelation called correlation time $\varkappa$ [15] and the modified equation becomes

$$\sigma_{I_N} = V \sigma_f \sqrt{\frac{\varkappa}{M}}. \tag{3.26}$$

The advantage of Monte Carlo scaling still remains assuming that correlation time does not increase faster than polynomially with the number of dimensions.

4 STATISTICAL PHYSICS

This chapter gives a short introduction to quantum statistical physics and how it is connected to path integral formalism.

4.1 Expectation value

As is evident from our discussion of the wave function of a particle and its interpretation as a probability amplitude we can not generally know where the particle is exactly located. The absolute square of the wave function integrated over an infinitesimal volume tells us the probability that the particle is located inside this volume. Now, measurements of the position x of the particle in several identical systems will give different values and we can only talk about the mean or expectation (expected) value of x. This will be given by the probability $P(x,t)$ that the particle is found on x, times the value of x and summed (integrated as x is continuous variable) over all possible values of x.

For more general case where we are interested not only in the position but some function of the position, for a system described by a wave function $\psi(x,t)$ the expectation value of a function $f(x)$ is [13, 17]

$$\langle f(x)\rangle = \frac{\int_{-\infty}^{\infty} \psi^*(x,t) f(x) \psi(x,t) \mathrm{d}x}{\int_{-\infty}^{\infty} \psi^*(x,t)\psi(x,t)\mathrm{d}x}. \tag{4.1}$$

Since we are working in the coordinate space this will suffice for us, but it should be noted that this form cannot be used to calculate expectation values for observables that can not be expressed as a function of x, only, such as spin.

If the wave function is properly normalized the denominator is one, but this is not the case usually, when carrying out Monte Carlo simulations as the volume V in Eq. 3.2 might be hard to calculate, and as we will see, it is usually not needed.

Again, using the importance sampling method with distribution function $|\psi(x,t)|$ and using Eq. (3.11) we can write the Monte Carlo estimate for the expectation value as

$$\langle f(x)\rangle \approx \langle f_M\rangle = \frac{\sum_{j=1}^{M} f(X_j)\,|\,\psi_M(X_j,t)\,|}{\sum_{j=1}^{M}|\,\psi_M(X_j,t)\,|}. \tag{4.2}$$

One advantage of this form is that we do not need to worry about the norm of the wave function since any constant prefactor will cancel out.

4.2 Quantum statistical physics

The following discussion follows that in the book *Quantum Mechanics and Path Integrals* [8].

In statistical physics the probability P_n that the system in thermal equilibrium in temperature T is in a state with energy E_n is proportional to the Boltzmann factor $\exp(-\beta E_n)$ where β is $\frac{1}{kT}$ and k is Boltzmann's constant [41]

$$P_n = \frac{1}{Z}\exp(-\beta E_n), \tag{4.3}$$

where Z in the normalizing factor is the partition function

$$Z = \sum_n \exp(-\beta E_n). \tag{4.4}$$

All the thermodynamic properties of a system can be computed [41] if the partition function is known. In a natural classical system Hamilton function $H(p,x)$ represents the energy of the system [18] and since x and p are continuous variables the sum in Eq. (4.4) is replaced by integrals [16]

$$Z = \int \frac{1}{2\pi\hbar}\exp\big(-\beta H(p,x)\big)\mathrm{d}p\mathrm{d}x. \tag{4.5}$$

For a d dimensional system the phase space integral is $\prod_{n=1}^{d}\int \frac{dp_n dx_n}{2\pi\hbar}$.
The interpretation is that the probability of the volume of the phase phase being occupied is proportional to the Bolzmann factor. It is also interesting to note how the reduced Planck's constant $\hbar$ appears in a purely classical equation. Historically,

the partition function in this form was determined only up to an unidentified constant factor with units of inverted action that determined the size of the phase space element [8].

Use of the eigenstates $\phi_n(x)$ of the Hamiltonian gives us a simple way to calculate the expectation value of $f(x)$ for a system in thermal equilibrium. The probability for the system to be in a particular state of energy E_n is given by Eq. (4.3) and the probability that a particular x is observed for given ϕ_n is given by the absolute square of the wave function and so the probability of observing x is

$$P(x) = \frac{1}{Z}\sum_n \phi_n^*(x)\phi_n(x)\exp(-\beta E_n) \tag{4.6}$$

and so the expectation value is

$$\langle f(x)\rangle = \frac{1}{Z}\sum_n \int_{-\infty}^{\infty} \phi_n^*(x) f(x)\phi_n(x)\exp(-\beta E_n)\mathrm{d}x \tag{4.7}$$

where the eigenstates $\phi_n(x)$ are properly normalized.

The statistical density matrix at temperature T is defined as

$$\rho(x', x) = \sum_n \phi_n(x')\phi_n^*(x)\exp(-\beta E_n). \tag{4.8}$$

Because integral of $P(x)$ over all x is normalized to 1 we see from Eq. (4.6) that

$$Z = \int \rho(x, x)\mathrm{d}x \equiv \mathrm{Tr}\{\rho\}. \tag{4.9}$$

We can now write the expectation value as

$$\langle f(x)\rangle = \frac{1}{Z}\int f(x)\rho(x, x)\mathrm{d}x. \tag{4.10}$$

If we are interested in expectation values of $f(x, p)$, then we need also the off diagonal elements of the density matrix [16], but the conventional thermodynamic variables can be evaluated directly from $Z \equiv \mathrm{Tr}\{\rho\}$.

We can write Eq. (4.8) slightly differently

$$\rho(x_b, u_b; x_a, u_a) = \sum_n \phi_n(x_b)\phi_n^*(x_a)\exp\Big(-\frac{1}{\hbar}E_n(u_b - u_a)\Big) \tag{4.11}$$

where $x_b = x'$, $x_a = x$, $u_b = \hbar\beta$ and $u_a = 0$. If we compare this to the real-time

propagator of Eq. (2.41) we see that they are formally similar. The requirement that the Hamiltonian is time independent is automatically implied, when our system is in thermal equilibrium. We have already shown how to calculate the propagator as a path integral (see Eq. (2.28) and its derivation) and so we can write

$$\rho(x_b, x_a, \hbar\beta) = \int_{x_a}^{x_b} \exp\Big\{ -\frac{1}{\hbar} \int_0^{\hbar\beta} \big[\frac{m}{2}\dot{x}^2(u) + V\big(x(u)\big) \big] \mathrm{d}u \Big\} \mathscr{D}x(u). \qquad (4.12)$$

By the same analogy as before we can give statistical description of a quantum mechanical system by summing over all possible paths that the particle can "move" from x_a to x_b in "time" $\hbar\beta$. For the partition function we need to consider closed paths only, that begin and end at the same position in space.

It is interesting to note that our description is fully quantum mechanical but we no longer have the imaginary unit in the equation. This allows much easier numerical calculations, as now, the importance sampling technique is readily usable. We also have much clearer picture how each path contributes to the integral as they are weighted by the negative exponential as opposed to the real time where each path has equal weight.

4.3 Symmetry considerations

The symmetry of the multi particle wave function is ultimately linked to the fact that particles in nature are identical as can be seen by considering the two particle wave function $\psi(x_1, x_2)$. If the particles are identical this means that we do not have any way of identifying which particle is which. This means that the probability of finding particle 1 at some position s_1 and particle 2 at some position s_2 must be the same as probability of finding particle 1 in position s_2 and particle 2 in position s_1, which in mathematical terms means that the absolute square of the wave function must be unchanged under the operation of interchanging its arguments.

$$|\,\psi(x_1, x_2)\,|^2 \quad = \quad |\,\psi(x_2, x_1)\,|^2\,. \qquad (4.13)$$

From this it follows that

$$\psi(x_1, x_2) = \pm\psi(x_2, x_1). \tag{4.14}$$

Nature has cleverly taken use of both possible signs and particles with symmetric solution are called bosons

$$\psi(x_1, x_2) = +\psi(x_2, x_1) \tag{4.15}$$

and those with antisymmetric solution are called fermions

$$\psi(x_1, x_2) = -\psi(x_2, x_1). \tag{4.16}$$

Thus, for a system of identical particles the Eq. (4.12) is not actually complete. The reason is that even though other solutions to Schrödinger's equation exist, only symmetric (Bosons) and antisymmetric (Fermions) ones appear in nature [8], and so, the sum in Eq. (4.4) should only include energies of the appropriate solutions.

Let us consider a bosonic system of N identical particles. Any function $f(x_1, x_2)$ can be made symmetric by replacing it by a combination $f(x_1, x_2) + f(x_2, x_1)$ and so the energy eigenfunction

$$\phi'(x_i) = \sum_P \phi(P x_i), \tag{4.17}$$

is symmetrical. Here $P x_i$ means permutation of pair of x_i:s. Suppose that E_k is an energy eigenvalue for which Schödinger equation does not have a symmetric solution, and so, $\sum_P \phi_k(Px)$ must vanish. This implies that the operation defined by Eq. (4.17) selects only symmetric solutions. Since there are $N!$ ways of permuting N patricles, we can write

$$\sum_P \phi_n(Px) = \begin{cases} N!\phi_n(x), & \text{if } \phi_n \text{ is symmetric.} \\ 0, & \text{otherwise.} \end{cases} \tag{4.18}$$

This means that if $\phi_n(x)$ in Eq. (4.11) is replaced with this sum it will then select only the symmetric solutions multiplied by $N!$ and the way to write the symmetric

form of Eq. (4.12) is

$$\rho_{\mathrm{sym}}(x_b, x_a, \hbar\beta) = \frac{1}{N!}\sum_P \int_{x_a}^{Px_b} \exp\Big\{-\frac{1}{\hbar}\int_0^{\hbar\beta} \big[\frac{m}{2}\dot{x}^2(u) + V\big(x(u)\big)\big]\mathrm{d}u\Big\}\mathscr{D}x(u). \tag{4.19}$$

For fermions the form is similar except that we need to include antisymmetric wave function and extra factor of ± 1 (positive for even permutations and negative for odd permutations) [8].

Inclusion of these changes will yield the correct quantum statistics where fermions are described by Fermi–Dirac distribution and bosons by Bose–Einstein distribution [41].

One might wonder, if we need to take into account similar symmetry considerations when using real time propagator of Eq. (2.28). There, this symmetry is automatically included in the path integral calculations as we calculate all the paths (including those were the particles swap positions) and by the symmetry of the original wave function (see Eq. (2.31)).

However, in practical simulations this is only true when our walker distribution conforms to the actual symmetry. Instead of making sure that we have a walker representing the wave function for each permutation of particles we can also implement these permutations directly into the kernel and reduce the number of needed walkers by $N!$ where N is the number of identical particles.

4.4 Fermion sign problem

As was discussed above, the advantage of Monte Carlo integration is that the error does not grow exponentially with the number of dimensions and the integral can be evaluated to any desired accuracy in polynomial time [42].

Usually we are interested in calculating expectation values of certain physical quantities. If the quantity in question has a simple multiplicative form in position basis then using Eq. (4.10) this can be calculated as

$$\langle O(x)\rangle = \frac{\int O(x)\rho(x,x)\mathrm{d}x}{\int \rho(x,x)\mathrm{d}x} \tag{4.20}$$

and using Monte Carlo estimate of Eq. (3.2) as

$$\langle O(x)\rangle = \frac{\sum_i O(x_i)\rho(x_i)}{\sum_i \rho(x_i)}. \tag{4.21}$$

If all weights $\rho(x_i)$ are positive the standard Monte Carlo methods can be used to calculate the expectation value. In fermionic systems the weights can be positive or negative as discussed in the section 4.3 and the approach needs to be modified. The easiest solution is to take the sign $s(x_i)$ as a part of the sum and use the absolute value of $\rho(x_i)$ as the weight [42]

$$\langle O(x)\rangle = \frac{\sum_i O(x_i)s(x_i)\,|\,\rho(x_i)\,|\,/\sum_i\,|\,\rho(x_i)\,|}{\sum_i s(x_i)\,|\,\rho(x_i)\,|\,/\sum_i\,|\,\rho(x_i)\,|} \equiv \frac{\langle Os\rangle}{\langle s\rangle} \equiv \frac{\langle Os\rangle}{Z/Z'} \tag{4.22}$$

where Z and Z' are the partition functions of the fermionic and bosonic systems, respectively. This allows Monte Carlo calculations but the error increases exponentially with the number of particles N and the inverse temperature β. This is because the partition functions are exponentials of the corresponding free energies, so their ratio is exponential of the difference in free energy densities Δf [42, 56],

$$\frac{Z}{Z'} = \exp(-\beta N \Delta f). \tag{4.23}$$

The relative error becomes

$$\frac{\delta_s}{\langle s\rangle} = \frac{\sqrt{(\langle s^2\rangle - \langle s\rangle^2)/M}}{\langle s\rangle} = \frac{\sqrt{1-\langle s\rangle^2}}{\sqrt{M}\langle s\rangle} \sim \frac{\exp(\beta N \Delta f)}{\sqrt{M}}. \tag{4.24}$$

This grows exponentially with N and β and so the advantage of Monte Carlo is lost. This is the infamous "fermion sign problem" one comes across, when running Monte Carlo simulations. There are many schemes [27, 43, 44, 45, 56, 61] to tackle this problem but the general solution has not been found. There are also arguments [42] that it cannot be solved, as general solutions would yield the solution for all computational NP problems and hence would mean NP = P, which is generally not believed to be the case. NP (Nondeterministic Polynomial) stands for a class of problems, for which the correctness of the answer can be checked in polynomial time but for which there exists no general algorithm that can compute the answer in polynomial time. P (Polynomial) means problems for which polynomial time

algorithms are known.

5 IMAGINARY TIME METHODS

This chapter gives a brief introduction to the conventional state-of-the-art Quantum Monte Carlo (QMC) methods. QMC methods form a collection of robust, imaginary time approaches to study quantum many-particle systems [38]. With QMC the central benefit is that one can deal with multi-dimensional systems, where standard grid based methods become computationally too heavy. Imaginary time path integral and Green's function approaches take the many-body effects and correlations into account without introducing approximations and evaluate them within numerical accuracy, which is limited by the computational resources, only. Furthermore, if starting from the first-principles, also the systematic errors are avoidable. Thus, for the field of electronic structure calculations, with QMC one can benchmark the energetics and structure of atoms and molecules with desired accuracy. It is even straightforward in cases where the wave function is everywhere positive or can be considered as piecewise positive between given or calculated nodes.

5.1 Path integral Monte Carlo

In Path Integral Monte Carlo (PIMC) approach the Metropolis Monte Carlo method is used to sample the density matrix in Eq. (4.12) or Eq. (4.19), though the latter is not as straightforward for fermions [27]. For bosons this has proven to be very efficient method of calculating quantum statistical properties of finite, non-zero temperature systems [15, 46, 47].

In practical simulations the short time approximation is usually used, which is called the primitive approximation in this context. It can be derived by using the fact that amplitudes for events occurring in succession are multiplicative [8]. The "time" $\hbar\beta$ is divided into M equal parts and the density matrix can then then be

written as

$$\rho(x', x, \hbar\beta) = \int \rho(x', x_1, \hbar\tau)\rho(x_1, x_2, \hbar\tau)...\rho(x_{M-1}, x, \hbar\tau)\mathrm{d}x_1\mathrm{d}x_2...\mathrm{d}_{M-1}, \quad (5.1)$$

where $\tau = \beta/M$. M is often called the Trotter number and it should be noted that the equation is exact for any M.

In case, the particles are assumed to be distinguishable Eq. (4.8) is used to write Eq. (5.1) as

$$\rho(x_{i-1}, x_i, \hbar\tau) = \sum_n \phi_n(x_{i-1})\exp(-\tau\hat{H})\phi_n^*(x_i) \quad (5.2)$$

$$= \sum_n \phi_n(x_{i-1})\exp(-\tau\hat{T} - \tau\hat{V})\phi_n^*(x_i) \quad (5.3)$$

$$\approx \sum_n \phi_n(x_{i-1})\exp(-\tau\hat{T})\exp(-\tau\hat{V})\phi_n^*(x_i). \quad (5.4)$$

In the last line the commutator between $\hat{T}$ and $\hat{V}$ is ignored (see Eq. 2.11), and thus, this is exact at the limit $\tau \to 0$ *i.e.*, $M \to \infty$. Because potential energy is diagonal in position space the last equation can be written as

$$\rho(x_{i-1}, x_i, \hbar\tau) = \sum_n \phi_n(x_{i-1})\exp(-\tau\hat{T})\ \phi_n^*(x_i)\exp(-\tau V(x_i)) \quad (5.5)$$

$$\equiv \rho_0(x_{i-1}, x_i, \hbar\tau)\exp(-\tau V(x_i)), \quad (5.6)$$

where ρ_0 is the free particle density matrix. It can be calculated analytically [15] by inserting free particle eigenfunctions (plane waves) and eigenenergies into Eq. 5.5. Then, assuming we can approximate the sum by an integral it can be calculated the same way the momentum integrals of Eq. (2.17) were done in chapter 1. The free particle density matrix then takes the form

$$\rho_0(x', x) = (4\pi\lambda\tau)^{-dN/2}\exp\Big[-\frac{(x'-x)^2}{4\lambda\tau}\Big] \quad (5.7)$$

where $\lambda = \hbar^2/2m$, d is the dimensionality of the system and N is the number of

particles with mass m. Eq. (5.1) can now be written as

$$\rho(x',x,\hbar\beta)=\int(4\pi\lambda)^{-dNM/2}\exp(-\sum_{i=1}^{M}\Big[-\frac{(x_{i-1}-x_i)^2}{4\lambda\tau}+\tau V(x_i)\Big]\mathrm{d}x_1...\mathrm{d}x_{M-1}. \tag{5.8}$$

There is a useful classical analogy for this equation. It is the configuration integral for a chain of beads that are connected with springs *i.e.,* harmonic potential. Because of this classical isomorphism, many properties of a quantum system can be understood purely in terms of classical statistical mechanics. For thermodynamical properties we only need the trace of this matrix ($x = x'$) and so the chain becomes closed to a ring.

5.2 Diffusion Monte Carlo

Diffusion Monte Carlo (DMC) method is another typical representative of QMC, where imaginary time evolution is used to find the ground state of the system at zero temperature. It has been demonstrated in several cases to be a simple, yet accurate approach [14, 38] and both bosonic [15, 54] and fermionic [55, 56, 60] systems have been successfully considered. A recent example is benchmarking the hydrogen molecule and its simple reaction conformations with ever increasing accuracy [57, 58, 59].

The time-dependent Schrödinger wave equation for the many-body wave function $\psi(x,t)$ is

$$\mathrm{i}\hbar\frac{\partial\psi(x,t)}{\partial t}=(H-E_T)\psi(x,t), \tag{5.9}$$

where H is the hamiltonian, x stands for all coordinates of particles in one or more spatial dimensions and E_T is an arbitrary reference energy or shift of zero level. Now, by replacing the real time t by imaginary time $\tau=\frac{i}{\hbar}t$, this becomes

$$-\frac{\partial\psi(x,\tau)}{\partial\tau}=(H-E_T)\psi(x,\tau), \tag{5.10}$$

which is of the form of a diffusion equation. Its solutions can be expressed in terms

of eigenfunctions $\phi_n(x)$ of the hamiltonian as

$$\psi(x,\tau) = \sum_{n=0}^{\infty} C_n \phi_n(x) \exp[-(E_n - E_T)\tau]. \tag{5.11}$$

As τ increases the eigenfunction with the lowest eigenvalue starts to dominate the sum. In other words, imaginary time propagation with large enough τ produces the ground state of the system.

Using Eq. (2.34) we can write the solution as

$$\psi(x_b,\tau_b) = \int_a G(x_b,\tau_b;x_a,\tau_a)\psi(x_a,\tau_a)\mathrm{d}x_a, \tag{5.12}$$

where $G(x_b,\tau_b;x_a,\tau_a)$ is the propagator, the position space representation of the time evolution operator $\exp[-(H-E_T)(\tau_b-\tau_a)]$. Since DMC is usually presented without resorting to path integrals and instead using Green's function formalism [14] the propagator is called Green's function of the system in this context.

As the exact analytical form of the Green's function is rarely known it needs to be approximated. Use of the so called short time approximation [14] (see also Eqs. (2.12) and (6.5)) to separate the kinetic and potential energy contributions, T and V, gives

$$\exp[-(H-E_T)\Delta\tau] = \exp[-(T+V-E_T)\Delta\tau] \approx \exp[-T\Delta\tau]\exp[-(V-E_T)\Delta\tau]. \tag{5.13}$$

Since T and V do not commute, in general, this approximation is exact only at the limit $\Delta\tau \to 0$ but accurate for small $\Delta\tau$ for potentials bound from below [14].

At this limit the Green's function can be separated into two parts, kinetic and potential (or diffusion and branching),

$$G(x_b,\tau_b;x,\tau_a) \approx G_{\mathrm{diff}}(x_b,\tau_b;x,\tau_a)G_B(x_b,\tau_b;x,\tau_a). \tag{5.14}$$

As this Green's function satisfies the imaginary time Schrödinger equation [14] we can write

$$-\frac{\partial G_{\text{diff}} G_B}{\partial \tau} = (H - E_T) G_{\text{diff}} G_B \tag{5.15}$$

$$= -\frac{\hbar^2}{2m} \nabla^2 G_{\text{diff}} G_B - (E_T - V) G_{\text{diff}} G_B \tag{5.16}$$

$$\tag{5.17}$$

and differentiating the left hand side yields

$$\frac{\partial G_{\text{diff}}}{\partial \tau} G_B + G_{\text{diff}} \frac{\partial G_B}{\partial \tau} = \frac{\hbar^2}{2m} \nabla^2 G_{\text{diff}} G_B + (E_T - V) G_{\text{diff}} G_B. \tag{5.18}$$

From this we get two equations

$$\frac{\partial G_{\text{diff}}}{\partial \tau} = \frac{\hbar^2}{2m} \nabla^2 G_{\text{diff}} \tag{5.19}$$

and

$$\frac{\partial G_B}{\partial \tau} = (E_T - V) G_B. \tag{5.20}$$

Solutions to these equations are well known [14, 38], a Gaussian spreading in $\Delta\tau$ and an exponential function:

$$G_{\text{diff}}(x_b, x_a; \Delta\tau) = (4\pi D \Delta\tau)^{-dN/2} \exp[-(x_b - x_a)^2 / 4D\Delta\tau] \tag{5.21}$$

and

$$G_B(x_b, x_a; \Delta\tau) = \exp[-(\frac{1}{2}[V(x_a) + V(x_b)] - E_T)\Delta\tau], \tag{5.22}$$

where the diffusion constant is $D = \hbar^2/2m$ ($= 1/2$ in atomic units for the electron), d is the dimensionality and N is the number of particles with mass m. Note that the diffusion part of Eq. (5.21) and the free particle density matrix of PIMC Eq. (5.7) are the same.

With these equations one can simulate random-walk-with-branching procedure to find the imaginary time evolution. Carrying out the simulation iteratively with short enough time step $\Delta\tau$, large enough population of random walkers and adjusting the "trial energy" E_T to keep the simulation stationary will finally converge to the ground state wave function distribution of walkers and trial energy to the corre-

sponding energy eigenvalue.

Diffusion Monte Carlo method is generally used with trial wave functions [14, 26], which makes DMC a significantly more powerful tool than without, in which case it usually deals with the ground states. Trial wave functions enable studies of larger system sizes, helps finding the lowest energy states of given symmetries and use of sc. mixed estimators for evaluation of physical quantities. Also, use of wave function nodes, if available, allows simulation of excited states [27, 28].

6 REAL TIME METHODS

Finally, the novel real time path integral (RTPI) methods of this thesis will be given in this chapter. We will first introduce improvements to the propagator from both physical and numerical viewpoint. Second, we will present a novel technique that we call the "incoherent propagation". This method allows us to use real time propagation to calculate the eigenstates of the system. Unlike the imaginary time methods, this approach can also be used on excited states straightforwardly. A Monte Carlo method, where the calculated real part of the wave function is used to guide the evolution of the walkers, is introduced for the simulations of incoherent propagation. Coherent propagation *i.e.*, actual dynamics is also demonstrated. The real time diffusion Monte Carlo method is presented. This technique transforms the complex propagator into four real valued propagators, which can be used, similarly to the conventional Diffusion Monte Carlo method, as probabilities for walker evolution. This will remove the need of calculating propagators between all walkers making the calculations computationally substantially lighter. Both incoherent and coherent propagations are simulated with this method.

6.1 Propagator and its approximations

At first look the equations for imaginary time evolution Eqs. (4.12), (5.12) and real time evolution Eq. (2.34) look very similar but the imaginary unit in the exponent makes an essential difference. While the imaginary time evolution is local like diffusion the real time one is not. This makes most of the useful features discussed in the previous section unavailable for real time simulations. In principle, we can use importance sampling but we do not generally have an efficient way of producing the desired distribution and we end up summing highly oscillatory terms that makes calculations inefficient.

Explicit forms of the propagator are known for simple cases, only, such as the

particle with mass m in the one dimensional constant linear potential $V(x) = -fx$ [8, 21],

$$K(x_b, x_a; \Delta t) = \left[\frac{m}{2\pi \mathrm{i}\hbar \Delta t}\right]^{1/2} \exp\left[\frac{\mathrm{i}}{\hbar}\left(\frac{m}{2\Delta t}(x_b - x_a)^2 - \frac{\Delta t}{2}(V(x_a) + V(x_b)) - \frac{\Delta t^3 f^2}{24m}\right)\right], \quad (6.1)$$

which reduces to the free particle propagator with $f = 0$ or to the propagator of particle in a box if confined by infinite potentials.

For the one dimensional forced harmonic oscillator

$$V(x,t) = \frac{m\omega^2}{2}x^2 - f(t)x \quad (6.2)$$

the exact explicit propagator takes the form [8, 22]

$$K(x_b, x_a; \Delta t) = \exp(-i\theta)\left[\frac{m\omega}{2\pi\hbar\,|\sin(\omega\Delta t)\,|}\right]^{1/2} \exp\left[\frac{\mathrm{i}}{\hbar}S_{\mathrm{cl}}\right], \quad (6.3)$$

where S_{cl} is the classical action and $\theta = \frac{\pi}{4}(1 + 2\,\mathrm{trunc}(\omega t/\pi))$. Here, "trunc$(x)$" denotes the truncation function, the largest integer less than or equal to x. For $f \equiv 0$ the classical action is

$$S_{\mathrm{cl}} = \frac{m\omega}{2\sin(\omega\Delta t)}\left[(x_b^2 + x_a^2)\cos(\omega\Delta t) - 2x_b x_a\right]. \quad (6.4)$$

In general, the exact Kernel is rarely known and approximations are needed. A usual approximation is sc. "symmetrized short time approximation" or "symmetrized Trotter kernel" as it is also called [1, 19, 23, 24]

$$K(x_b, x_a; \Delta t) \approx \left[\frac{m}{2\pi \mathrm{i}\hbar \Delta t}\right]^{d/2} \exp\left[\frac{\mathrm{i}}{\hbar}\left(\frac{m}{2\Delta t}(x_b - x_a)^2 - \frac{\Delta t}{2}(V(x_a) + V(x_b))\right)\right]. \quad (6.5)$$

Here d is the dimensionality of the system. As was discussed before, if part of the dimensionality consists of multiple particles with different masses the above equation must be modified accordingly. This equation follows directly from operator factorization Eq. (2.12), and so, it becomes exact as $\Delta t \to 0$. Some physical intuition can be gained by comparing this with Eqs. (2.27) and (2.28) and noting that this

describes a particle or particles moving along a straight line with constant speed and in constant potential.

In Paper I the performance of Trotter kernel is tested and the fundamental problem associated with it in real time simulations is discussed. While the approximation is accurate only when Δt is small, this causes the integrand to become highly oscillatory which increases the numerical error in the Monte Carlo estimate. So, unlike in imaginary time, where decreasing time step systematically increases the accuracy of the result, in real time the best numerical result is achieved at some $\Delta t_{\text{optimal}}$, where the Trotter approximation is good enough and the numerical error from Monte Carlo integration is manageable.

One approach to improve this propagator is sc. semi-classical or WKB approximation [8, 16, 19], where the particle moves along the classical paths only. This approximation is exact for linear and quadratic potentials [8] and it has been claimed that the only propagators, for which we can find exact analytical form, are of this type [19]. For the semi-classical propagator all the classical trajectories connecting x_a and x_b in time Δt must be found. This is not trivial for most systems, such as for the Coulomb problem [29, 30]. Another semi-classical method is the sc. cellular dynamics [31], where the propagator is computed by dividing the phase space into small Gaussian cells where within each of the classical dynamics can be linearized and the resulting Gaussian integrals performed.

A different approach is to keep higher-order terms in Eq. (2.12) to reduce the error from non-zero time-step [25]. Other schemes include construction of effective non-oscillatory propagators [23] and calculating those numerically on a grid [24].

In Paper II we introduce a couple of simple improvements for the kinetic and potential part of the propagator. Looking at the form of Eq. (6.5) we see that the potential part is just the average of potentials in starting point and end point. Keeping the straight line path and constant speed we can replace this two point average with the actual average along that path

$$V_{\text{avg}} = \frac{1}{|\, x_b - x_a \,|} \int_{x_a}^{x_b} V(x) dx. \tag{6.6}$$

In one dimensional space for two particles this yields for the harmonic potential

$$V_{\rm avg}^{\rm H} = \frac{\omega^2}{6}\left[\frac{x_{1b}^3 - x_{1a}^3}{x_{1b} - x_{1a}} + \frac{x_{2b}^3 - x_{2a}^3}{x_{2b} - x_{2a}}\right] \tag{6.7}$$

and for the Coulomb potential

$$V_{\rm avg}^{\rm C} = \frac{\ln(r_b/r_a)}{r_b - r_a}, \tag{6.8}$$

where x_1 and x_2 are the particle coordinates, and $r_a = x_{1a} - x_{2a}$ and $r_b = x_{1b} - x_{2b}$ are the initial and final distances between the particles.

In numerical simulations the highly oscillatory nature of the propagator raises serious problems. This sign problem will be discussed more thoroughly later, but we will introduce here a method of smoothing the kinetic part of the propagator.

The kinetic part of the propagator is the free particle propagator, see Eq. (6.1) and related comments, and it tells us how delta functions evolve in time, see Eq. (2.35). When working in coordinate space the wave function can be thought of as a linear combination of Dirac delta functions

$$\psi(x) = \int_{-\infty}^{\infty} \psi(x')\delta(x' - x)\mathrm{d}x'. \tag{6.9}$$

In numerical simulations we have a finite number of grid points, so the representation of the wave function is always an approximation and using a finite number of δ-functions only, leads to numerical errors.

The initial wave function $\psi(x_a, t_a)$ presented pointwise in a grid of walkers can be "smoothened" to a "gaussianwise" presentation in the same grid by using Gaussian basis function with variance $\frac{\epsilon^2\hbar}{2m}$ [2], where ϵ must be small enough that the overlap of the Gaussians is not too large. The kinetic part in the propagator is now replaced by the well known time-evolution of Gaussian wavepacket [17, 32]

$$\left[\frac{m}{2\pi \mathrm{i}\hbar\Delta t}\right]^{d/2} \exp\left[\frac{\mathrm{i}}{\hbar}\frac{m}{2\Delta t}(x_b - x_a)^2\right] \rightarrow \left[\frac{m}{2\pi\hbar(\mathrm{i}\Delta t + \epsilon^2)}\right]^{d/2} \exp\left[\frac{\mathrm{i}}{\hbar}\frac{m}{2(\Delta t - \mathrm{i}\epsilon^2)}(x_b - x_a)^2\right], \tag{6.10}$$

which converges back to the pointwise presentation as $\epsilon \to 0$. It is interesting to note that mathematically this smoothening is equivalent with replacing Δt with $\Delta t - i\epsilon^2$ and this complex time corresponds to the physical system, where the initial state of the particle is not a pure state but a probabilistic mixture of them [33].

We could do the same modification for the potential part of the propagator, but as this would only play a role, when the potential energy becomes very large ($V(x) \sim \Delta x^2/\Delta t^2$) it is usually not needed. In the case of singular potential it could provide similar numerical stability.

Also, it should be noted that path integral algorithms allow easy parallel computing since we can compute each x_b separately and even do the sum over all x_a's as a sum of partial sums (or vice versa).

6.2 Numerical sign problem

When running Monte Carlo simulations in real time, at first, it might seem that the fermion sign problem does not manifest in a similar way as it does in imaginary time. We can calculate the wave function using Eq. (3.11) and then use Eq. (4.2) to calculate the expectation value of the desired observable. This is because in real time the phase factor can be separated from the wave function, see Eq. (3.11), and as the wave function is multiplied by its complex conjugate when calculating the expectation value, see Eq. (4.1), the phase factors will cancel out.

The problem with real time is that in Eq. (3.11) the Kernel is usually a highly oscillatory function as the time step Δt gets smaller. This can can be seen by the form of short time propagator of Eq. (6.5) and is illustrated in Fig. 6.1. This causes the variance and the error of Monte Carlo estimate to increase, until the error becomes as large as the value of the integral and the whole Monte Carlo estimate becomes meaningless. This problem is related to the ratio of the size of the positive and negative areas of the integrand, so that the closer they are in size, the worse the problem. This is emphasized when the dimensionality increases and even an integral of a function that is only mildly oscillatory in one dimension becomes exponentially harder to evaluate accurately with Monte Carlo technique [48]. That is why the improvements in the kernel, such as making it less oscillatory and more exact are so crucial in real time path integral calculations.

Intuitively it can be seen how both the fermion and numerical sign problem are

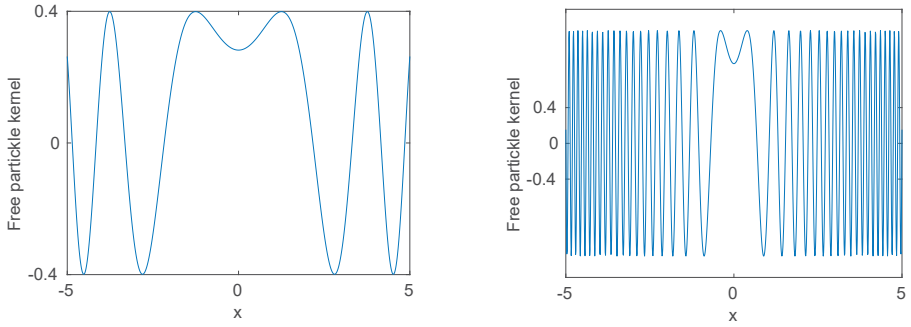

Figure 6.1 Real part of the free particle kernel for one dimensional electron in atomic units with $x_a = 0$, $\Delta t = 1$ (left) and $\Delta t = 0.1$ (right). Kernel is the probability amplitude for the electron to arrive at various distances x from the origin after a time Δt. Shorter wavelengths correspond to a higher classical momentum according to the de Broglie relation $\lambda = h/p$

manifestations of same phenomena. We are trying to calculate something that is very small by subtracting two large numbers, when the error in those numbers is proportional to the size of that number. This means that the error could be larger than the result we are trying to calculate.

So, in real time, instead of a fermion specific sign problem we have a sign problem that affects all systems, whether they are bosonic, eigenstates, dynamical, etc.

6.3 Incoherent propagation

In real time evolution, propagator and wave functions are complex valued functions with modulus and argument, latter of which we call phase in this context. The phase factor is the description of all the interference effects for the coherent propagation.

In Paper I we present the method of incoherent propagation, where we use real time propagation to find eigenstates of the system. Unlike the imaginary time DMC this method can be used also to find excited states and since it deals with static distributions we can use Metropolis Monte Carlo to find them.

The real-time solution of the wave Eq. (5.9) has the form

$$\psi(x,t) = \sum_{n=0}^{\infty} C_n \phi_n(x) \exp[-\frac{\mathrm{i}}{\hbar}(E_n - E_T)t], \tag{6.11}$$

analogously with the imaginary time solution of Eq. (5.11). By using the small angle approximation for short enough Δt the time evolution can be written [1] as

$$\psi(x,\Delta t) \approx \sum_{n=0}^{\infty} C_n \phi_n(x)\{1-[(E_n-E_T)\frac{\Delta t}{\hbar}]^2/2 - \mathrm{i}[(E_n-E_T)\frac{\Delta t}{\hbar}]\}. \qquad (6.12)$$

Now dropping off the imaginary part and keeping the real part of $\psi = \psi_R + \mathrm{i}\psi_I$, only, the single step time evolution leads to projection onto the real axis

$$\psi_{\mathrm{R}}(x,\Delta t) = \sum_{n=0}^{\infty} C_n \phi_n(x)\{1-[(E_n-E_T)\frac{\Delta t}{\hbar}]^2/2\}. \qquad (6.13)$$

Repetition of wave function projection onto its real part removes the coherent phase factor in every time step. Therefore, we call this iteration of Eqs. (2.34) and (6.13) as incoherent propagation or quantum Zeno propagation [49].

Now, it is easy to see that this incoherent propagation (iRTPI) converges to one of the real eigenstates of the system. The dominant term in the sum in (6.13) is the one, where $\mid E_n - E_T \mid$ is least. Therefore, the iterative incoherent propagation of $\psi_{\mathrm{R}}(x,t)$ will converge to the real eigenstate ϕ_k with eigenenergy E_k closest to E_T, unless the initial $\psi_{\mathrm{R}}(x,t)$ is orthogonal to ϕ_k ($C_k = 0$). However, even in such case we can expect the numerical inaccuracies to generate a small seed of any eigenstate ($C_k \neq 0$), and eventually, to lead to the expected convergence. In case of degeneracy it is to be expected that this procedure will find some superposition of the degenerate states.

This effect is demonstrated in Fig. 6.2, where the incoherent propagation simulation of a one dimensional harmonic oscillator starting from superposition of the 1st and 2nd excited states, first finds the first excited state but eventually falls to the ground state.

All the simulations in this thesis are done using atomic units, where $m = \hbar = a_0 = 1$, where a_0 is the Bohr radius and the unit of time is $(ma_0^2)/\hbar \approx 24$ as.

By writing the first terms of the Taylor series of Eq. (5.11)

$$\psi(x,\tau) = \sum_{n=0}^{\infty} C_n \phi_n(x)\{1-(E_n-E_T)\frac{\Delta t}{\hbar} + \frac{[(E_n-E_T)\frac{\Delta t}{\hbar}]^2}{2}\}. \qquad (6.14)$$

and comparing it to the (6.13) we see that the imaginary time propagation can con-

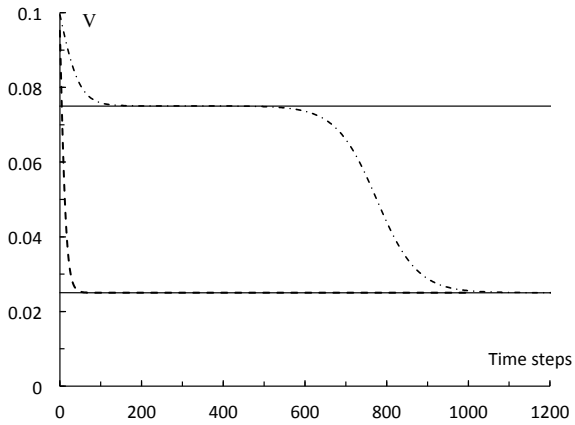

Figure 6.2 Incoherent time evolution of the superposition states to the ground state. Dashed line simulation starts from the superposition of the ground and 3rd excited state, whereas the dash dotted line starts from the superposition of the 1st and 2nd excited states. The calculated potential energy V, in atomic units, for each time step is shown. Solid lines show the potential energies of the ground and 1st excited states.

verge to the ground state of the system, only, while with the incoherent propagation E_T can be chosen arbitrarily to find any non-degenerate eigenstate ϕ_k. This is the benefit of iRTPI, when compared to DMC.

In a graphical interpretation of Eq. (6.13) the real wave function in a time step Δt rotates in complex plane clockwise an angle $(E_n - E_T)\Delta t/\hbar$, and then, becomes projected back to the real axis, walker by walker. The larger $(E_n - E_T)\Delta t$, the less of $\phi_n(x)$ contributes to the projection. The hypothetical problem arising from the 2π periodicity of the angle can be eliminated by changing, or in particular, decreasing the time step.

In Paper I we demonstrate the use of incoherent propagation and calculate ground states and some excited states of our test cases. As our target wave function is real, we use the Metropolis Monte Carlo method where the calculated wave function is used to guide the evolution of the walkers. In this way we have the wave function represented by the walker distribution, and also, by the values calculated for each walker. The advantage of this is, that it gives us a straightforward way to evaluate expectation values directly as can be seen from Eq. (4.2). We can also evaluate the total energy from the phase of the wave function before dropping the imaginary part, because we are finding the eigenstate for which it will be constant *i.e.*, the same for all walkers.

Table 6.1 Incoherent propagation in MC grid of the ODHO ground state with Trotter kernel. M is the number of walkers, Δt the time step, ΔV the deviations of expectation values of the potential energy from its exact value 0.025000 and σ the standard deviation of V from long simulations. All quantities are in atomic units.

M	Δt	$\Delta V/10^{-6}$	$\sigma/10^{-6}$
10^4	0.3	160	540
10^4	1	60	530
10^4	3	40	470
3×10^4	1	30	320

Using the short time approximation we find the potential energy with good accuracy. The table 6.1 will show the data for the one dimensional harmonic oscillator (ODHO).

6.4 Hooke's atom

Consider two electrons with Coulomb repulsion in a harmonic potential well. This system is called Hooke's atom. In atomic units $m=\hbar=a_0=1$, the Hamiltonian of the system is

$$H(x_1,x_2)=-\frac{1}{2}\nabla_1^2-\frac{1}{2}\nabla_2^2+\frac{1}{2}\omega^2x_1^2+\frac{1}{2}\omega^2x_2^2+\frac{1}{|x_1-x_2|}, \tag{6.15}$$

where x_1 and x_2 are the three coordinates of two electrons. The relative and center-of-mass (CM) motion of the electrons can now be separated by defining new three-dimensional variables

$$r=x_1-x_2 \qquad \text{and} \qquad R=\frac{x_1+x_2}{2} \tag{6.16}$$

Then, the Hamiltonian decouples as

$$H(r,R)=-\frac{1}{2\mu}\nabla_r^2+\frac{1}{2}\mu\omega^2r^2+\frac{1}{|r|}-\frac{1}{2M}\nabla_R^2+\frac{1}{2}M\omega^2R^2\equiv H_r+H_R, \tag{6.17}$$

where $\mu = \frac{1}{2}$ and $M = 2$ are the reduced and the total mass of the electrons. The six dimensional wave function and total energy separates as $\psi_6(r,R) = \phi_3(r)\Phi_3(R)$ and $E = E_r + E_R$, respectively.

The CM motion is simple harmonic oscillation, which, of course, can further be separated into three one-dimensional components. The relative motion of the two electrons is harmonic oscillation with the Coulomb repulsion as a perturbation. This equation can be separated into radial and angular components similarly to the dynamics of the hydrogen atom.

With substitution $\phi_1(r) = u(r)/r$ where r is now one dimensional the radial equation of ground state takes the form

$$[-\frac{1}{2\mu}\frac{\mathrm{d}^2}{\mathrm{d}r^2} + \frac{1}{2}\mu\omega^2 r^2 + \frac{1}{r}]\, u(r) = E_r\, u(r). \tag{6.18}$$

To find the exact solution we must solve a three step recurrence equation [50], whose solutions are restricted to some specific values of confinement parameters, only.

Oseguera and Llano [51] have proven that the singularity of the attractive one-dimensional Coulomb potential acts as an impenetrable barrier and the space becomes divided into two independent regions. This is called the space splitting effect. Therefore, the solutions for positive and negative parts of relative coordinates are completely independent. Due to the space spitting effect of the one dimensional Coulomb potential, the wave function of the two particles should vanish where their relative coordinate becomes zero.

As a consequence of this, the relative dynamics in one dimension is that of the radial part in three dimensions for the angular momentum quantum number $\ell = 0$, Eq. (6.18), [50]. With the definitions of r and R in Eq. (6.16), in one dimension

$$\psi(r,R) = u(r)\Phi(R), \tag{6.19}$$

where now $u(r)$ is the relative motion wave function in one dimension Eq. (6.18). It is related to the three-dimensional relative motion wave function with zero angular momentum via $r\phi(r) = u(r)$. In the one dimensional space the CM dynamics is simply that of one of the three R-components in Eq. (6.17).

In Papers II and III the incoherent propagation with the wave function guided walkers is applied to Hooke's atom and the strong correlation between electrons is examined. Again the method yields good accuracy for energetics, for both the

Table 6.2 Accuracy and distribution of ground state energetics of 1D Hooke's atom (ω = 0.5) from incoherent RTPI simulations of the ground state. M is the number of walkers ($\mathrm{k} = 10^3$), Δt the time step, ΔE deviation of expectation values from the exact value 1.5000, ΔV deviation of the expectation value from the exact value 1.0856..., σ standard deviation in 20 blocks of data with 50 iterations in block and ϵ^2 the "gaussian width of walkers" discussed in section 7.1. All quantities are in atomic units.

M	Δt	ΔE	σ_E	ΔV	σ_V	ϵ^2
100k	0.3	—0.0152	0.0008	0.0109	0.0017	0.005
100k	0.1	0.0032	0.0014	0.0039	0.0021	0.005
100k	0.03	0.0601	0.0135	0.0054	0.0014	0.005
30k	0.3	—0.0185	0.0016	0.0161	0.0042	0.005
30k	0.1	0.0046	0.0058	0.0172	0.0111	0.005
30k	0.03	0.1544	0.0333	0.0221	0.0247	0.005
10k	0.3	—0.0220	0.0030	0.0126	0.0062	0.005
10k	0.1	0.0077	0.0123	0.0296	0.0505	0.005
10k	0.03	0.4324	0.0653	0.0154	0.0045	0.005

ground and excited states. We also show how perturbation theory (PT) provides an accurate approach in the strong confinement regime. Tables 6.2 and 6.3 show the results of simulations with $\omega = 0.5$ and comparison with the exact value and value from pertubation theory, where available. ω is the angular frequency of the oscillator and for the chosen value exact results for the ground state can be found [50]

Using the Virial theorem for one dimensional harmonic oscillator, we have [52]

$$< T_{CM} >=< V_{H,CM} >= (n + \frac{1}{2})\frac{\hbar\omega}{2} \tag{6.20}$$

T_{CM} is the kinetic energy of center of mass motion and $V_{H,CM} = \frac{1}{2}M\omega^2R^2$ is the CM harmonic potential. Here, for $n = 1$ and $\omega = 0.5$ this gives $3/8 = 0.375$. Table 6.3 shows the RTPI, PT and analytical exact values (where available) for kinetic and potential energies of Hooke's atom. As one can see the results are in very good agreement with the exact solution.

The energetics of the second excited state is shown in the Table 6.4.

There is a systematic error arising from the short time approximation which is

Table 6.3 The first excited state ($\omega = 0.5$) and its expectation values. The first excited state is the combination of the first excited state of CM motion and ground state of relative motion. The expectation values of $T_r{}^*$ and $T_{CM}{}^*$ are calculated directly from normalized wave functions. Potential energy$^\dagger = V_c + V_{H,r} + V_{H,CM}$ and its components are calculated as RTPI output and total energy‡ is calculated (independent from potential and kinetic energies) directly from the phase of the wave function. The number of walkers M is 300k and Δt = 0.1.

	Exact value	RTPI	1^{st} order PT	2^{nd} order PT	3^{th} order PT
V_c	0.4474	0.4530(4) †	0.4354	0.4443	0.4466
$V_{H,r}$	0.5131	0.5117(1) †	0.5161	0.5218	0.5181
T_r	0.2894	0.2870(9) *	0.3028	0.2847	0.2861
$V_{H,CM}$	0.375	0.3722(1) †	0.375	0.375	0.375
T_{CM}	0.375	0.3765(15) *	0.375	0.375	0.375
Potential energy	1.3355	1.3369(3) *	1.3265	1.3412	1.3397
Total energy	2	1.9969(6) ‡	2.0043	2.0010	2.0009

Table 6.4 The second excited state ($\omega = 0.5$) and its energetics as in the Table 6.3. The second excited state is a combination of the CM ground state and the first excited state of relative motion. Analytical exact values for this state are not available. Notations are the same as in Table 6.3

	Exact value	RTPI	1^{st} order PT	2^{nd} order PT	3^{th} order PT
V_c	-	0.4234(9)†	0.4233	0.4074	0.4119
$V_{H,r}$	-	0.9811(9)†	0.9530	1.0074	1.0043
T_r	-	0.786(4) *	0.8159	0.7771	0.7753
$V_{H,CM}$	0.125	0.1620(3) †	0.125	0.125	0.125
T_{CM}	0.125	0.0986(7) *	0.125	0.125	0.125
Potential Energy	-	1.5665(6) *	1.5013	1.5399	1.5413
Total Energy	-	2.4331(2)‡	2.4423	2.4420	2.4417

largest near the singularity of the potential of Eq. 6.18) *i.e.*, where the two electrons come close to each other. Other errors come from the sparsity of the grid where the absolute value of the wave function is small and from the error of using Monte Carlo to calculate the highly oscillatory integral of Eq. (3.11). The effect of these errors on energy calculations is lessened by the fact that they all are most prominent in the areas where the absolute value of the wave function is small, and so, contribute relatively little to the value of the expectation value of Eq. (4.2).

This can be seen from the following snapshots of Monte Carlo simulation that show the error in phase for each walker, Figs. 6.3 - 6.5.

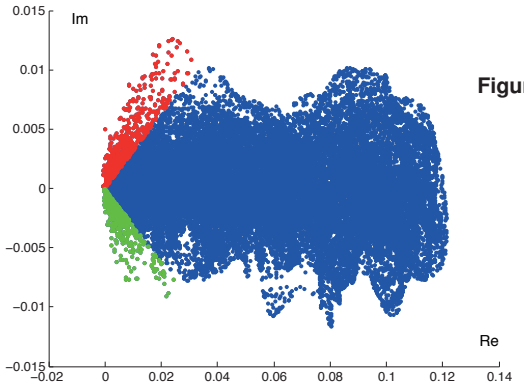

Figure 6.3 Snapshot of the complex wave function phase evolution in one time step. Color coding: red for $\Delta\varphi > 0.3$ and green for $\Delta\varphi < -0.3$. These values correspond to 20% of the known expectation value of energy. M = 30000, Δt = 0.1 and $\epsilon^2 = 0.005$.

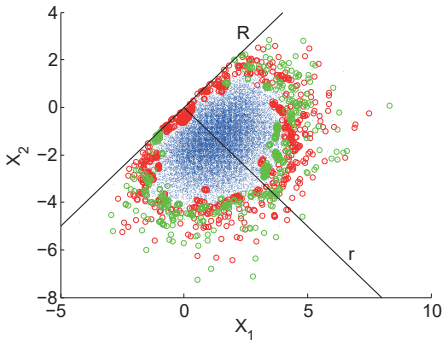

Figure 6.4 Complex wave function phase evolution of the real ground state after one time step in a plane of coordinates of electrons (x_1, x_2) in atomic units. Trial energy $E_T = 2$ is the exact value for the total energy, so the wave function is rotated back to the real axis ($\Delta\varphi = 0$ expected). The colors show which walkers are more than 20% off from the known expectation value of energy. Color coding: red for $\Delta\varphi > 0.3$ and green for $\Delta\varphi < -0.3$, size of blue and other walkers is smaller and larger, respectively. M = 30000, Δt = 0.1 and $\epsilon^2 = 0.005$. The CM and relative coordinate axes are also shown.

6.4.1 Coherent RTPI simulation of quantum dynamics

To test the time evolution of Hooke's atom, a short time pulse of spatially linear electric field (linear in space and Gaussian in time) has been considered as a perturbation. We chose the external potential as

$$U(x,t) = \frac{U_0}{\sqrt{\pi\alpha}} x \exp(-\frac{(t-t_0)^2}{\alpha}), \tag{6.21}$$

where $U_0 = 1, \alpha = 0.1$ and $t_0 = 1$, in atomic units.

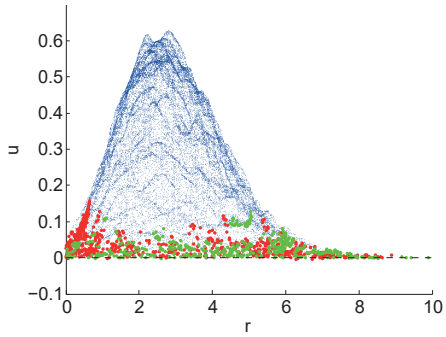

Figure 6.5 Snapshot of the calculated wave function in the relative motion coordinates with M = 30000, Δt = 0.1 and $\epsilon^2 = 0.005$. The units, the walkers and the color coding are the same as in the Fig. 6.4.

As can be seen from the potential energies in figure 6.6 the walker size ϵ affects the results much more than in incoherent propagation. Too large ϵ cuts out higher energy eigenstates and results in incorrect energies (blue line) and too small ϵ increases the incidental numerical error from the kinetic energy part of propagator (green line). That is expected as it cuts out higher energy eigenstates, which are not present in the simulation of lower eigenstates but contribute to the real time evolution. For the real-time dynamics ϵ must be chosen smaller than that for the optimal incoherent propagation [1, 2].

There is a delay in the system response to such an ultrafast transient process. It is due to the inertia of electrons. After the external pulse the total energy is conserved and the electrons remain in harmonic oscillation.

Figure (6.7) shows the different contributions to the potential energy. As expected, the Coulomb interaction remains unchanged during the time evolution, and the effects of the external electric field just appear in a short time interval.

6.4.2 RTPI extension to DMC

Now, we consider the conventional DMC and how RTPI can be used in conjunction with it. Since Hooke's atom does not involve attractive singular Coulomb potentials, but only $+\frac{1}{r}$, the Trotter break-up is valid and the branching term in Eq. (5.22) does not diverge. Therefore, the simple DMC can be expected to give accurate results with sufficiently small imaginary time time step and large enough number of walkers.

The data in Table 6.5 shows that the total energy converges to its exact value as

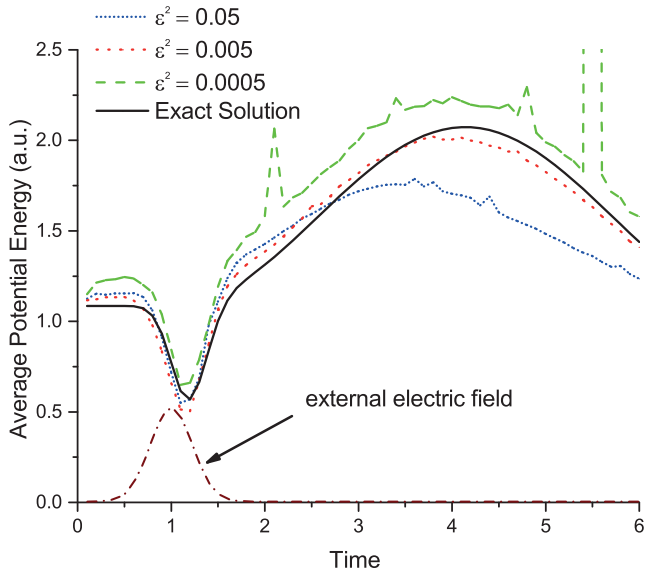

Figure 6.6 Potential energy in atomic units from one MC simulation $\Delta t = 0.1$ and $M = 100000$ with different walker size ϵ in atomic units. Blue short dot line $\epsilon^2 = 0.05$, red dot line $\epsilon^2 = 0.005$ and green dash line $\epsilon^2 = 0.0005$. The black solid line represents the exact solution.

the imaginary time step $\tau \to 0$. By comparing the RTPI data in Table 6.2 we see that with optimal parameters and the same number of walkers M, RTPI gives similar accuracy as simple DMC, if only the number of Monte Carlo steps matters.

However, RTPI is computationally much more demanding. This stems from the fact, that for each MC step in DMC algorithm, only M moves of walkers guided by the potential function is needed, but with the present incoherent RTPI we need to calculate $M \times M$ real time propagations to evaluate the guiding distribution before moving the walkers.

The expectation value of an observable, such as potential energy V, is

$$\langle V \rangle = \frac{\langle \psi \mid V \mid \psi \rangle}{\langle \psi \mid \psi \rangle}. \tag{6.22}$$

For direct sampling of the matrix elements, another representation of the wave function, ket or bra vector, is needed.

The simple DMC algorithm samples the nodeless ground state distribution, which makes it cumbersome and inefficient to evaluate expectation values for observables

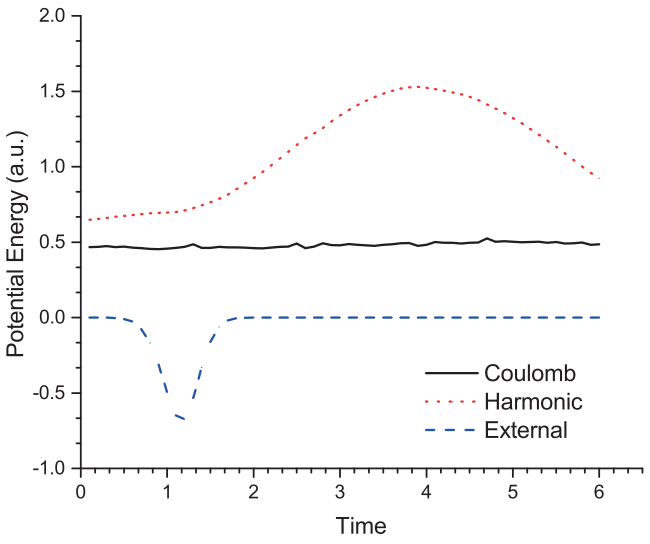

Figure 6.7 Contributions to the potential energy in atomic units from Coulombic (black solid line), harmonic (red dot line) and external potential (blue dash line) effects from one MC simulation with $M = 100000$ and $\epsilon^2 = 0.005$.

other than the total energy, even as simple as the potential energy. This is due to the availability of the wave function in form of walker distribution, only. Thus, in evaluation of the expectation value matrix elements the walker distribution implicitly contributes as one wave function, but the other one is not available.

For this purpose the incoherent RTPI on DMC walkers can be used. Similarly, expectation values of any local multiplicative operators become directly available. Also, another total energy estimate is obtained from the wave function phase evolution in real time.

Furthermore, the incoherent RTPI can be used to evaluate, not only the ground state, but also the excited states with the positive and negative amplitudes, and thus, it provides means for locating the nodal surfaces. We can combine the two approaches for evaluation of excited states, or in general, states with nodes in the spirit of released nodes idea [53]; RTPI would be used in finding the nodes and evaluating another wave function, as well as another total energy, while DMC is used to sample the walkers for RTPI.

In Table 6.6 we show the data evaluated with the combined approach, for the

Table 6.5 Accuracy and distribution of energetics in DMC simulations of the stationary ground state. Number of walkers is $M = 30\text{k}$, τ is the imaginary time step, ΔE deviation of the expectation value from its exact value 1.5000 and σ is the standard deviation of 20 blocks of data. Each block consists of 50 iterations. A new energy estimate was calculated after each block.

τ	ΔE	σ
1	—0.0526	0.0008
0.3	—0.0197	0.0016
0.1	—0.0096	0.0034
0.03	—0.0063	0.0049
0.01	—0.0041	0.0085
0.001	0.0137	0.0235

Table 6.6 Energetics of the one-dimensional Hooke's atom in ground state, calculated with incoherent RTPI combined with DMC. The walker distribution $M = 30k$ is sampled by DMC with ($\tau = 0.01$) and RTPI step length is $\Delta t = 0.1$. Evaluated expectation values and DMC total energy are given with their standard deviations. Notations are the same as in the previous Tables. DMC is calculated from 20 blocks of data with 50 iterations per block. RTPI step is run once for every other block.

	ΔE	σ_E	ΔV	σ_V	ϵ^2
RTPI	0.0033	0.0060	0.0022	0.0039	0.005
DMC	—0.0041	0.0085			

ground state of one-dimensional Hooke's atom. The underlying DMC has been run with $\tau = 0.01$, see Table 6.5 and RTPI on top of that with $\Delta t = 0.1$ with the optimal choice of other parameters, see above. RTPI step has been run once for every other block of 50 DMC steps.

We find that DMC sampling of walkers from the distribution derived from the potential function leads to smoother spatial distribution than that of guided by the wave function amplitude from RTPI. This can be seen by comparing the distributions in Figs. 6.4 and 6.8, and also, the amplitudes in Figs. 6.5 and 6.9. This also yields better energetics which can be seen by comparing the values from Tables. 6.2 and 6.6. In the latter one there are less stray walkers at very low density region. The reason for this is in the different nature of the guiding distribution: for DMC it is stable well-defined potential, while for the Metropolis algorithm in RTPI it is the

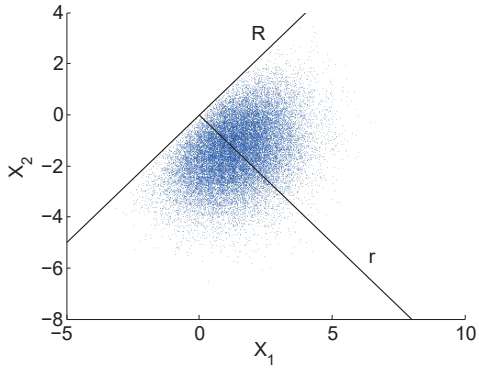

Figure 6.8 DMC simulation snapshot of walker distribution in a plane of coordinates of electrons (x_1, x_2) and separated coordinates (r, R), in atomic units. Parameters $\tau = 0.001$ and $M = 30000$ were used.

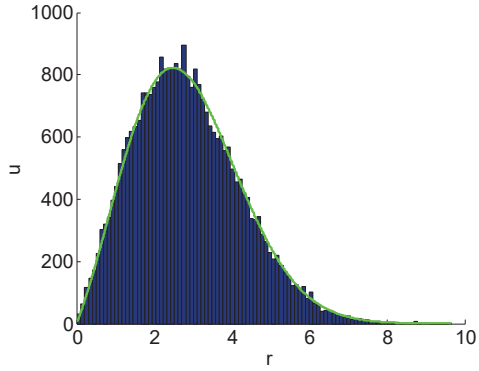

Figure 6.9 Snapshot histogram of walker distribution in DMC simulation with $\tau = 0.001$ and M = 30000. Green line is the analytical solution fitted to the data. u is the number of walkers in each bin and r is given in atomic units.

calculated amplitude presented in the Monte Carlo grid.

If more stability is needed and larger number of walkers becomes too expensive, it may be necessary to use cumulative distribution of the amplitude from several previous RTPI steps. According to our preliminary testing, the same type of problem may arise in locating the nodal surfaces accurately enough. Use of the cumulative distributions calls for numerical algorithms for efficient interpolation and updating the collected data.

6.5 Real time diffusion Monte Carlo

The DMC diffusion like procedure can be used directly to solve the integral in Eq. (5.12) but not that in Eq. (2.34) for ψ, because the kernel K, as a path integral, is a complex valued functional of interfering paths coupling all of the walkers. Thus, K can not be interpreted as a probability [23, 24, 61], and furthermore, it is delocalised with complex exponential tails oscillating in whole space, the more the shorter the time step Δt.

In Paper IV we introduce real time diffusion Monte Carlo method (RTDMC) with which we regain the probability interpretation of the propagator, and thus, we are able to use walker distributions to represent the whole complex wave function.

6.5.1 Separation of kernel

In RTDMC [4] method we separate the integrand in Eq. (2.34) into terms, which can be considered as "positive probabilities", and second, normalization is accomplished by restricting the space of integration. Similarly both the kernel $K \propto \exp(\mathrm{i}\phi)$ [8] and the wave function $\psi(a)$ at the right hand side of Eq. (2.34) are separated into four parts as

$$\begin{aligned} K(b,a) &= C\exp(\mathrm{i}\phi) = C\left[\cos(\phi)+\mathrm{i}\sin(\phi)\right] = C\left[\cos(\phi)+\mathrm{i}\cos(\frac{\pi}{2}-\phi)\right] \\ &= C\left[\cos^2(\frac{\phi}{2})-\sin^2(\frac{\phi}{2})+\mathrm{i}\left(\cos^2\left(\frac{\frac{\pi}{2}-\phi}{2}\right)-\sin^2\left(\frac{\frac{\pi}{2}-\phi}{2}\right)\right)\right] \\ &= K_+(b,a)-K_-(b,a)+\mathrm{i}K_{+\mathrm{i}}(b,a)-\mathrm{i}K_{-\mathrm{i}}(b,a) \end{aligned} \tag{6.23}$$

and

$$\psi(a) = \psi_+(a)-\psi_-(a)+\mathrm{i}\psi_{+\mathrm{i}}(a)-\mathrm{i}\psi_{-\mathrm{i}}(a). \tag{6.24}$$

This splits the integrand into 16 terms. Here C and ϕ are some functions of a and b, that can be chosen so that C is real and positive. Rearrangement of these terms

allows splitting the left hand side of (2.34) with the same principle as

$$\begin{aligned}
\psi_+(b) &= \int_a K_+\psi_+ dx_a + \int_a K_-\psi_- dx_a + \int_a K_{+i}\psi_{-\mathrm{i}} dx_a + \int_a K_{-i}\psi_{+\mathrm{i}} dx_a \\
\psi_-(b) &= \int_a K_+\psi_- dx_a + \int_a K_-\psi_+ dx_a + \int_a K_{+i}\psi_{+\mathrm{i}} dx_a + \int_a K_{-i}\psi_{-\mathrm{i}} dx_a \\
\psi_{+\mathrm{i}}(b) &= \int_a K_+\psi_{+\mathrm{i}} dx_a + \int_a K_-\psi_{-\mathrm{i}} dx_a + \int_a K_{+i}\psi_+ dx_a + \int_a K_{-i}\psi_- dx_a \\
\psi_{-\mathrm{i}}(b) &= \int_a K_+\psi_{-\mathrm{i}} dx_a + \int_a K_-\psi_{+\mathrm{i}} dx_a + \int_a K_{+i}\psi_- dx_a + \int_a K_{-i}\psi_+ dx_a,
\end{aligned} \tag{6.25}$$

each of which is everywhere real and positive. Here, all of the K_{sub} and ψ_{sub} on the right-hand side stand for $K_{\mathrm{sub}}(b,a)$ and $\psi_{\mathrm{sub}}(a)$, respectively, where $a = (x_a, t_a)$, $b = (x_b, t_b)$ and $\mathrm{sub} = \{+, -, +i, -i\}$. Thus, the complete wave function at the end of the time step $t = t_b - t_a$ can be written as

$$\psi(b) = \psi_+(b) - \psi_-(b) + \mathrm{i}\psi_{+\mathrm{i}}(b) - \mathrm{i}\psi_{-\mathrm{i}}(b). \tag{6.26}$$

The approach is reminiscent of an old DMC method of Arnow *et.al.* [55], where positive and negative walkers were used for the respective parts of the wave function. The main differences are the following. Here, we have four types of walkers and each walker generates all other types of walkers. Therefore, all parts of Eqs. (6.25) are coupled and unlike in DMC [55] they do not separately converge to the ground state, but instead, they can be used to simulate time evolution of the full complex time-dependent wave function.

In Eqs. (6.25), we have a fully delocalized piecewise everywhere positive probability density to sample, which first needs to be normalised. In case of a wave function localized in a finite domain it is known that the contributions to $\psi(b)$ in Eq. (6.26) cancel outside the domain and close to the domain boundaries inside. Thus, the partial probabilities of Eq. (6.23) can be normalized in a so chosen domain and diffusion localised in the domain, only, is considered. Inside the domain the evolution is not restricted and for example tunneling effects will be described accurately and without delay.

The four parts of the initial wave function $\psi(a)$ in Eq. (6.24) are presented with corresponding four sets of walkers. Neither real contributions $\psi_+(a)$ and $\psi_-(a)$ nor the imaginary contributions $\psi_{+i}(a)$ and $\psi_{-i}(a)$ should pairwise overlap as the

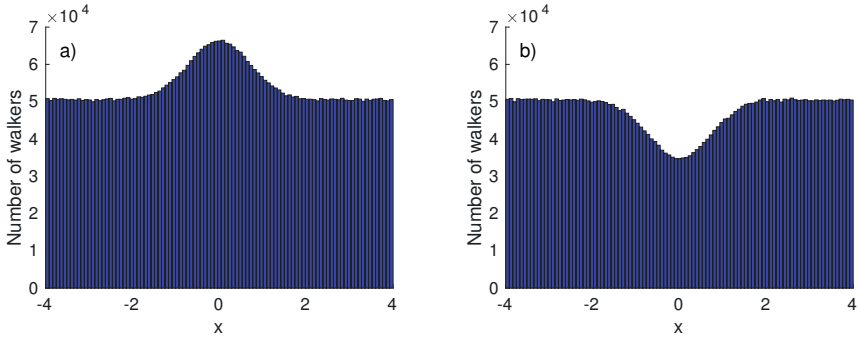

Figure 6.10 Distribution of a) positive and b) negative walkers ($\psi_+(b)$ and $\psi_-(b)$) after one time step $t = 0.1$ from gaussian real wave function $\psi_+(a)$ and $M(x_a) \approx 10^7$ walkers. Histogram bin width is 0.08. The complex components are not shown.

complex wave function should be single valued. Now, the real-time diffusion of these walkers according to the Eq. (6.25) results in four strongly delocalised and pairwise overlapping contributions, real $\psi_+(b)$ and $\psi_-(b)$, and imaginary $\psi_{+i}(b)$ and $\psi_{-i}(b)$. Then, the real and imaginary parts of the wave function are simply evaluated as the two sums of their positive and negative contributions. This means cancellation or pairwise annihilation of nearby walkers until the nodal surfaces between the positive and negative amplitudes appear. For the one dimensional case we define the walker touch parameter σ that determines the maximum distance at which pair of walkers with different signs will annihilate.

There is a large cancellation of walkers also in the box, *e.g.*, the wave function must vanish close to the domain boundaries, and similar strong cancellation turns out to dominate everywhere in the domain. In fact, it is only a small fraction of the generated walkers, which eventually remain presenting the wave function. Due to the massive cancellation of diffusing walkers all initial walkers need to be massively duplicated for each time step to maintain the total number of walkers.

A one-timestep real time diffusion is demonstrated in Fig. 6.10 and the numerical sign problem can be seen there, although it is only mild in this one dimensional case. The initial state is ODHO ground state gaussian real wave function, *i.e.*, $\psi(a) \equiv \psi_+(a)$. The real components $\psi_+(b)$ and $\psi_-(b)$ after propagation with the exact kernel (6.4) over a short time step t are shown. We see that most of the walkers will cancel out, leaving behind the initial real gaussian shape, but slightly scaled down. Similarly, the $\psi_{+i}(b)$ and $\psi_{-i}(b)$ after cancellation result in a small negative gaussian shape for the imaginary part, as expected, not shown in Fig. 6.10. This corresponds

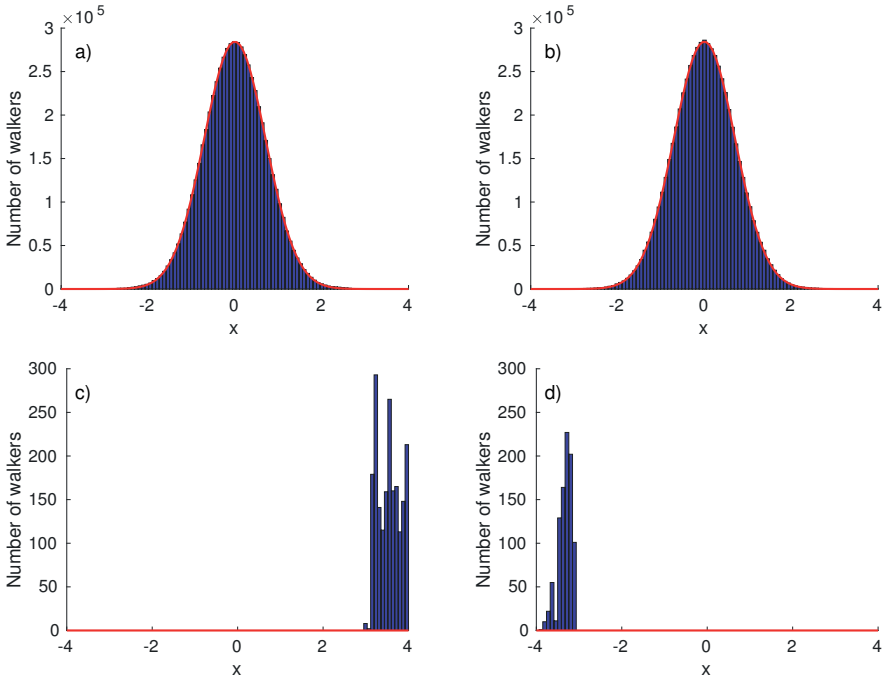

Figure 6.11 Distribution of walkers after the first time step, $\Delta t = \pi/4$, from the positive real ground state $\psi_+(a)$ of ODHO, followed by cancellation. All four components of the wave function are presented: a) positive real ($M \approx 6.27 \times 10^7$), b) negative imaginary ($M \approx 6.26 \times 10^7$), c) negative real ($M \approx 2.0 \times 10^3$) and d) positive imaginary ($M \approx 0.9 \times 10^3$) walkers. Note the different scaling of the vertical axes of the latter two. Red solid line is the properly normalized exact wave function and same normalization is used for all components. Notations are the same as in Fig. 6.10.

to rotation of the wave function from the real axis clockwise with a small angle, which is interpreted as multiplication with the phase factor $\mathrm{e}^{-iEt/\hbar}$.

6.5.2 Quantum dynamics

Even though all parts of the wave function in Eq. 6.24 are positive and real, the propagation is fully coherent and produces exact time evolution within numerical accuracy.

Dynamics of a particle in the potential $V(x) = \frac{1}{2}m\omega^2 x^2$ with $\omega = 2$ is shown in Figs. 6.11 and 6.12. Now, $\omega = 2$ corresponds to relatively strong confinement.

For the stationary ground state dynamics ($E = 1$), in each time step we expect to see the rotation of the phase factor $\exp(-iE\Delta t/\hbar) = \exp(-i\Delta t)$, only, without any

change in the absolute value of the wave function. Thus, the dynamics is expected to be simple oscillation of the real and imaginary parts of the ground state wave function in a phase difference of $\pi/2$. The initial phase is chosen to be zero at $t_0 = 0$, *i.e.*, $\psi(0) = \psi_+(a)$ as before. We start with $M(a) = 10^7$ and run the simulation with the exact kernel (6.3), time steps $\Delta t = \pi/4$ and duplicating walkers in x_a enough so that after the cancellation $M(b) \geq M(0)$. Fig. 6.11 shows the distribution of remaining walkers after the first time step, $t = \pi/4$. Time step can be chosen relatively large, since we are working with the exact kernel.

As expected, we find the same copy of the starting gaussian as the positive real and imaginary parts and small remnants of incomplete cancellation in both opposite sign parts, as a numerical error. Here, with the walker touch parameter $\delta = 0.01$, the remaining opposite sign walkers are less than the proper walkers with a factor smaller than 10^{-4}. Thus, the cancellation is almost perfect.

In Fig. 6.12 we show the negative imaginary part of the wave function from further simulation, at times $t = \pi/4,\ 2\pi/4,\ 3\pi/4$, and $4\pi/4$. Clearly, the evolution is correct and at $t = \pi$ the wave function is purely real and negative with zero imaginary contribution.

6.5.3 Observables and eigenenergies

Evaluation of transient expectation values of local operators, like multiplicative potential energy faces the same problem with RTDMC as it does with the conventional DMC, the wave function is given by the walker density, only. Application of operators on the wave function or even finding the square of the wave function $\psi^*\psi$ numerically is not straightforward. In sec. 6.4.2 we have demonstrated, that for DMC one can easily evaluate the complex valued wave function of the system at each DMC walker by using our direct real time path integral (RTPI) approach [1]. The RTPI time step is heavy to calculate, and therefore, could be restricted only to a few DMC iteration steps, where needed.

Now, the RTPI can be used together with RTDMC, similarly as with DMC, where the wave function is purely real or imaginary. This becomes relevant and useful with eigenstates and incoherent dynamics, as discussed in the next section.

With the eigenstates we should be able to monitor the phase factor of the wave function to find the corresponding eigenenergies. Now, we cannot evaluate the local

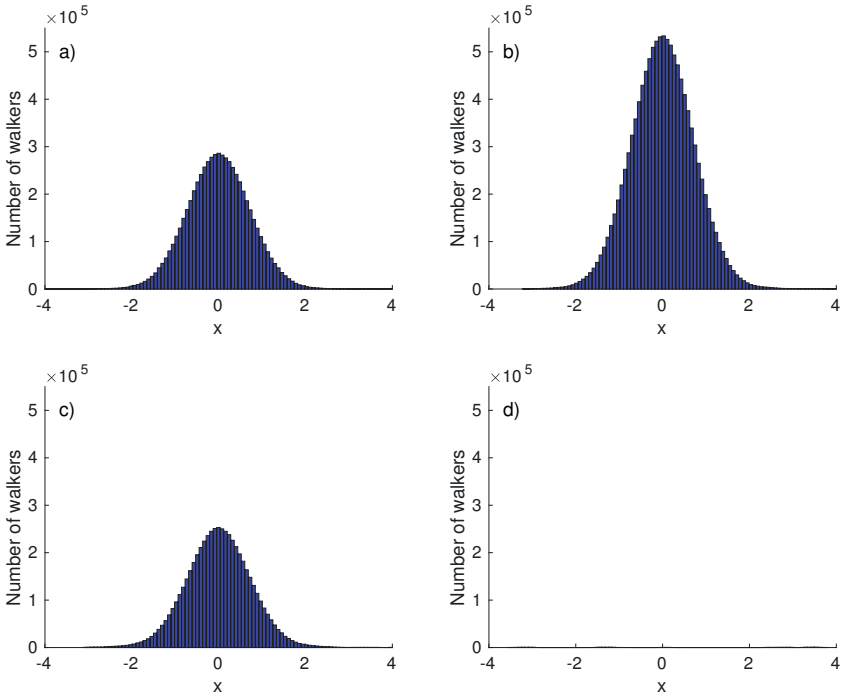

Figure 6.12 Distribution of negative imaginary walkers at a) $t = \pi/4$, b) $t = 2\pi/4$, c) $t = 3\pi/4$ and d) $t = 4\pi/4$ in the dynamics started in Fig. (6.11). Notations are the same as in Fig. 6.11.

energy for each walker as can be done with RTPI [1]. However, we can evaluate the change in the ratio of the number of real and imaginary walkers to approximate the average collective change in the phase factor. Thus, for the eigenenergy we write [4]

$$E = -\frac{\theta\hbar}{\Delta t} = -\tan^{-1}\left(\frac{\psi_{\mathrm{Im}}}{\psi_{\mathrm{Re}}}\right)\frac{\hbar}{\Delta t} \approx \tan^{-1}\left(\frac{M(x_{\mp i})}{M(x_{\pm})}\right)\frac{\hbar}{\Delta t}. \tag{6.27}$$

For this to be accurate the time step should be short enough that the phase angle θ is small, but also, the ratio $M(x_{\mp i})/M(x_{\pm})$ should be close to one so that the noise effect is minimised. Furthermore, one should keep track of the quadrants of the complex plane and corresponding changes of sign, where relevant.

If the wave function is not that of an eigenstate but a superposition, for a short time step and small angle we can approximate

$$-\frac{\theta\hbar}{\Delta t} = -\tan^{-1}\left(\frac{\sum_i c_i \sin(\theta_i)}{\sum_i c_i \cos(\theta_i)}\right)\frac{\hbar}{\Delta t} \approx -\tan^{-1}\left(\frac{\sum_i c_i\theta_i}{\sum_i c_i}\right)\frac{\hbar}{\Delta t} \approx \frac{\sum_i c_i E_i}{\sum_i c_i} = E \tag{6.28}$$

where the sum goes over the eigenstates with contributions c_i.

6.5.4 Excited eigenstates

The imaginary time DMC simulation converges to the lowest eigenstate (ground state) by adjusting the potential zero reference parameter E_T in Eq. (5.22) to the lowest eigenvalue. The convergence is usually unstable and needs continuous regulation with E_T. In section 6.3, we have shown that the incoherent propagation of real time path integral dynamics RTPI drives the system to an eigenstate, which is closest to the zero reference of the potential energy [1]. Furthermore, the convergence is stable and does not need careful adjustment of potential zero reference.

Here too, we can insert the zero reference parameter E_T into the Eq. (6.5) and use it to choose the energy, for which we want to find the closest excited state. Also, we can scan the parameter E_T to find all eigenstates within a given range.

Fig. 6.13 shows a superposition of walkers of the ODHO real ground state and those of the real first excited state. We see that representation of the superposition is not unique, as there are overlapping negative and positive parts of the wave function. Here we demonstrate, that the cancellation of the walkers with different sign is not mandatory for the correct propagation, but if this is not done, after couple of time steps the relevant information will be lost in the "noise" of positive and negative walkers.

Fig. 6.14 shows the energetics of RTDMC simulation starting with this initial wave function and run 100 time steps of length $\Delta t = 0.1$ with $M = 10^6$ walkers. The zero reference is set as $E_T = 0$. The exact value $E = 1.0000$ is expected. It can be seen that the convergence has been achieved in about 60 time steps to about $E = 1.1$. Thus, there is some systematic error left, which we trace coming from the short time step. With a too short time step false positive imaginary walkers appear, although all correct imaginary contribution should be negative. This seems to relate also with the size of the domain, 8 atomic units. Now, increasing the time step to $\Delta t = 0.8$ after 100 steps improves the energy estimate as clearly seen in the last ten time steps. Then, the energy estimate from simulation is 0.9974 ± 0.0030 (2 SEM).

The first excited state can be found by using the incoherent propagation and starting from the same initial superposition state shown in Fig. 6.13. Now, the potential zero reference is set as $E_T = 2.5$ and we expect to find the eigenenergy of 3.

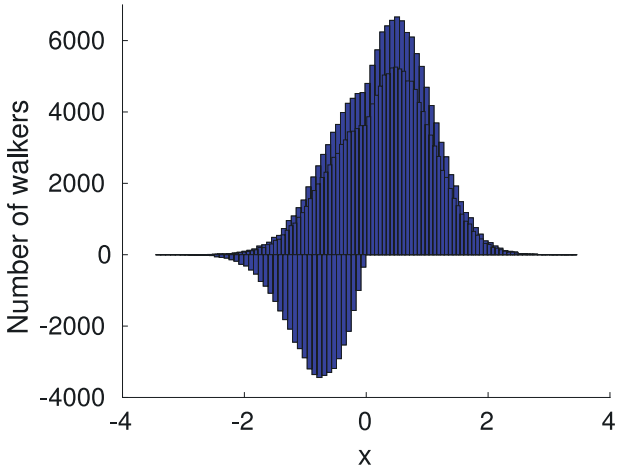

Figure 6.13 Positive ($M = 150 \times 10^3$) and negative walkers ($M = 50 \times 10^3$) of the superposition of ODHO 1st excited and the ground state ($M = 100 \times 10^3$ each). Other notations are the same as in above figures.

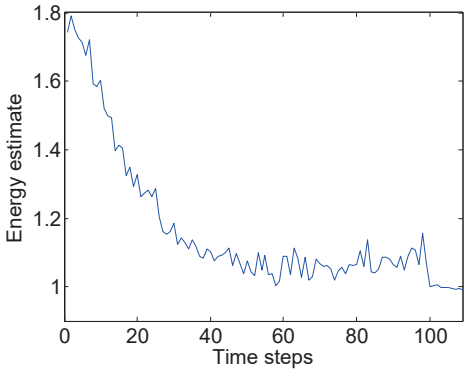

Figure 6.14 Estimated energy that demonstrates convergence starting from the superposition of the ODHO 1st excited state and ground state in incoherent RTDMC ending to the ground state. The exact ground state eigenenergy is one, $E = 1.0000$. $M \approx 10^6$, and $\Delta t = 0.1$ for the first 100 time steps and then $\Delta t = 0.8$.

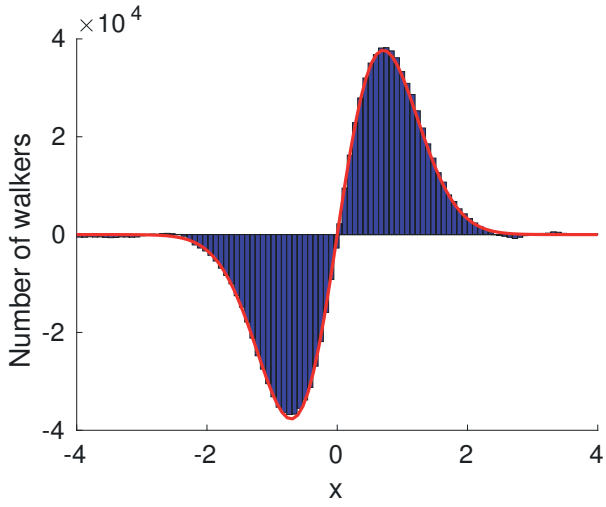

Figure 6.15 Distribution of positive ($M \approx 0.57 \times 10^6$) and negative ($M \approx 0.56 \times 10^6$) real walkers after the system has converged to its 1st excited state. Red solid line is the properly normalized exact wave function.

By using a time step $\Delta t = \pi/12$ the first excited state is found as shown in Fig. 6.15 and the eigenenergy becomes as 3.0199 ± 0.0076 (2 SEM). Fig. 6.15 shows the distribution of walkers after 100 timesteps to the convergence. As the figure shows, the node of the wave function is clear and sharp. By fitting to the histogram we get 0.0191, which is close to the exact value of 0.0000.

This approach may be one of the practical ways to locate nodal surfaces for other QMC methods like DMC, and thus, give help in finding the practical solutions to the fermion sign problem.

7 CONCLUSIONS

We have shown how our novel RTPI methods can be used for electronic structure calculations. Real time calculations are computationally laborious, as are most methods that use space and time as basis, but they include correlations between particles exactly, within numerical accuracy and they are easy to parallelize. Monte Carlo integration can be used to alleviate the sc. "curse of dimensionality". Irregular Monte Carlo grid is also free from artificial diffraction patterns of paths that may arise when using regular grids.

Use of the Trotter kernel, which is practical in imaginary time simulations, suffers from numerical errors from evaluation of highly oscillatory complex integral in real time simulations. Increasing the length of the time step will reduce this, but it increases the systematic error from the short time approximation used in derivation of this kernel. By increasing the number of walkers, shorter time steps can be evaluated accurately. In simulations of the actual dynamics of the system, these errors may accumulate, and if this is the case, only events over relatively short times can be simulated accurately. Improving the propagator from a physical point of view allows use of larger time steps and smoothening techniques decrease the numerical instability. If the exact kernel is known or can be calculated numerically, time steps of any lengths can be performed and the aforesaid issues do not appear.

Incoherent propagation method is a novel approach using real time propagator for searching the stationary states. It can be used to find the excited states, unlike the conventional diffusion Monte Carlo, which is restricted to the ground state. Another advantage is that it provides one with the wave function explicitly, and thus, evaluation of local multiplicative expectation values becomes straightforward.

It is also shown here, that this can be used in combination with conventional diffusion Monte Carlo, where the latter is used to move the walkers and the former to provide the value of the wave function on these walkers. Another novel technique, how combining the two methods could prove advantageous, is to use incoherent

propagation to find the nodal surfaces related to the excited states, that can then be used in conventional Diffusion Monte Carlo simulations.

If using calculated wave function to guide the evolution of the walkers, the errors from each time step may accumulate. This effect can be reduced if we find some way of driving the walkers that is independent of the accrued errors.

With the novel real-time diffusion Monte Carlo method we show how the complex valued kernel can be separated into real, positive and normalizable components, that can be interpreted as probabilities to drive the walkers. It incorporates the essential features of the conventional imaginary time diffusion Monte Carlo method. In addition, we can also find the excited states and the wave function nodes with incoherent propagation, and simulate proper dynamics of the system with coherent propagation.

In future, the methods presented here are to be applied to higher dimensional systems where the increase of configuration space presents its own challenges. Also, even though repulsive Coulomb potential was studied with Hooke's atom, attractive case needs more considerations. There particles tend to cluster and so paths where the potential energy and its gradient are large will become more relevant and the Trotter approximation becomes less accurate.

REFERENCES

[1] I. Ruokosenmäki and T. T. Rantala. Numerical Path Integral Approach to Quantum Dynamics and Stationary Quantum States. *Communications in Computational Physics* 18 (2015), 91–103. DOI: 10.4208/cicp.180914.161214a.

[2] I. Ruokosenmäki, H. Gholizade, I. Kylänpää and T. T. Rantala. Numerical Path Integral Solution to Strong Coulomb Correlation in One Dimensional Hooke's Atom. *Computer Physics Communications* 210 (2017), 45–53. DOI: 10.1016/j.cpc.2016.09.012.

[3] H. Gholizadehkalkhoran, I. Ruokosenmäki and T. T. Rantala. Eigenstates and Dynamics of Hooke's Atom: Exact Results and Path Integral Simulations. *Journal of Mathematical Physics* 59 (2018). DOI: 10.1063/1.5028503.

[4] I. Ruokosenmäki and T. T. Rantala. Real-Time Diffusion Monte Carlo Method. *Communications in Computational Physics* 25 (2019), 347–360. DOI: 10.4208/cicp.OA-2018-0048.

[5] D. Hanneke, S. Fogwell and G. Gabrielse. New measurement of the electron magnetic moment and the fine structure constant. *Physical Review Letters* 100 (2008), 120801.

[6] T. Aoyama, M. Hayakawa, T. Kinoshita and M. Nio. Tenth-order electron anomalous magnetic moment: Contribution of diagrams without closed lepton loops. *Physical Review D* 91 (2015), 033006.

[7] J. von Neumann. *Mathematische Grundlagen der Quantenmechanik*. Springer-Verlag, 1932.

[8] R. P. Feynman and A. R. Hibbs. *Quantum Mechanics and Path Integrals*. McGraw-Hill, New York, 1965.

[9] R. P. Feynman. Space-time approach to non-relativistic quantum mechanics. *Review of Modern Physics* 20 (1948), 367.

[10] D. R. Hartree and W. Hartree. Self-consistent field, with exchange, for beryllium. *Proceedings of the Royal Society A* 150 (1935), 869.

[11] P. Hohenberg and W. Kohn. Inhomogeneous Electron Gas. *Physical Review* 136 (1964), B864.

[12] W. Kohn and L. J. Sham. Self-Consistent Equations including Exchange and Correlation Effects. *Physical Review* 140 (1965), A1133–A1138.

[13] P. Atkins and R. Friedman. *Molecular Quantum Mechanics*. 4th ed. Oxford University Press Inc., 2005.

[14] B. L. Hammond, W. A. Lester Jr. and P. J. Reynolds. *Monte Carlo Methods in Ab initio Quantum Chemistry*. World Scientific, 1994.

[15] D. M. Ceperley. Path integrals in the theory of condensed helium. *Reviews of Modern Physics* 67 (1995), 279.

[16] H. Kleinert. *Path Integrals in Quantum Mechanics, Statistics, Polymer Physics, and Financial Markets*. 3rd ed. World Scientific Publishing Co., 2004.

[17] S. Gasiorowicz. *Quantum Physics*. 3rd ed. Wiley, 2003.

[18] T. W. B. Kibble and F. H. Berkshire. *Classical Mechanics*. 5th ed. Imperial College Press, 2004.

[19] L. S. Schulman. *Techniques and Applications of Path Integration*. Dover Publications, 2005.

[20] S. Bochner and K.Chandrasekharan. *Fourier Transforms*. Princeton University Press, 1949.

[21] L. S. Brown and Y. Zhang. Path-Integral for the motion of a particle in a linear potential. *American Journal of Physics* 62 (1994), 806–808.

[22] N. S. Thornber and E. F. Taylor. Propagator for the simple harmonic oscillator. *American Journal of Physics* 66 (1998), 1022–1024.

[23] N. Makri. Feynman path integration in quantum dynamics. *Computer Physics Communications* 63 (1991), 389–414.

[24] N. Makri. Improved Feynman propagators on a grid and non-adiabatic corrections within the path integral framework. *Chemistry Letters* 193 (1992), 435–445.

[25] M. Suzuki. Hybrid exponential product formulas for unbounded operators with possible applications to Monte Carlo simulations. *Physics Letters A* 201 (1995), 425–428.

[26] C. J. Umrigar, M. P. Nightingale and K. J. Runge. A diffusion Monte Carlo algorithm with very small time-step errors. *The Journal of Chemical Physics* 99 (1993), 2865.

[27] D. M. Ceperley. Fermion nodes. *Journal of Statistical Physics* 63 (1991), 1237.

[28] N. M. Tubman, I. Kylänpää, S. Hammes-Schiffer and D. M. Ceperley. Beyond the Born-Oppenheimer approximation with quantum Monte Carlo methods. *Physical Review A* 90 (2014), 042507.

[29] S. M. Blinder. Two-point characteristic function for the Kepler-Coulomb problem. *Journal of Mathematical Physics* 16 (1975), 2000.

[30] S. M. Blinder. Semiclassical approximation for the nonrelativistic Coulomb propagator. *Journal of Mathematical Physics* 52 (1984), 1771.

[31] E. J. Heller. Cellular dynamics: A new semiclassical approach to time-dependent quantum mechanics. *The Journal of Chemical Physics* 94 (1991), 2723–2729.

[32] S. M. Blinder. Evolution of a Gaussian wavepacket. *American Journal of Physics* 36 (1968), 525.

[33] G. Stefanucci and R. van Leeuwen. *Nonequilibrium Many-Body Theory of Quantum Systems*. Cambridge University Press, 2013.

[34] Planck Collaboration et al. Cosmological parameters. *Astronomy&Astrophysics* 594 (2016), A13.

[35] W. Kohn. *Nobel lecture*. 1999.

[36] F. James. Monte Carlo theory and practice. *Reports on Progress in Physics* 43 (1980), 1145–1189.

[37] N. J. Giordano and H. Nakanishi. *Computational Physicss*. 2nd ed. Pearson Prentice Hall, 2006.

[38] J. Thijssen. *Computational Physics*. 2nd ed. Cambridge University Press, 2007.

[39] G. Steinbrecher and W. T. Shaw. Quantile mechanics. *European Journal of Applied Mathematics* 19 (2008), 87–112.

[40] N. Metropolis, A. W. Rosenbluth, M. N. Rosenbluth, A. H. teller and E. Teller. Equation of state calculations by fast computing machines. *The Journal of Chemical Physics* 21 (1953), 1087.

[41] D. V. Schroeder. *An Introduction to Thermal Physics*. Addison Wesley Longman, 2000.

[42] M. Troyer and U.-J. Wiese. Computational complexity and fundamental limitations to fermionic quantum Monte Carlo simulations. *Physical Review Letters* 94 (2005), 170201.

[43] S. Chandrasekharan and U.-J. Wiese. Meron-cluster solution of fermion Sign problems. *Physical Review Letters* 83 (1999), 3116–3119.

[44] G. Aarts. Can stochastic quantization evade the sign problem? The relativistic Bose gas at finite chemical potential. *Physical Review Letters* 102 (2009), 131601.

[45] Z.-X. Li, Y.-F. Jiang and H. Yao. Majorana-time-reversal symmetries: A fundamental principle for sign-problem-free quantum Monte Carlo simulations. *Physical Review Letters* 117 (2016), 267002.

[46] I. Kylänpää. First-principles Finite Temperature Electronic Structure of Some Small Molecules. PhD thesis. Tampere University of Technology, 2011.

[47] J. Tiihonen. Thermal Effects in Atomic and Molecular Polarizabilities with Path Integral Monte Carlo. PhD thesis. Tampere University, 2019.

[48] N. Makri. Information guided noise reduction for Monte Carlo integration of oscillatory functions. *Chemical Physics Letters* 400 (2004), 446–452.

[49] B. Misra and E. C. G. Sudarshan. The Zeno's paradox in quantum theory. *Journal of Mathematical Physics* 18 (1977), 756.

[50] M. Taut. Two electrons in an external oscillator potential: Particular analytic solutions of a Coulomb correlation problem. *Physical Review A* 48 (1993), 3561.

[51] U. Oseguera and M. de Llano. Two singular potentials: The space splitting effect. *Journal of Mathematical Physics* 34 (1993), 4575.

[52] L. D. Landau and E. Lifshitz. *Quantum Mechanics: Non-Relativistic Theory*. Elsevier, 1981.

[53] D. Ceperley and B. J. Alder. Quantum Monte Carlo for molecules: Green's function and nodal release. *The Journal of Chemical Physics* 81 (1984), 5833–44.

[54] M. H. Kalos, D. Levesque and L. Verlet. Helium at zero temperature with hard-sphere and other forces. *Physical Review A* 9 (1974), 2178.

[55] D. M. Arnow, M. H. Kalos, M. A. Lee and K. E. Schmidt. Green's function Monte Carlo for few fermion problems. *The Journal of Chemical Physics* 77 (1982), 5562.

[56] D. M. Ceperley. Path Integral Monte Carlo Methods for Fermions. Ed. by K. Binder and G. Ciccotti. Editrice Compositori, 1996.

[57] J. B. Anderson, C. A. Traynor and B. M. Boghosian. Quantum chemistry by random walk: Exact treatment of many-electron systems. *The Journal Of Chemical Physics* 1991 (1995), 7418–7425.

[58] K. E. Riley and J. B. Anderson. Higher accuracy quantum Monte Carlo calculations of the barrier for the H+H_2. *The Journal Of Chemical Physics* 118 (2003), 3437–3438.

[59] J. B. Anderson. "Exact" quantum Monte Carlo calculations of the barrier for the H+H_2 reaction at the sub-microhartree level. *The Journal Of Chemical Physics* 144 (2016), 166101.

[60] M. H. Kalos and F. Pederiva. Exact Monte Carlo method for continuum fermion systems. *Physical Review Letters* 85 (2000), 3547.

[61] T. D. Kieu and C. J. Griffin. Monte Carlo simulations with indefinite and complex-valued measures. *Physical Review E* 49 (1994), 3855–3859.

PUBLICATIONS

PUBLICATION

I

Numerical Path Integral Approach to Quantum Dynamics and Stationary Quantum States

I. Ruokosenmäki and T. T. Rantala

Communications in Computational Physics 18.(2015), 91–103
DOI: 10.4208/cicp.180914.161214a

Commun. Comput. Phys.
doi: 10.4208/cicp.180914.161214a

Vol. **18**, No. 1, pp. 91-103
July 2015

Numerical Path Integral Approach to Quantum Dynamics and Stationary Quantum States

Ilkka Ruokosenmäki and Tapio T. Rantala*

Department of Physics, Tampere University of Technology, Finland.

Communicated by Michel A. Van Hove

Received 18 September 2014; Accepted (in revised version) 16 December 2014

Abstract. Applicability of Feynman path integral approach to numerical simulations of quantum dynamics of an electron in real time domain is examined. Coherent quantum dynamics is demonstrated with one dimensional test cases (quantum dot models) and performance of the Trotter kernel as compared with the exact kernels is tested. Also, a novel approach for finding the ground state and other stationary sates is presented. This is based on the incoherent propagation in real time. For both approaches the Monte Carlo grid and sampling are tested and compared with regular grids and sampling. We asses the numerical prerequisites for all of the above.

AMS subject classifications: 81-08, 65R20

PACS: 71.15.-m, 31.15.X-, 73.21.-b

Key words: Path integral, real time domain, quantum dynamics, incoherent propagation, stationary states.

1 Introduction

Feynman path integral (PI) approach offers an intuitively welcome description of non-relativistic quantum mechanics [1, 2], where classical mechanics emerges transparently from disappearing wave nature of particles along with vanishing Planck constant. In PI approach the presentation of the quantum dynamics with a propagator also in stationary quantum states is transparent, in contrast with the conventional approaches, where time evolution is seen in the phase factor, only. However, working out analytical or computational solutions to practical problems becomes more demanding with PI [3, 4], and obviously, this is one of the main reasons for path integrals not being a popular choice for considering quantum dynamics, not to mention the stationary quantum states.

*Corresponding author. *Email addresses:* Ilkka.Ruokosenmaki@tut.fi (I .Ruokosenmäki), Tapio.Rantala@tut.fi (T. T. Rantala)

For the above reasons the dynamical phenomena in nonrelativistic quantum mechanics are conventionally considered by searching or simulating solutions to the time dependent Schrödinger equation. This is almost trivial for a single particle, but becomes laborious and needs a number of approximations with growing complexity in a many-body system. In contrast, with PI the many-body interactions are included transparently and exactly within numerical accuracy. Often, the PI approach is implemented with a stochastic sampling of paths or by analytical formulations like the Kleinert's variational perturbation theory [5].

Out of other approaches than the present, it is worth mentioning the path integral Monte Carlo (PIMC), which has proven to be successful in simulations of periodic imaginary time propagation of many-particle systems, which leads to the finite temperature equilibrium statistical physics description of the many-particle system in terms of mixed state density matrix [6, 7]. By treating all particles with the same PIMC approach it is possible to evaluate the finite temperature electronic structure with exact account of many-body effects and beyond Born–Oppenheimer approximation as demonstrated, already [8,9]. PIMC is also robust enough to be used in various applications in nanoscience [10, 11].

Beyond the analytical solutions to stationary states or quantum dynamics, which are very few [3, 4, 12, 13], numerical simulation of coherent real time propagation faces substantial challenges related to the interference of paths: how to choose or sample the relevant paths in a balanced way, *i.e.* weighting the ones with most contribution through constructive interference and avoiding waste of efforts to those with negligible contribution due to destructive interference. In practice, time evolution of the complex many-body wave function in a space with high number of dimensions leads to even higher dimensional path integrals, which obviously can be sampled efficiently with the Monte Carlo technique, only. There, the interference related slow convergence has been called as "numerical sign problem" [12, 13] or phase (sign) problem. Sophisticated "stationary phase weighting" methods have been developed to overcome this without Monte Carlo technique [14, 15].

There are still no preferable solutions to these problems, although many approaches and approximations for certain types of systems have been found [16, 17]. Basically these methods rely on effective propagators [18] with desired properties. They are relatively well behaving and use the advantageous features of the PI formalism, *e.g.*, reduction of the total system into two parts: the lower dimensional system of interest and the effect of an environment modeled with an influence functional [1]. Often, the effect of the environment can be approximated classically, leaving only a lower dimensional system to be inspected quantum mechanically. Such methods have been shown to be successful in evaluation of the time evolution of a quantum-classical many-body systems [19] for heavier particles than electrons.

Since there is no perfect method for solving dynamical full quantum many-body problems in practice, it is useful to look at different methods, how they can be used, what are their strengths and weaknesses and what is needed in implementation of those

methods.

In this paper, we deal with real time quantum dynamics with both coherent and incoherent propagation. Next, we present the basic theory, exact kernels and the approximate Trotter kernel, and in Section 3, the numerical approach to evaluation of propagation and expectation values. In Section 4 we define one dimensional electron-in-quantum-dot models chosen for testing. In Section 5 we analyze results for coherent quantum dynamics and in Section 6 we finally present a novel approach to search for stationary quantum states and the ground state, in particular. The last section presents our conclusions.

2 Path integral and propagators

Consider non-relativistic particle propagation in one, two or three dimensional space Ω from x_a to x_b in time interval from t_a to t_b along all possible paths $x(t)$. The path integral over all paths defines the propagator

$$K(b,a)=\int_a^b \exp\left[\frac{\mathrm{i}}{\hbar}S_x[b,a]\right]\mathcal{D}x(t), \tag{2.1}$$

where $S_x[b,a]=\int_a^b L_x \mathrm{d}t$ is the action of the path $x(t)$ from $a=(x_a,t_a)$ to $b=(x_b,t_b)$ and L_x is the corresponding Lagrangian [1,2]. Time evolution of the probability amplitude, *i.e.*, the wave function $\psi(x,t)$ in space Ω can now be written as

$$\psi(x_b,t_b)=\int_\Omega K(x_b,t_b;x_a,t_a)\psi(x_a,t_a)\mathrm{d}x_a, \tag{2.2}$$

where $t_a<t_b$. From this relation the time dependent Schrödinger equation can be derived [1], or alternatively, the time dependent wave function $\psi(x,t)$ can be directly evaluated from the initial state $\psi(x_a,t_a)$, in case the kernel $K(x,t;x_a,t_a)$ is known.

However, general explicit forms of the propagator are known for simple cases, only, such as the particle with mass m in the one dimensional constant linear potential $V(x)=-fx$,

$$K(x_b,x_a;t)=\left[\frac{m}{2\pi\mathrm{i}\hbar t}\right]^{1/2}\exp\left[\frac{\mathrm{i}}{\hbar}\left(\frac{m}{2t}(x_b-x_a)^2-\frac{t}{2}(V(x_a)+V(x_b))-\frac{t^3f^2}{24m}\right)\right], \tag{2.3}$$

which reduces to the free particle propagator with $f=0$ [1] or to the propagator of particle in a box with surrounding infinite potential.

For the one dimensional forced harmonic oscillator

$$V(x,t)=\frac{m\omega^2}{2}x^2-f(t)x \tag{2.4}$$

the exact explicit propagator takes the form [1]

$$K(x_b,x_a;t)=\left[\frac{m\omega}{2\pi\mathrm{i}\hbar\sin(\omega t)}\right]^{1/2}\exp\left[\frac{\mathrm{i}}{\hbar}S_{\mathrm{cl}}\right], \tag{2.5}$$

where $S_{\rm cl}$ is the classical action. For $f\equiv 0$ this is

$$S_{\rm cl}=\frac{m\omega}{2\sin(\omega t)}\left[(x_b^2+x_a^2)\cos(\omega t)-2x_bx_a\right]. \tag{2.6}$$

For numerical approaches robust approximations are needed. It is advantageous that also in nontrivial forms of potential the propagation is straightforward to evaluate and with increasing numerical accuracy the propagator approaches the exact limit. With this in mind we discretize the time $t=t_b-t_a$ to a number of short steps Δt. This is straightforward, because

$$K(b,a)=\int_\Omega K(b,c)K(c,a)\mathrm{d}x_c, \tag{2.7}$$

for $t_a<t_c<t_b$. This follows from additivity of action $S[b,a]=S[b,c]+S[c,a]$ for any path [1].

Now, with a small Δt the quantum paths can be expected to give the main contribution close to the classical path, for which $\Delta x=x_b-x_a$ is also small. This follows from the canceling kinetic energy T contributions due to the destructive interference of paths in long path propagation. This presumes, of course, smooth enough potential V, for which also the commutator $[T,V]$ is small.

Furthermore, for numerical approaches it is essential that the chosen discretization also converges to the exact formalism at the limit $\Delta t\to 0$, and the faster the better for practical purposes. Also, it is preferable that computational efforts are not wasted for computation of almost canceling contributions more than needed for the chosen target accuracy.

Now, Eq. (2.3) gives numerically useful approximation, which can be further simplified by neglecting the last term, cubic in Δt, for short enough time steps. Thus, we arrive at the symmetrized Trotter kernel [12,13]

$$K(x_b,x_a;\Delta t)\approx\left[\frac{m}{2\pi\mathrm{i}\hbar\Delta t}\right]^{D/2}\exp\left[\frac{\mathrm{i}}{\hbar}\left(\frac{m}{2\Delta t}(x_b-x_a)^2-\frac{\Delta t}{2}(V(x_a)+V(x_b))\right)\right], \tag{2.8}$$

where D is the dimensionality of space.

This propagator can also be found from the hamiltonian formulation [4]. For a time independent hamiltonian $H=T+V$, where T and V are the kinetic and potential energies, the propagator can be written as [4]

$$K(x_b,x_a;\Delta t)=\left\langle x_b\middle|\exp\left[-\frac{\mathrm{i}}{\hbar}H\Delta t\right]\middle|x_a\right\rangle=\left\langle x_b\middle|\exp\left[-\frac{\mathrm{i}}{\hbar}(T+V)\Delta t\right]\middle|x_a\right\rangle, \tag{2.9}$$

where $\Delta t=t_b-t_a$. Now, by using the Zassenhaus formula [4,22]

$$\begin{aligned}\exp\left[-\frac{\mathrm{i}}{\hbar}(T+V)\Delta t\right]=&\exp\left[-\frac{\mathrm{i}\Delta t}{\hbar}T\right]\exp\left[-\frac{\mathrm{i}\Delta t}{\hbar}V\right]\\&\times\exp\left\{\left(\frac{\mathrm{i}\Delta t}{\hbar}\right)^2\frac{[T,V]}{2}\right\}\mathcal{O}\left\{1+\left(\frac{\mathrm{i}\Delta t}{\hbar}\right)^3\right\}\end{aligned} \tag{2.10}$$

and by neglecting factors which approach one in the second order or higher in Δt, as $\Delta t \to 0$, and using the path integral formulation, we arrive at the approximation (2.8). Thus, this approximation is accurate almost to the second order in Δt for a smooth potential with $[T,V] \to 0$ as $\Delta x \to 0$ or $\Delta t \to 0$. In fact, this is what the kernel in Eq. (2.3) also suggests.

Clearly, in numerical approaches it is the kinetic energy part, which brings in the challenges as $\Delta t \to 0$, but as pointed out above, already, the resulting large momentum – short wave length oscillations of the propagator interfere destructively and should be damped out without wasting computational efforts. The potential energy part behaves the opposite way with respect to the time step, and becomes laborious only in case of large potential gradient at possible singularities in the potential function.

We consider and test the Trotter kernel Eq. (2.8) against the exact kernels Eqs. (2.3) and (2.5) in numerical simulations of one-dimensional harmonic oscillator (ODHO) and quantum well (QW), both in stationary eigenstates and wave packet propagation.

3 Numerical evaluation of propagation and expectation values

Numerical evaluation of the integral Eq. (2.2) is the core problem, here. For that, we span grids $\mathbf{g}_a = \{x_{ai}\}_{i=1}^{N_a}$ and $\mathbf{g}_b = \{x_{bj}\}_{j=1}^{N_b}$ for wave functions at a and b. It is practical to define the grid density profiles or distribution functions $g_a(x)$ and $g_b(x)$, as (possibly normalized) inverse average grid spacing. With small enough time step Δt we can assume the same restricted space Ω for both ψ_a and ψ_b, and for simple cases, also the same grid $\mathbf{g} = \mathbf{g}_a = \mathbf{g}_b$ with the same size $N = N_a = N_b$.

The simplest equally spaced regular grid, *i.e.*, with g constant, between end points may generate fake constructive diffraction patterns. This is the diffraction grating effect, which can be removed out by increasing the grid size N. Usually, a better choice is some other regular distribution of g, like gaussian or some other, related to the probability density or (the absolute value of) the wave function, itself.

Of course, Monte Carlo grids with given distributions g serve well, if smooth and sizable enough. There are methods for the analysis of "smoothness" of the distribution, such as Kolmogorov-Smirnov test [21]. In fact, with the increasing number of dimensions Monte Carlo grids may remain as the only practical choice. Further smoothing and averaging out accumulative errors is attained with a continuous random change of the MC grids, within the predefined density profiles. For restricted range of dynamics, it may be practical to use identical distributions, *i.e.*, $g_a(x) = g_b(x)$, but $\mathbf{g}_a \neq \mathbf{g}_b$.

Ongoing random evolution of $\{x_i\}_{i=1}^{N_i}$ also means sampling of continuous space, instead of a discrete grid. This evolution can be adapted to follow the time evolution of the wave function or some related distributions like the absolute value or the probability distribution of the wave function, *i.e.*, $g(x,t) \propto |\psi(x,t)|^n$, $n = 1$ or 2, for example.

The distribution function $g(x)$ appears as an inbuilt weight factor in the integration of Eq. (2.2). In the one-dimensional space it is straightforward to write $g(x) = \mathrm{d}G(x)/\mathrm{d}x$, in

terms of the cumulative distribution function G. Thus, Eq. (2.2) becomes in form $\psi(b)=\int_0^1 K(b,a)\psi(a)\ g_a^{-1}(a)\mathrm{d}G_a$. For propagation over the time interval $\Delta t=t_b-t_a$ with $t_a=0$, numerical calculation can be carried out as

$$\begin{aligned}\psi(x_j,\Delta t)&=\int_0^1 K(x_j,\Delta t;x_i,0)\frac{\psi(x_i,0)}{g_a(x_i)}\mathrm{d}G_a(x_i)\\&\approx\sum_{i=1}^{N_a}\frac{K(x_j,x_i;\Delta t)\psi(x_i,0)}{g_a(x_i)}.\end{aligned}\tag{3.1}$$

Hence, it seems obvious that $\psi(a)$ should decay faster than g_a in order to avoid numerical instabilities. For real $\psi(a)$ or for its absolute value this can be easily established, whereas for the two parts of complex $\psi(a)$ this can be expected to be more tricky. The phase factor of calculated $\psi(b)$ relates to the "local total energy", and therefore, it serves as a good indicator of numerical stability. Therefore, it seems possible to find phase factor based algorithms for stabilization of propagation and for removing numerical errors.

In principle, the distribution $g_a(x)$ needs not to be known analytically, if $g_a(x_i)$ can be evaluated from the wave function, for example. Furthermore, negative sign can be assigned to $g_a(x)$ at some range of x, if relevant for some reason.

Monte Carlo evaluation of expectation values of local operators, like the multiplicative potential $V(x)$, at time t_a, can be done with

$$\langle V\rangle=\int_0^1\frac{\psi^\star(x_i,t)V(x_i)\psi(x_i,t)}{g(x_i)}\mathrm{d}G(x_i)\approx\sum_{i=1}^{N}\frac{V(x_i)|\psi(x_i,t)|^2}{g(x_i)},\tag{3.2}$$

where the operator can be time dependent, too.

Similarly, we calculate the total energy from

$$\langle E\rangle\approx\sum_{i=1}^{N}\frac{E_L(x_i)|\psi(x_i,t)|^2}{g(x_i)},\tag{3.3}$$

where the local energy is evaluated from the increase in wave function phase $-\Delta\phi(x)$ within a time step Δt as $E_L(x)=-\Delta\phi(x)\hbar/\Delta t$. Then, the kinetic energy $\langle T\rangle$ can be evaluated from $\langle E\rangle=\langle T\rangle+\langle V\rangle$.

4 One-dimensional harmonic oscillator and quantum well

We first consider the one-dimensional harmonic oscillator (ODHO), *i.e.*, a particle in the potential of Eq. (2.4) with $f(t)\equiv 0$. Thus, we have the time-independent potential

$$V(x)=\frac{1}{2}m\omega^2x^2.\tag{4.1}$$

We choose the parameters describing an electron in an atom size "quantum dot" to maximize the quantum effects and challenge for simulation of dynamics. We use atomic units,

where $\hbar = 4\pi\varepsilon_0 = e = m = a_0 = 1$, the last three being the charge, mass and Bohr radius of the electron. This leads to the atomic unit energy of Hartree, Ha $= \hbar^2/(ma_0^2) \approx 27.211384$ eV, which also defines the unit of the potential in Eq. (4.1). The atomic time unit becomes as $t_0 = (ma_0^2)/\hbar \approx 24.18884 \times 10^{-18}$ s ≈ 24 as.

Now, by substituting $m = 1$ and $\omega = 0.1$ ($= \hbar\omega$), we have the corresponding eigenenergies E_ν with equal contributions from kinetic and potential energies and eigenstates $\psi_\nu(x) = (2^\nu \nu!/\sigma_0)^{-1/2}\pi^{-1/4}H_\nu(x/\sigma_0)\exp(-x^2/2\sigma_0^2)$, where H_ν are Hermite polynomials and $\sigma_0 = \sqrt{\hbar/m\omega} \approx 3.16$. For the ground state we have $\psi_0(x) = \pi^{-1/4}\sigma_0^{-1/2}\exp(-x^2/2\sigma_0^2)$ and $E_0 = 0.050$. Thus, $E_1 = 0.150$.

The one-dimensional quantum well (QW) or "particle in a box"

$$V(x) = \begin{cases} 0 & \text{for} |x| < L/2, \\ \infty & \text{otherwise,} \end{cases} \quad \text{and} \tag{4.2}$$

with $L = 20$ is also used as a test case, where relevant. Here, we have the free particle eigenstates with energies $E_\nu = \frac{1}{2}k^2$, where $k = 2\pi/\lambda$ and $\nu\lambda/2 = L$. Thus, $E_1 = \frac{1}{2}(\pi/L)^2 \approx 0.01234$ and $E_2 = 2(\pi/L)^2 \approx 0.04935$.

5 Coherent dynamics

5.1 Stationary states

First, we searched for numerical parameters, which keep the eigenstates stationary with an acceptable accuracy. The three lowest eigenstates of ODHO ($\hbar\omega = 0.1$), Eq. (4.1), turn out to remain stable in a simulation with an even spaced grid of size $N = 10^3$ in the domain $-12 < x < 12$ with the time step $\Delta t = 1$. The potential energy expectation value (3.2) fluctuates around the time average $\overline{\langle V_0 \rangle} = 0.02503$ with a standard deviation $\sigma \approx 3 \times 10^{-5}$, and correspondingly, the total energy (3.3) becomes as $\overline{\langle E_0 \rangle} = 0.05002$ with $\sigma \approx 4 \times 10^{-9}$. Thus, a small grid related error remains.

We find that the time step should be small enough ($\Delta t_{\max} \approx 4$) to justify the Trotter approximation, Eq. (2.8), for ODHO. Shortening the time step calls for more accurate grid due to increasing kinetic energy, *i.e.*, oscillatory nature of the exponential in Eq. (2.8). The potential energy contribution to phase oscillations is roughly two orders of magnitude less. In general, we found the maximum time step and even grid size proportion to be related roughly as $\Delta t_{\max} \times N \geq 10^3$ for the Trotter kernel, Eq. (2.8).

The exact kernel Eqs. (2.5)–(2.6) of ODHO, however, allows unlimited time step and the accuracy depends on the grid, only. Even so, the time steps of a multiple of half oscillation period can not be used, because $\sin(\omega t)$ in the denominator causes divergence of both (2.5) and (2.6). With other time steps $1 \leq \Delta t \leq 500$ and $N = 10^3$ the potential energy keeps correct in 5 digits. The total energy $\overline{\langle E_0 \rangle}$ becomes evaluated with same accuracy.

For the QW with constant potential the Trotter kernel is nearly exact [4]. However, numerical accuracy suffers from inaccurate description of discontinuities of the potential

function Eq. (4.2) at $|x| = L/2$. Thus, the accuracy is limited by the grid spacing Δx. Obviously for this reason, we found the time propagation to be somewhat unpredictable.

For this case, we found that the Monte Carlo grid with a constant distribution function solves the problem. Time evolution of the grid, with $g(x) =$ constant, samples the space continuously. We found the grid size $N = 10^3$ sufficient for a stable simulation of the ground state in a QW $L = 20$ with the total energy $\overline{\langle E_0 \rangle}$ accurate in a few digits, for a few steps, already. Obviously, other non divergent but adapted distributions $g(x)$ will perform even better.

5.2 Wave packet propagation

Next, we consider real time evolution of gaussian wave packet oscillation in the harmonic potential (ODHO), above. As a test case we use the Glauber state, also called coherent or quasi-classical state, because of classical like oscillation retaining the wave packet shape rigid. In fact, the width of the Glauber state gaussian is that of the ground state, in the present case $\psi(x) = \pi^{-1/4}\sigma_0^{-1/2}\exp(-x^2/2\sigma_0^2)$. The oscillation frequency is, of course, $\omega = 0.1$ and period $T = 2\pi/\omega \approx 62.83$, for any oscillation amplitude A.

With the Trotter kernel and grid size $N = 10^4$ the time step dependence is small. With $A = \sqrt{20}$ and starting from rest, the total energy is that of the first excited state, see Fig. 1. Both $\Delta t = 2\pi/60$ and $\Delta t = 2\pi/200$, and wave packet propagation of one period leads to potential energy error of -0.0027, only. With the exact kernel, Eqs. (2.5)–(2.6), arbitrarily long time steps can be taken, except those, for which $\sin(\omega\Delta t) \approx 0$, as pointed out above.

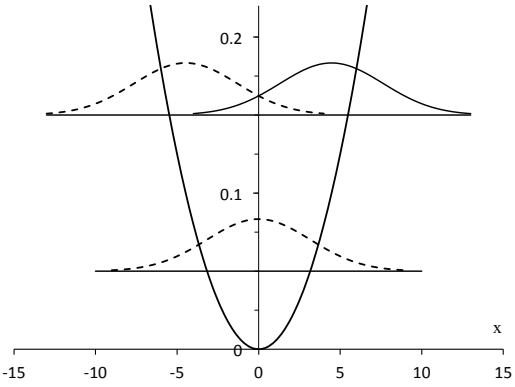

Figure 1: The ODHO potential and the starting Glauber state (full curves). Dashed curves show the two other extreme phases of oscillation. Horizontal lines indicate the ground and the first excited state energies.

6 Incoherent dynamics

6.1 Stationary state search

With the path-integral approach, simulation of stationary eigenstates is no more trivial than that of explicitly time dependent wave functions. In both cases full propagation in the whole space needs to be similarly considered within each time interval. This points to the inherent nonlocality of the wave function and quantum phenomena, in general.

An arbitrary pure quantum state can be expanded as a superposition of stationary eigenstates as $\Psi=\sum_k c_k\psi_k$ and its time evolution in Δt is $\Delta\Psi=\sum_k \exp(-\mathrm{i}E_k\Delta t)c_k\psi_k=\sum_k[\cos(E_k\Delta t)-\mathrm{i}\sin(E_k\Delta t)]c_k\psi_k$. By using the small angle approximation for short enough Δt, this can be written as $\Delta\Psi\approx\sum_k[1-(E_k\Delta t)^2/2-\mathrm{i}(E_k\Delta t)]c_k\psi_k$.

Consider now stepwise decoherence of the wave function in each time step, that is driven by removal of the small imaginary part. Such incoherent time evolution,

$$\Delta\Psi(\Delta t)=\sum_k[1-(E_k\Delta t)^2/2)]c_k\psi_k, \tag{6.1}$$

converges to quantum Zeno propagation at the limit $\Delta t\to 0$, if the eigenstate is real. However, with a finite but short enough Δt it increases the contribution of the eigenstate with smallest absolute eigenvalue with respect to the chosen reference energy, if $E_k\Delta t\ll 1$ for all k. At the end, this state dominates and contributions from the other states die out.

This is what we call incoherent propagation, here, and demonstrate the respective time evolution in ODHO with the Trotter propagator in evenly spaced grid, see Fig. 2. Incoherent evolution depends on the initial state as shown. In case where the ground state ψ_0 contribution is initially considerable, $c_0\neq 0$, the convergence is fast. However, in

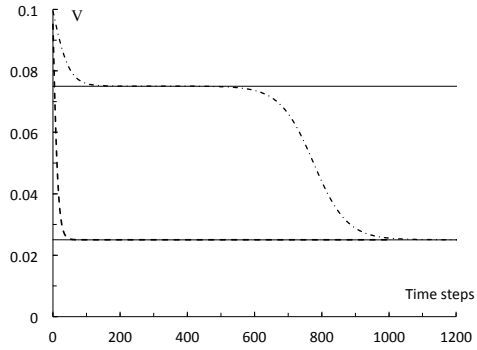

Figure 2: Incoherent evolution of the superposition states to the ground state. Dashed line starts from the superposition of the ground and 3rd excited state, whereas the dash dotted line starts from the superposition of the 1st and 2nd excited states. Solid lines show the potential energies of the ground and 1st excited states.

case where initially $c_0 = 0$, lowest of the states contributing to the initial wave function is found. The ground state is found only after a small seed of ψ_0 has been sown from numerical errors in propagation.

By shifting the zero reference of ODHO close to the first excited state eigenvalue, in Fig. 2, we find the incoherent propagation locking to the first excited state, similarly to finding the ground state, above.

6.2 Ground state evaluation

Finally, we consider accurate evaluation of the ground state, or another stationary state, after first finding it by the "stationary state search" described in the previous section. With the incoherent propagation in ODHO by using the Trotter propagator we found accuracy of about five digits for the ground state energetics, independent of the grid size ($N = 10^3$ to 3×10^4) and accidentally with the time step $\Delta t \approx 0.3$. Obviously, there remains a systematic error due to the grid and propagator.

Therefore, we again employ the Monte Carlo grid to sample the continuous space. We also simplify the propagation, Eq. (3.1), to increase accuracy in the spirit of diffusion Monte Carlo (DMC) approach, where it is the distribution of walkers, which is the target ground state wave function. This allows comparison of our approach to DMC, which is known as a robust and accurate method for finding and evaluation of properties of the ground state.

Close enough the ground state we set $g(x) = \psi(x) \approx \psi_0(x)$, and consequently, approximate Eqs. (2.2) and (3.1) for numerical Monte Carlo evaluation as

$$\begin{aligned}\psi(x_j,\Delta t) &= \int K(x_j,\Delta t;x_i,0)g(x_i)\mathrm{d}x_i \\ &= \int_0^1 K(x_j,\Delta t;x_i,0)\mathrm{d}G(x_i) \approx \sum_{i=1}^{N_a} K(x_j,x_i;\Delta t),\end{aligned} \tag{6.2}$$

and therefore, $\{x_i\}_{i=1}^{N_a}$ are random numbers from distribution $g(x)$ with the cumulative distribution function $G(x)$, as discussed above. Thus, in practice we run incoherent propagation

$$\psi(x_b,\Delta t) = \int K(x_b,\Delta t;x_a,0)\psi(x_a,0)\mathrm{d}x_a, \tag{6.3}$$

without an explicit starting amplitude $\psi(x_a,0)$, but hidden in the walker distribution, and assuming good convergence of the distribution to the ground state wave function. To sample continuous space, Metropolis Monte Carlo (MMC) can be used to carry out evolution of the walker distribution $g(x)$, and if needed, stability can be increased by using the "time average" $\overline{g(x)}$ from a longer simulation and partly overlapping grids $\mathbf{g}_a = \{x_{ai}\}_{i=1}^{N_a}$ and $\mathbf{g}_b = \{x_j\}_{j=1}^{N_b}$, with $N_a = N_b = N$.

It is worth noting that in a simulation, as described above, we have the ground state wave function at each step both in the walker distribution $g(x) = \psi(a)$ and evaluated from

Table 1: Incoherent propagation in MC grid of the ODHO ground state with Trotter kernel. N is the grid size, Δt the time step, ΔV the deviations of expectation values of the potential energy from its exact value 0.025000 and σ the standard deviation from long simulations.

N	Δt	$\Delta V/10^{-6}$	$\sigma/10^{-6}$
10^4	0.3	160	540
10^4	1	60	530
10^4	3	40	470
3×10^4	1	30	320

propagation as $\psi(b)$. Though the latter is guiding the evolution of the former through MMC, $g(x)$ can be kept stable by settings of the MMC parameters, whereas the stability of the evaluated amplitude $\psi(b)$ depends primarily on the propagation parameters: grid size and time step length. As a test case we present evaluation of the potential energy from Eq. (3.2), which depends on both distributions.

To maximize variance (standard deviation) in this test, we use fully random and non overlapping grids $\mathbf{g}_a$ and $\mathbf{g}_b$ from exact gaussian distribution to assess the statistical performance of the Trotter kernel for evaluation of the ground state energetics of ODHO. The obtained data from incoherent propagation is shown in Table 1 and Fig. 3.

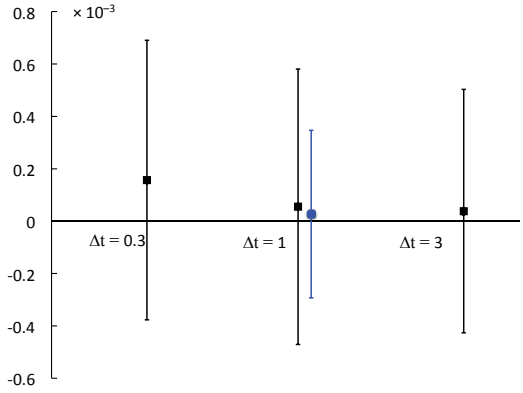

Figure 3: Incoherent propagation in MC grid of the ODHO ground state with Trotter kernel. Deviations of expectation values of the potential energy from its exact value 0.025 (dots) and standard deviations (bars) shown (in au $\times10^{-6}$) from long simulations, with time steps 0.3, 1 and 3, and grid sizes 10^4 (black fullsquare) and 3×10^4 (blue fullcircle). The $2\times$SEM error bars are smaller than the square/circle size.

We find that accuracy of the achieved ground state energetics (ΔV) and distribution depends on the grid size and the time step. Note, that the "error bars" (σ) do not describe accuracy. Grid size dependence is as expected: larger grid increases accuracy. Time step

dependence, however, is weak and longer step leads to higher accuracy. Overall, this is what one can expect from the Trotter kernel.

The vertical bars in Fig. 3 describe simulation length independent standard deviation σ arising from Monte Carlo sampling. It can be used to estimate the statistical accuracy (precision) of evaluated expectation values in form of standard error of mean, SEM $=$ $\sigma/\sqrt{N_{\mathrm{MC}}}$, where N_{MC} is the number of uncorrelated Monte Carlo steps. Usually, $2\times$SEM limits (95%) are assumed as a statistical error estimate. Thus, the longer the simulations, the smaller the $2\times$SEM error bars become. The precision of the squares and the dot in Fig. 3 is good enough to demonstrate the systematic error from Trotter approximation and size of test grid sizes.

Finally, by using the Trotter kernel, we carried out a search of an electron in the ground state of the two-dimensional quantum dot, 2DHO, with $N=3\times10^4$ and $\Delta t=0.3$. For the expectation value of ΔV and σ (in units 10^{-6}, cf. Table 1) we obtained -2000 and 600, respectively.

7 Conclusions

We have demonstrated the path integral approach to the time domain coherent quantum dynamics with numerical simulations of simple one dimensional test cases, relevant as quantum dot models. Generally, we find the PI approach more laborious as compared to the conventional evaluation of the solution from the time dependent Schrödinger equation, as expected [1,2].

With PI approach a regular periodic grid may give rise to diffraction patterns on the evaluated amplitude, while Monte Carlo grids are free from such artifact. Also as usual, with Monte Carlo technique for path sampling, the PI approach becomes more attractive in case of complex geometry or increasing number of spatial dimensions.

The cases where the exact kernel is known are special. There, the time step length is not limited, even in practice, which offers a huge advantage over the conventional simulation of single particle quantum dynamics. On the other hand, the straightforward incorporation of many-body correlations presumes short time steps. Therefore, the Trotter kernel, which becomes exact at the zero step length limit, becomes accurate enough with practical time step lengths. However, shorter time steps require more dense grids, as discussed above.

With the incoherent real time dynamics we have demonstrated a novel approach for searching the stationary states and the ground state, in particular. Monte Carlo sampling of the continuous space turns out to increase accuracy as compared to the use of a regular discrete grid. The Monte Carlo version has further advantages, similar to the conventional "high accuracy" diffusion Monte Carlo method. Here, we have carried out the first tests of the convergence and accuracy of the new method, which seems promising with its novel features.

Acknowledgments

For computational resources we like to thank the Techila Technologies facilities at Tampere University of Technology, and also, the facilities of Material Sciences National Grid Infrastructure (Akaatti, Merope) and Finnish IT Center for Science (CSC). The authors also want to thank Dr. I. Kylänpää for his comments on the manuscript.

References

[1] R.P. Feynman and A.R. Hibbs, Quantum Mechanics and Path Integrals (McGraw-Hill, New York, 1965).
[2] R.P. Feynman, Rev. Mod. Phys. **20**, 367 (1948).
[3] I.H.Duru and H.Kleinert, Phys. Lett. **84B**, 185 (1979) and H.Kleinert, Path Integrals in Quantum Mechanics, Statistics, Polymer Physics, and Financial Markets. World Scientific Publishing Co. Pte. Ltd. Singapore (2004). The 5th edition.
[4] L.S.Schulman, Techniques and Applications of Path Integration (Wiley, New York, 1981).
[5] K.-Y. Wong, Commun. Comput. Phys. **15**, 853 (2014).
[6] D.M. Ceperley, Rev. Mod. Phys. **67**, 279 (1995).
[7] I. Kylänpää, PhD Thesis (Tampere University of Technology 2011).
[8] I. Kylänpää and T.T. Rantala, J. Chem. Phys. **133**, 044312 (2010), I. Kylänpää and T.T. Rantala, J. Chem. Phys. **135**, 104310(2011) and I. Kylänpää and T.T. Rantala, Phys. Rev. A **80**, 024504(2009).
[9] Militzer and D.M. Ceperley, Phys. Rev. B **63**, 066404 (2001).
[10] S. Weiss and R. Egger, Phys. Rev. B **72**, 245301 (2005).
[11] E. Gull *et al.*, Rev. Mod. Phys. **83**, 349 (2011).
[12] N. Makri, Comp. Phys. Comm. **63**, 389–414.
[13] N. Makri, Chem. Phys. Lett. **193**, 435 (1992).
[14] V.S. Filinov, Nucl. Phys. B **271**, 717–725 (1986).
[15] H. Wang *et al.*, J. Chem. Phys. **115**, 6317(2001).
[16] N. Makri, Ann. Rev. Phys. Chem. **50**, 167–191 (1999) and V. Jadhao and N. Makri, J. Chem. Phys. **132**, 104110 (2010).
[17] T.L. Marchioro and T.L. Beck, J. Chem. Phys. **96**, 2966 (1992).
[18] N. Makri, Comp. Phys. Comm. **63**, 389–414 (1991) and N. Makri, J. Math. Phys. **36**, 2430–56 (1995).
[19] R. Lambert and N. Makri, J. Chem. Phys. **137** 22A552 and 22A553 (2012).
[20] D.E. Makarov and N. Makri, Chem. Phys. Lett. **221**, 482 (1994).
[21] A. Kolmogorov, G.Ist.Ital.Attuari **4**, 83 (1933).
[22] M. Suzuki, Phys. Lett. A **201**, 425–428 (1995).
[23] N. Metropolis, A.W. Rosenbluth, M.N. Rosenbluth, H. Teller and E. Teller, J. Chem. Phys. **21**, 1087 (1953).
[24] P. Atkins and R. Friedman, Molecular Quantum Mechanics (Oxford University Press Inc., New York, 2005). The 4th edition.
[25] K. Schulten, "Notes on Quantum Mechanics" (University of Illinois at UrbanaChampaign, 2000).

PUBLICATION

II

Numerical Path Integral Solution to Strong Coulomb Correlation in One Dimensional Hooke's Atom

I. Ruokosenmäki, H. Gholizade, I. Kylänpää and T. T. Rantala

Computer Physics Communications 210.(2017), 45–53
DOI: 10.1016/j.cpc.2016.09.012

Computer Physics Communications 210 (2017) 45–53

Contents lists available at ScienceDirect

Computer Physics Communications

journal homepage: www.elsevier.com/locate/cpc

Numerical path integral solution to strong Coulomb correlation in one dimensional Hooke's atom

Ilkka Ruokosenmäki *, Hossein Gholizade, Ilkka Kylänpää, Tapio T. Rantala

Department of Physics, Tampere University of Technology, Finland

ARTICLE INFO

Article history:
Received 14 October 2015
Received in revised form
21 March 2016
Accepted 21 September 2016
Available online 4 October 2016

Keywords:
Path integral
Quantum dynamics
First-principles
Monte Carlo
Strong correlation
Hooke's atom

ABSTRACT

We present a new approach based on real time domain Feynman path integrals (RTPI) for electronic structure calculations and quantum dynamics, which includes correlations between particles exactly but within the numerical accuracy. We demonstrate that incoherent propagation by keeping the wave function real is a novel method for finding and simulation of the ground state, similar to Diffusion Monte Carlo (DMC) method, but introducing new useful tools lacking in DMC. We use 1D Hooke's atom, a two-electron system with very strong correlation, as our test case, which we solve with incoherent RTPI (iRTPI) and compare against DMC. This system provides an excellent test case due to exact solutions for some confinements and because in 1D the Coulomb singularity is stronger than in two or three dimensional space. The use of Monte Carlo grid is shown to be efficient for which we determine useful numerical parameters. Furthermore, we discuss another novel approach achieved by combining the strengths of iRTPI and DMC. We also show usefulness of the perturbation theory for analytical approximates in case of strong confinements.

1. Introduction

Feynman path integral (PI) approach offers an intuitive description of quantum mechanics [1,2], where classical mechanics emerges transparently from disappearing wave nature of particles along with vanishing Planck constant. Therefore, it is robust in numerical calculations in cases close to classical ones, like molecular quantum dynamics in real time [3], but becomes more challenging and laborious for states of electrons, where the wave nature plays larger role. Furthermore, the PI presentation of stationary states also involves full time-dependent quantum dynamics, in contrast with the conventional solution of the time-dependent Schrödinger equation, where time evolution appears as simple change of the wave function phase, only.

We have already demonstrated that numerical solutions to stationary states and quantum dynamics of single electrons in one dimensional potentials can be reliably found, both in regular and Monte Carlo grids, by using real time path integral (RTPI) propagation [4]. We have also assessed the usefulness and accuracy of the Trotter kernel as compared to the exact kernels and pointed out the advantages of the Monte Carlo grid in avoiding spurious interference effects. For search and evaluation of the single particle eigenstates we found a novel approach based on the *incoherent propagation* [4], *i.e.*, collapsing the wave function to its real component after each short time step. This is the starting point of the present study.

RTPI approach can be expected to show most of its proficiency in simulation of many-electron systems, where correlation phenomena turn out to be in major role — the same way and partly for same reasons as it has been found to be with the more conventional path integral Monte Carlo (PIMC), simulation of the imaginary time propagation [5–8]. It may be pertinent to point out, that while PIMC simulation yields the finite temperature equilibrium description of the system of quantum particles, RTPI simulation finds the zero-Kelvin real time quantum dynamics. Furthermore, RTPI can also be used to find and simulate the eigenstates, as indicated above. Thus, for finding and simulation of the ground state, RTPI can be compared to the diffusion Monte Carlo (DMC) simulation [9]. Thus, combination of these two can be expected to offer novel features, which turns out to be the case.

To assess the performance of incoherent RTPI as compared with DMC we choose the Hooke's atom in one dimension as the test bench, presenting a case of an extremely strong correlation.

Three dimensional Hooke's atom is a helium-like system of two electrons with Coulomb repulsion, where electron–nucleus attraction is replaced by a confining parabolic or harmonic

* Corresponding author.
E-mail addresses: ilkka.ruokosenmaki@tut.fi (I. Ruokosenmäki), hossein.gholizadehkalkhoran@tut.fi (H. Gholizade), ilkka.kylanpaa@tut.fi (I. Kylänpää), Tapio.Rantala@tut.fi (T.T. Rantala).

http://dx.doi.org/10.1016/j.cpc.2016.09.012
0010-4655/

potential. It is one of the few non-trivial systems with exact solutions for certain strengths of confinement (harmonic force constant) [10], and therefore, it is a good test case for our new approach. As shown below, separation of the three dimensional problem in relative coordinates yields two problems, one of which is the one dimensional Hooke's atom once the angular momentum degrees of freedom are taken out. In one dimension, the Coulomb repulsion is strong enough to split the space to two independent domains defined by exchange of the electrons [11–14].

In this paper we will demonstrate the novel incoherent RTPI in finding the ground state of one dimensional Hooke's atom by using a Monte Carlo grid. We also analyze performance of the simulation by comparison with DMC simulation, and furthermore, discuss another new idea to combine the strengths of incoherent RTPI and DMC. Accuracy of the numerical approaches is analyzed by using analytical solutions and those from perturbation theory (PT), where relevant.

2. Ground state

Finding or simulation of the ground state is perhaps the most general problem to work out in dealing with quantum systems. Here, we present our novel approach to this based on the incoherent real time propagation [4] using the path integral formalism. First however, we briefly present the well known diffusion Monte Carlo (DMC) method [9] using imaginary time propagation, to be used as a reference. These both are numerical methods and the former one in its robust form also using Monte Carlo technique. For the specified test case, one dimensional Hooke's atom, we also compare with the analytical solutions, where available, and approximate solutions otherwise.

To keep notations simple, we use the atomic units, where $m_e = e = \hbar = 4\pi\epsilon_0 = 1$ throughout the paper, unless otherwise stated.

2.1. Imaginary time propagation: DMC

The time-dependent Schrödinger wave equation for the many-body wave function $\psi(x, t)$ is

$$\mathrm{i}\frac{\partial\psi(x,t)}{\partial t} = (H - E_T)\psi(x,t), \tag{1}$$

where H is the hamiltonian, x stands for all coordinates of particles in one or more spatial dimensions and E_T is an arbitrary reference energy or shift of zero level. Now, by replacing the real time t by imaginary time $\tau = it$, this becomes

$$-\frac{\partial\psi(x,\tau)}{\partial\tau} = (H - E_T)\psi(x,\tau), \tag{2}$$

which is of the form of a diffusion equation. Its solutions can be expressed in terms of eigenfunctions $\phi_n(x)$ of the hamiltonian as

$$\psi(x,\tau) = \sum_{n=0}^{\infty} C_n\phi_n(x)\exp[-(E_n - E_T)\tau]. \tag{3}$$

As Monte Carlo methods are useful for evaluation of integrals, the differential equation is transformed into an integral equation. This is done by using Green's function formalism [9] and we seek the solution of the form

$$\psi(x_b,\tau_b) = \int_a G(x_b,\tau_b;x_a,\tau_a)\psi(x_a,\tau_a)dx_a, \tag{4}$$

where $G(x_b, \tau_b; x_a, \tau_a)$ is the Green's function of the system, the position space representation of the time evolution operator $\exp[-(H - E_T)(\tau_b - \tau_a)]$.

The exact analytical form of the Green's function is rarely known, and therefore, it needs to be approximated. Use of the so called short time approximation [9] to separate the kinetic and potential energy contributions, T and V, gives

$$\begin{aligned}\exp[-(H - E_T)\Delta\tau] &= \exp[-(T + V - E_T)\Delta\tau] \\ &\approx \exp[-T\Delta\tau]\exp[-(V - E_T)\Delta\tau].\end{aligned} \tag{5}$$

Since T and V do not commute, in general, this approximation is exact only in the limit $\Delta\tau \to 0$ but accurate for small $\Delta\tau$ for potentials bound from below [9].

The Green's function can be separated into two parts, kinetic and potential (or diffusion and branching),

$$G(x_b,\tau_b;x,\tau_a) \approx G_{\mathrm{diff}}(x_b,\tau_b;x,\tau_a)G_B(x_b,\tau_b;x,\tau_a). \tag{6}$$

As this Green's function satisfies the imaginary time Schrödinger equation, it gives one equation for both parts of the Green's equation with kinetic part satisfying diffusion equation and potential part satisfying rate equation. Solutions to these equations are well known, a Gaussian spreading in $\Delta\tau$ and an exponential function:

$$G_{\mathrm{diff}}(x_b,x_a;\Delta\tau) = (4\pi D\Delta\tau)^{-N/2}\exp[-(x_b - x_a)^2/4D\Delta\tau] \tag{7}$$

and

$$G_B(x_b,x_a;\Delta\tau) = \exp\left[-\left(\frac{1}{2}[V(x_a) + V(x_b)] - E_T\right)\Delta\tau\right], \tag{8}$$

where the diffusion constant is $D = \hbar^2/2m_e$ (=1/2 in atomic units for the electron).

With these equations one can simulate random-walk-with-branching procedure to find the imaginary time evolution. Carrying out the simulation iteratively with short enough time step $\Delta\tau$, large enough population of random walkers and adjusting the "trial energy" E_T to keep the simulation stationary will finally converge to the ground state wave function distribution of walkers and trial energy as the corresponding energy eigenvalue.

We should note, that Diffusion Monte Carlo method is generally used with trial wave functions [9,15], which makes DMC a significantly more powerful tool than without, in which case it deals with the ground states, only. Trial wave functions enable studies of larger system sizes, finding the lowest energy states of given symmetries and use of sc. mixed estimators for evaluation of physical quantities. Also, use of wave function nodes, if available, allows simulation of excited states [16,17].

Here, we use the simple DMC without trial wave functions to compare the features of DMC and our iRTPI approach, and more importantly, to be able to consider combination of these two Monte Carlo methods as another novel approach.

2.2. Real time propagation: RTPI

For the real time dynamics of a quantum many-body system $\psi(x, t)$ we define the Feynman path integral as

$$K(x_b,t_b;x_a,t_a) = \int_{x_a}^{x_b}\exp(\mathrm{i}S[x_b,x_a])\mathcal{D}x(t), \tag{9}$$

where $S[x_b, x_a] = \int_{t_a}^{t_b} L_x dt$ is the action of the path $x(t)$ from (x_a, t_a) to (x_b, t_b) and L_x is the corresponding Lagrangian [1,2]. This is the kernel (or real time Green's function) of the propagation.

Now, the time evolution of the wave function $\psi(x, t)$ (or probability amplitude), can be written as

$$\psi(x_b,t_b) = \int_a K(x_b,t_b;x_a,t_a)\psi(x_a,t_a)\mathrm{d}x_a, \tag{10}$$

where $t_a < t_b$. A more complete discussion about numerical time-dependent coherent PI solution for the full quantum dynamics is given elsewhere [4].

Now, we see the analogy of Eqs. (4) and (10), and the two propagators G and K. The latter of these is complex, bringing in the phase and interference of paths, an additional complication to numerical approaches, called "numerical sign problem" [18].

2.3. Incoherent RTPI

Here, we present the principle of incoherent real time propagation based on the numerical evaluation of $\psi(x, t)$ in discretized time grid, stepwise with Δt.

The real-time solution of the wave equation (1) has the form

$$\psi(x, t) = \sum_{n=0}^{\infty} C_n \phi_n(x) \exp[-\mathrm{i}(E_n - E_T)t], \tag{11}$$

analogously with the imaginary time solution, Eq. (3). By using the small angle approximation for short enough Δt this can be written [4] as

$$\psi(x, \Delta t) \approx \sum_{n=0}^{\infty} C_n \phi_n(x)\{1 - [(E_n - E_T)\Delta t]^2/2 - \mathrm{i}[(E_n - E_T)\Delta t]\}. \tag{12}$$

Now dropping off the imaginary part and keeping the real part of ψ, only, the single step time evolution leads to projection

$$\psi_{\mathrm{R}}(x, \Delta t) = \sum_{n=0}^{\infty} C_n \phi_n(x)\{1 - [(E_n - E_T)\Delta t]^2/2\}. \tag{13}$$

Repetition of wave function projection onto its real part removes the coherent phase factor in every time step. Therefore, we call this iteration of Eqs. (10) and (13) as incoherent propagation.

Now it is easy to see that this incoherent propagation (iRTPI) converges to one of the real eigenstates of the system. The dominant term in the sum in (13) is the one, where $\|E_n - E_T\|$ is least. Therefore, the iterative propagation of $\psi_{\mathrm{R}}(x, t)$ will converge to the real eigenstate ϕ_k with eigenenergy E_k closest to E_T, unless the initial $\psi_{\mathrm{R}}(x, t)$ is orthogonal to it ($C_k = 0$). However, even in such case we can expect the numerical inaccuracies to generate a small seed of any eigenstate ($C_k \neq 0$), and eventually, to lead to the expected convergence.

In comparison of Eqs. (3) and (13) we see that the imaginary time propagation can converge to the ground state of the system, only, while with the incoherent propagation E_T can be chosen arbitrarily to find any non-degenerate eigenstate ϕ_k. This seems to be the most essential difference between iRTPI and DMC.

In a graphical interpretation of Eq. (13) the real wave function rotates in complex plane clockwise an angle $(E_n - E_T)\Delta t/\hbar$, and then, becomes projected back to the real axis, walker by walker. The larger $(E_n - E_T)\Delta t$, the less of $\phi_n(x)$ remains in the projection. The hypothetical problem arising from the 2π periodicity of the angle can be eliminated by changing or decreasing the time step.

2.4. Kernel and its approximations

In general, the exact Kernel is rarely known and approximations are needed. A usual approximation is sc. "short time approximation" [19,3,4]

$$K(x_b, x_a; \Delta t) \approx \left[\frac{1}{2\pi \mathrm{i}\Delta t}\right]^{N/2} \exp\left[\frac{\mathrm{i}}{2\Delta t}(x_b - x_a)^2 - \frac{\mathrm{i}\Delta t}{2}(V(x_a) + V(x_b))\right], \tag{14}$$

which becomes exact as $\Delta t \to 0$. This is also called as Trotter kernel.

The product of Green's functions in Eqs. (7) and (8) is formally very similar to the propagator in Eq. (14), the exponential in the latter being complex causing oscillating wave behavior and numerical sign problem. This prevents interpretation of the Kernel straightforwardly as a probability. We use the kernel of Eq. (14) for simulation of time evolution, as in Eq. (10) in a short time step grid. Regular grids may work, but as discussed earlier [4], Monte Carlo grids generate less artificial interferences. We let the calculated real wave function $\psi_{\mathrm{R}}(x)$ guide evolution of the grid in the role of walkers by using Metropolis Monte Carlo algorithm [20]. Thus, in addition of the eigenenergy we obtain the wave function twice: calculated from the incoherent propagation, but also, represented by the walker distribution.

Wave oscillations in Eq. (14) are strongest for large distances $|x_a - x_b|$ and small time steps Δt. Therefore, the contributions of most paths (far from extrema of action) cancel efficiently by destructive interference, and in numerical calculations it is important not to waste time and efforts to those. Instead, it is necessary to choose or weight the paths with most constructive interference, *i.e.*, those with large wave function amplitude.

Increase of the number of walkers (grid size) will also damp the artificial interference [4] and there are other methods to make the kinetic term less oscillatory, *e.g.*, by using effective propagators [21,22]. Monte Carlo grids remove the interference arising from regularity, but bring in the roughness from randomness. This may cause lack of sufficient destructive interference of paths where the walker density is low, *i.e.*, where the wave function decays to zero. Smoothening of the roughness can be expected to help [4].

Our approach here is the following. The initial wave function $\psi(x_a, t_a)$ presented pointwise in a grid of walkers is "smoothened" to a "gaussianwise" presentation in the same grid by using Gaussian width parameter ϵ. We make it by modifying the kinetic part of the propagator as

$$\left[\frac{1}{2\pi \mathrm{i}\Delta t}\right]^{N/2} \exp\left[\frac{\mathrm{i}}{2\Delta t}(x_b - x_a)^2\right] \to \left[\frac{1}{2\pi(\mathrm{i}\Delta t + \epsilon^2)}\right]^{N/2} \exp\left[\frac{\mathrm{i}}{2(\Delta t - \mathrm{i}\epsilon^2)}(x_b - x_a)^2\right], \tag{15}$$

which converges back to the pointwise presentation as $\epsilon \to 0$.

The second part of kernel contributes to the numerical sign problem, if the potential is strongly variant along the paths, *i.e.*, if in Eq. (14) the change from $V(x_a)$ to $V(x_b)$ is far from linear or if $(V(x_a)+V(x_b))$ is locally variant for nearby paths. To the latter, only increase of walker density helps, whereas to the former, averaging over the path or decrease of the time step Δt is needed. Decrease of Δt leads essentially to decrease of $|x_a - x_b|$ due to the "destructive kinetic interference".

Averaging over the path could be done with some pseudo-potential. Such approximation could be tailored to include all the paths from x_a to x_b and remove the singularities, like the Δt dependent pair potential approximation widely used for the imaginary time propagation [5].

Here, we adopt a straightforward single path average approximation

$$V_{\mathrm{avg}} = \frac{1}{x_b - x_a}\int_{x_a}^{x_b} V(x)dx. \tag{16}$$

In one dimensional space this yields for the harmonic potential

$$V_{\mathrm{avg}}^{\mathrm{H}} = \frac{\omega^2}{6}\left[\frac{x_{1b}^3 - x_{1a}^3}{x_{1b} - x_{1a}} + \frac{x_{2b}^3 - x_{2a}^3}{x_{2b} - x_{2a}}\right] \tag{17}$$

and for the Coulomb potential

$$V_{\mathrm{avg}}^{\mathrm{C}} = \frac{\ln(r_b/r_a)}{r_b - r_a}, \tag{18}$$

where x_1 and x_2 are the particle coordinates, and $r_a = x_{1a} - x_{2a}$ and $r_b = x_{1b} - x_{2b}$ are the initial and final distances, as defined in the next section.

This result can also be acquired from a more sophisticated analysis and it is usually called semi-classical approximation [5].

3. Hooke's atom

The problem of two electrons in a harmonic potential, Hooke's atom, has been investigated by several authors [10,23–32]. There are even analytical solutions, but only for some specific parameters [10]. There are also numerical solutions and some approximate approaches, but to the ground state energy and wave function, only [33–40].

3.1. Separation of three dimensional problem

Consider two electrons with Coulomb repulsion in a harmonic potential well. With $m_e = 1$ the Hamiltonian of the system is

$$H(x_1, x_2) = -\frac{1}{2}\nabla_1^2 - \frac{1}{2}\nabla_2^2 + \frac{1}{2}\omega^2 x_1^2 + \frac{1}{2}\omega^2 x_2^2 + \frac{1}{|x_1 - x_2|}, \quad (19)$$

where x_1 and x_2 are the three coordinates of two electrons. The relative and center-of-mass (CM) motion of the electrons can now be separated by defining new three dimensional variables

$$r = x_1 - x_2 \quad \text{and} \quad R = \frac{x_1 + x_2}{2}. \quad (20)$$

Thus, the Hamiltonian decouples as

$$H(r, R) = -\frac{1}{2\mu}\nabla_r^2 + \frac{1}{2}\mu\omega^2 r^2 + \frac{1}{|r|} - \frac{1}{2M}\nabla_R^2 + \frac{1}{2}M\omega^2 R^2 \equiv H_r + H_R, \quad (21)$$

where $\mu = \frac{1}{2}$ and $M = 2$ are the reduced and the total mass of electrons. The wave function and total energy separates as $\psi(r, R) = \phi(r)\Phi(R)$ and $E = E_r + E_R$, respectively.

The CM motion is simple harmonic oscillation, which, of course, can further be separated into three one dimensional components. The relative motion of the two electrons is harmonic oscillation with the Coulomb repulsion as the perturbation. This equation can be separated into radial and angular components similarly to the dynamics of the hydrogen atom.

With substitution $\phi(r) = u(r)/r$ the radial equation of ground state takes the form

$$\left[-\frac{1}{2\mu}\frac{\mathrm{d}^2}{\mathrm{d}r^2} + \frac{1}{2}\mu\omega^2 r^2 + \frac{1}{r}\right] u(r) = E_r u(r). \quad (22)$$

To find the exact solution we must solve a three step recurrence equation [10], for which the solutions are restricted to some specific values of confinement parameters, only. For example, $\omega = \frac{1}{2}$ is one of the viable and the strongest confinement with ground state eigenenergy $E_r = \frac{10}{8}$ and wave function [10]

$$u(r) = r\phi(r) = r\frac{\mathrm{e}^{-r^2/8}\left(\frac{|r|}{2} + 1\right)}{\sqrt{\left(8 + 5\sqrt{\pi}\right)}}. \quad (23)$$

3.2. Analytical solutions for one dimensional hooke's atom

Oseguera and Llano [11] have proven that for the attractive one-dimensional Coulomb potential, the singularity acts as an impenetrable barrier and the space becomes divided into two independent regions (space splitting effect). Therefore, the solutions for positive and negative values of the relative coordinates of two particle are completely independent. Due to the space spitting effect for one dimensional Coulomb potential, the wave function of the two particles should vanish where their relative coordinate becomes zero.

Because of this, the relative dynamics in one dimension is that of the radial part in three dimensions for the angular momentum quantum number $\ell = 0$, Eq. (22), [10]. With the definitions of r and R in Eq. (20), in one dimension

$$\psi(r, R) = u(r)\Phi(R), \quad (24)$$

where $u(r)$ is the relative motion wave function in one dimension Eqs. (22)–(23). It is related to the three dimensional relative motion wave function with zero angular momentum via $r\phi(r) = u(r)$. In the one dimensional space the CM dynamics is simply that of one of the three R-components in Eq. (21). Thus, the ground state solution of $H_R\Phi = E_R\Phi$ is

$$\Phi(R) = \left(\frac{M\omega}{\pi}\right)^{1/4} \mathrm{e}^{-M\omega R^2/2}, \quad (25)$$

where $M = 2$ for electrons, and the corresponding energy is $E_R = \frac{1}{2}\hbar\omega$.

We have chosen this as the test case for the numerical methods, below. Thus, the ground state wave function $\psi(r, R) = u(r)\Phi(R)$ for one dimensional Hooke's atom with $\omega = \frac{1}{2}$ is given by Eqs. (23) and (25), which yields the energy of

$$E_0 = E_R + E_r = E_R + E_r^{\mathrm{kin}} + E_r^{\mathrm{pot}} = 0.25 + 0.28941 + 0.96058 = 0.25 + 1.25 = 1.5. \quad (26)$$

The exact relative coordinate wave function is illustrated as a solid line in Fig. 1, where it is also compared to those from PT. The differences between second order and third order perturbative solutions and exact solution are shown in Fig. 2.

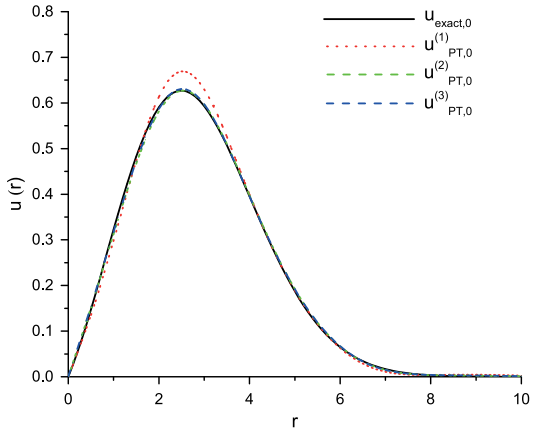

Fig. 1. Wave function of the ground state relative motion $u_0(r)$ for $\omega = 1/2$, exact (solid line) [10] and from the three lowest order PT (red dotted, green dash-dotted and blue dashed lines). (For interpretation of the references to color in this figure legend, the reader is referred to the web version of this article.)

3.3. Solutions from perturbation theory

Now, let us consider the Coulomb interaction as perturbation in Eq. (22). Then, the unperturbed wave function and first order energy corrections are

$$u_n^0(r) = \frac{\frac{1}{\sqrt[4]{\pi}}\sqrt{\xi}\exp\left(-\xi^2 r^2/2\right) H_n(\xi r)}{\sqrt{2^n n!}}, \quad (27)$$

$$\delta E_n^1 = 2e^2 \int_0^\infty \frac{u_{2n+1}^{0*}(r) u_{2n+1}^0(r)}{|r|} dr, \quad (28)$$

$$\xi = \sqrt{\frac{\mu\omega}{\hbar}}, \quad (29)$$

where $H_n(r)$ are the Hermite Polynomials with $n = 0, 1, 2, \ldots$.

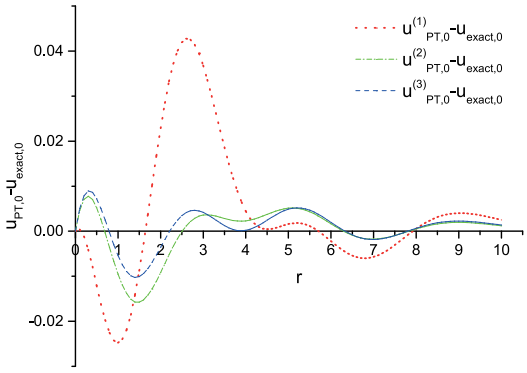

Fig. 2. The differences between the exact solution and different order PT results are shown. The first, second and third order corrections are shown by the dots (red), dot–dash (green) and dash (blue) lines respectively. The highest order PT has the best accuracy. (For interpretation of the references to color in this figure legend, the reader is referred to the web version of this article.)

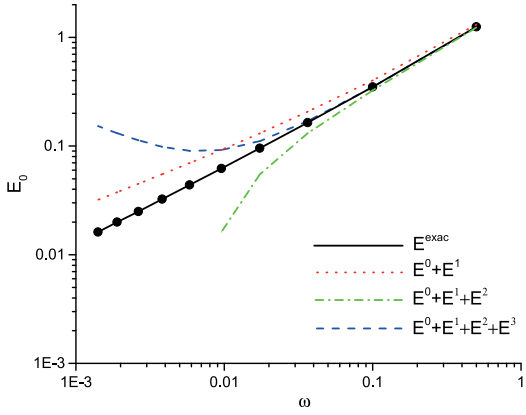

Fig. 3. Comparison of the ground state energies, exact [10] (black dots) and those from the PT (lines with the same notations as in Fig. 1). The highest energy dot ($\omega = 1/2$) corresponds the wave functions in Fig. 1.

To calculate the higher order energy corrections and wave function, we need matrix elements of the Coulomb potential. Generally, all of these cannot be found in closed form, but for the ground state we can write

$$V_{0,n} = \frac{e^2\xi\sqrt{2^{n+1}n!}}{n!\Gamma\left(1-\frac{n}{2}\right)}, \quad n \geq 1 \tag{30}$$

where Γ is the Gamma function.

Then, up to the second order, the perturbative approximation of the ground state energy is

$$E_0 = \frac{3}{2}\hbar\omega + 2e^2\sqrt{\frac{\mu\omega}{\pi\hbar}} + \sum_{n=1}^{\infty}\frac{|V_{0,2n+1}|^2}{-2n\omega\hbar}. \tag{31}$$

Fig. 3 shows the ground state energy as a function of ω. As the figure shows, for small values of ω the perturbative solutions do not converge to the exact values. We should notice that the PT is valid only as long as the condition $V_{nn} \ll |E_{n+1} - E_n|$ holds.

Average value of the kinetic energy can be used as a limit for validity of the perturbation method. In the first order perturbative approximation, the average kinetic energy of relative motion for ground state, becomes negative for $\omega < 4e^4\mu/9\pi\hbar^3 \approx 0.07073$ in au, and therefore, it can be chosen as the minimum acceptable frequency $\omega_{\min}$ in perturbation method for ground state.

Clearly, the perturbation theory, Eq. (31), works better for strong confinements, $\omega > 0.5$, where numerical approaches and other methods may become inaccurate. For $\omega = 0.5$ the ground state energy for relative motion is 1.25 and perturbation theory yields 1.314, 1.238 and 1.248 for the 1st, 2nd and 3rd order, respectively, whereas 0.75 and 1.1830 are found by approximations for strong (ignoring e–e interaction) and weak (harmonic approximation) confinements [10].

4. Monte Carlo simulations

We assess performance and accuracy of numerical solutions by using the above defined one dimensional Hooke's atom with $k = \omega^2 = 1/4$, *i.e.*, $\omega = 0.5$, as the test bench. First of all we consider our novel incoherent RTPI, as compared with diffusion Monte Carlo. Finally, we introduce one more novel method by combining these two.

4.1. Incoherent RTPI

To assess the performance of incoherent RTPI we first use constant width parameter $\epsilon^2 = 0.005$, see Eq. (15), and monitor the accuracy with respect to time step Δt and grid size N. The data is collected in Table 1 and partly also shown in Figs. 4 and 5 in graphical form.

We see that the accuracy improves with increasing grid size, as expected. We find an optimal size for the time step, roughly at $\Delta t = 0.1$, for the modified Trotter kernel. Shorter time steps strongly increase the error in the kinetic part of the propagator, whereas longer time steps increase that of the potential part, as discussed in sec. 2.4. Increasing time step also reduces the accuracy of Trotter kernel approximation. Shorter time steps can be used only with significantly larger grid size.

To allow estimation of convergence and statistical error of energies for practical calculations the standard deviations are given. It can be used to estimate the statistical accuracy (precision) of evaluated expectation values in form of standard error of mean, $\mathrm{SEM} = \sigma/\sqrt{N}$, where N is the number of uncorrelated Monte Carlo steps. Usually, $2 \times$ SEM limits (95%) are assumed as a statistical error estimate. For the present test cases evaluation of SEM is not relevant.

Next we keep the grid size and time step constant, $N = 30 \times 10^3$ and $\Delta t = 0.1$ and investigate the effect of the width parameter ϵ^2. The data is collected in Table 2. Obviously, the larger the grid size, the smaller ϵ can be used, increasing the accuracy. However, ϵ at least of the size of the average distance of walkers "smoothens" the wave function also increasing accuracy. On the other hand, the last line of Table 2 proves that $\epsilon \approx 0.3$ is still applicable, though the value $\epsilon \approx 0.07$. ($\epsilon^2 = 0.005$) was found the best with $N = 30 \times 10^3$.

In Fig. 6 the difference between calculated wave function and the exact one is shown in terms of the root-mean-square deviation as a function of time step length. This data have the same trends as the error in total energy in Fig. 4.

For more detailed analysis of the wave function we will consider the relative motion and CM motion separately. First, Fig. 7 shows a plot of all walkers (a snapshot of Monte Carlo grid points) as red dots at the walker coordinates $(r, u(r))$, *i.e.*, the relative coordinate and real amplitude. The green line shows the maximum amplitude given by Eq. (23). This is the simulation case of the last line of Table 2. We see that the wave function match is pretty good, but the energetics is not.

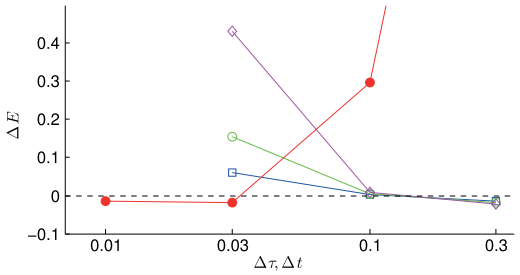

Fig. 4. Error in the calculated total energy ΔE from its exact value 1.5 as a function of time step in atomic units, Δt (iRTPI) and τ (DMC). Symbols for RTPI are magenta open diamonds, green open circles and blue open squares for $N = 10$k, 30k and 100k, respectively; and for DMC red full circles for 30k. Dashed line shows zero reference. (For interpretation of the references to color in this figure legend, the reader is referred to the web version of this article.)

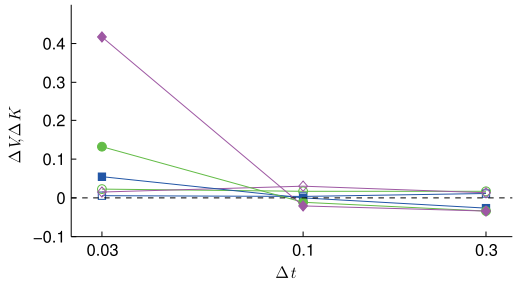

Fig. 5. Error in the calculated potential and kinetic energies, ΔV and $\Delta E - \Delta V$, from their exact values 1.0856 . . . and 0.4144 . . . respectively as a function of time step Δt. Open markers show the potential energy and filled markers the kinetic energy. Otherwise notations are the same as in Fig. 4. When comparing with Fig. 4 we can see that most of the error comes from kinetic energy.

Table 1
Accuracy and distribution of energetics in incoherent RTPI simulations of the ground state. N is the number of walkers ($k = 10^3$), Δt the time step, ΔE deviation of expectation values from the exact value 1.5, ΔV deviation of expectation value from the exact value 1.0856 . . ., σ standard deviation in 20 blocks of data with 50 iterations in block and ϵ^2 the "gaussian width of walkers" discussed in Section 2.2. (All quantities in atomic units).

N	Δt	ΔE	σ_E	ΔV	σ_V	ϵ^2
100k	0.3	−0.0152	0.0008	0.0109	0.0017	0.005
100k	0.1	0.0032	0.0014	0.0039	0.0021	0.005
100k	0.03	0.0601	0.0135	0.0054	0.0014	0.005
30k	0.3	−0.0185	0.0016	0.0161	0.0042	0.005
30k	0.1	0.0046	0.0058	0.0172	0.0111	0.005
30k	0.03	0.1544	0.0333	0.0221	0.0247	0.005
10k	0.3	−0.0220	0.0030	0.0126	0.0062	0.005
10k	0.1	0.0077	0.0123	0.0296	0.0505	0.005
10k	0.03	0.4324	0.0653	0.0154	0.0045	0.005

Another snapshot of walkers is shown in Fig. 8. This plot presents the complex amplitude in complex plane after one time step starting from the real wave function, Eq. (13), *i.e.*, starting from all the walkers lying in the real axis according to the amplitude. With the walkers perfectly representing the stationary state one expects no other changes than rotation of all walkers around origin corresponding to the phase $\varphi \propto (E_0 - E_T)/\Delta t$ and retaining their absolute value (modulus). Fig. 8 shows the case, where $E_T = E_0$, and thus, $\varphi = 0$ is expected. Therefore, deviations from the real axis present numerical or statistical error emerging from the random nature of Monte Carlo grid in the figure. Thus, the imaginary components of amplitude are zero in average and large deviations from the average, shown in red and green, point out the

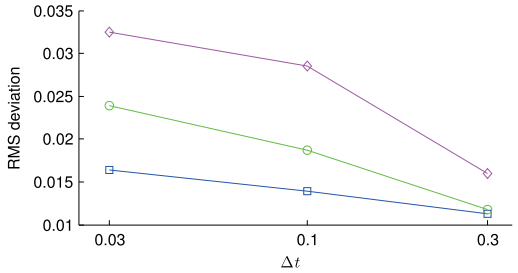

Fig. 6. RMS deviation of the calculated and analytical wave functions as a function of time step Δt. Notations are the same as in Fig. 4.

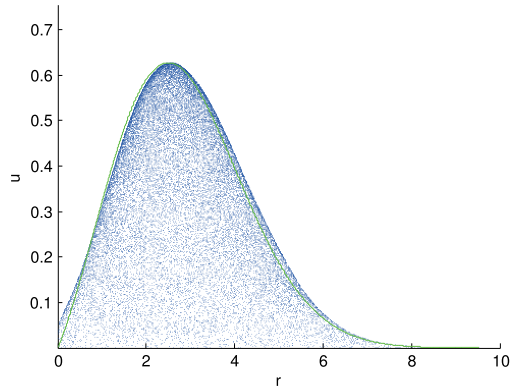

Fig. 7. Snapshot of the simulation for relative motion wave function with $N = 30$k, $\Delta t = 0.1$ and $\epsilon^2 = 0.1$. The blue dots show walkers projected onto the plane $(r, u(r))$. Green line shows the corresponding exact wave function $u(r)$, Eq. (23) for $R_{CM} = 0$. The maximum amplitude of walkers is scaled to match the maximum of the analytical maximum and r is in and atomic units. (For interpretation of the references to color in this figure legend, the reader is referred to the web version of this article.)

Table 2
Effect of the gaussian width of walkers. Notations are the same as in Table 1.

N	Δt	ΔE	σ_E	ΔV	σ_V	ϵ^2
30k	0.1	−0.0235	0.0068	0.0510	0.0168	0
30k	0.1	0.0025	0.0037	0.0146	0.0112	0.005
30k	0.1	−0.0118	0.0024	0.0848	0.0194	0.1

walkers with largest error. Note the different scaling of real and imaginary axes.

The same walkers as in Fig. 8 are shown in Fig. 9, but now in two dimensional cartesian coordinate system of (x_1, x_2), the coordinates of the two electrons in one dimension. Now, we see that the walkers showing the most erroneous phase in Fig. 8 are those in the region with the lowest density, where the wave function decays to zero. Obviously, the sparse walker density is not able to describe the amplitude smoothly, enough.

The sparse grid problem is expected but cannot be avoided, in case the walker density represents the wave function amplitude in the region of almost vanishing wave function. Increase of the walker width parameter ϵ^2 helps until it starts to adversely round the shape of the wave function in other regions, see Fig. 7.

In Figs. 10 and 11 two different projections of again the same set of walkers are shown. The real amplitude is presented as a function of the relative and CM coordinate, *i.e.*, walkers in planes $(r, u(r))$ and $(R, u(r))$, respectively. Thus, Fig. 10 is the same projection as

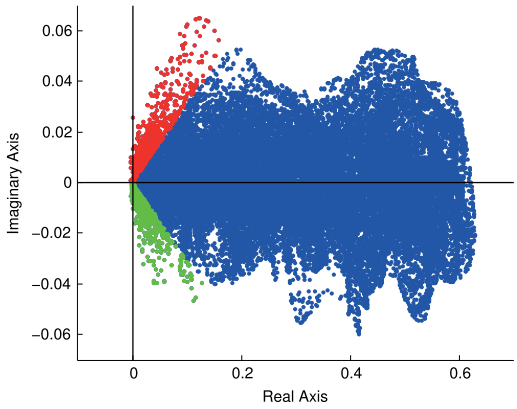

Fig. 8. The complex wave function phase evolution of the real ground state in one time step ($\Delta\varphi = 0$ expected.). Note the different scaling of axes. Color coding: red for $\Delta\varphi > 0.3$ and green for $\Delta\varphi < -0.3$. These walkers are more than 20% off from the known expectation value of energy. $N = 30{,}000$, $\Delta t = 0.1$ and $\epsilon^2 = 0.005$. (For interpretation of the references to color in this figure legend, the reader is referred to the web version of this article.)

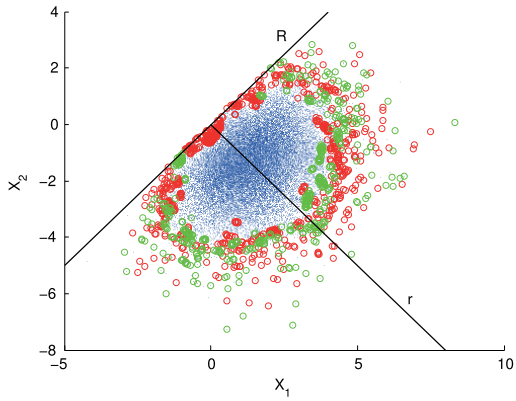

Fig. 9. Plot of the same walkers as in Fig. 8, but now in a plane of coordinates of electrons (x_1, x_2) in atomic units. The color coding is the same, but size of blue and other walkers is smaller and larger, respectively. The CM and relative coordinate axes are also shown. (For interpretation of the references to color in this figure legend, the reader is referred to the web version of this article.)

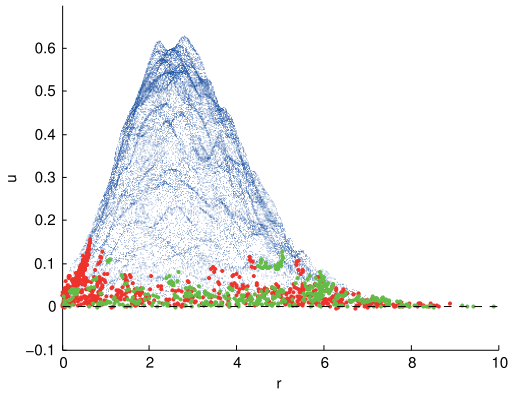

Fig. 10. Snapshot of the calculated wave function in the relative motion coordinates with $N = 30{,}000$, $\Delta t = 0.1$ and $\epsilon^2 = 0.005$. The walkers and the color coding are the same as in Figs. 8 and 9. Units are the same as in Fig. 7. (For interpretation of the references to color in this figure legend, the reader is referred to the web version of this article.)

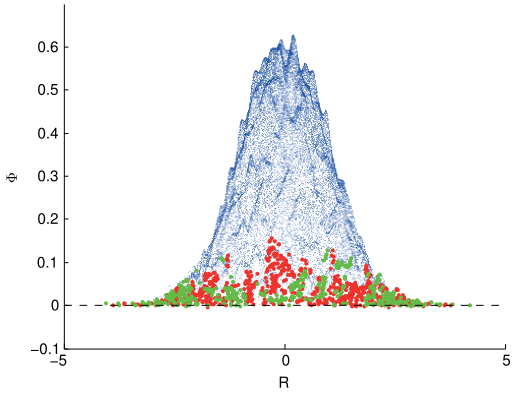

Fig. 11. Snapshot of the calculated wave function in the center of mass coordinates with $N = 30{,}000$, $\Delta t = 0.1$ and $\epsilon^2 = 0.005$. The walkers and the color coding are the same as in Figs. 8–10. Units are the same as in Fig. 7. (For interpretation of the references to color in this figure legend, the reader is referred to the web version of this article.)

that in Fig. 7, but now from a simulation with better numerical parameters as judged by the accuracy of energetics in Table 1.

Now, we see strong fluctuations in amplitude with the RMS deviation from the exact wave function given in Fig. 6. Cumulative averaging over the Monte Carlo simulation, however, smoothens these fluctuations away.

4.2. Simple DMC

Diffusion Monte Carlo in its most efficient form includes the use of trial wave functions. Here we introduced only the simple DMC approach in order to allow straightforward comparison with RTPI. Moreover, simple DMC and RTPI can be combined to a novel method with new practical properties that simplify the calculation of various observables, not just the total energy. This will be discussed in the next subsection in more detail.

Since Hooke's atom does not involve attractive singular Coulomb potentials, only $+\frac{1}{r}$, the Trotter break-up is valid and the branching term in Eq. (8) does not diverge. Therefore, sampling without a trial wave function can be expected to give accurate results with sufficiently small imaginary time step and large enough number of walkers.

The data in Table 3 shows that the total energy converges to its exact value as the imaginary time step $\tau \to 0$. By comparing the data in Table 1 we see that with optimal parameters and the same number of walkers N, RTPI gives similar accuracy as simple DMC, if only the number of Monte Carlo steps matters.

However, RTPI is computationally much more demanding. This stems from the fact, that for each MC step in DMC algorithm, only N moves of walkers guided by the potential function is needed, but with the present incoherent RTPI we need to calculate $N \times N$ real time propagations to evaluate the guiding distribution before moving the walkers.

4.3. Combination of DMC and RTPI

The simple DMC algorithm samples the nodeless ground state distribution, which makes it cumbersome and inefficient to

Table 3
Accuracy and distribution of energetics in DMC simulations of the ground state. Number of walkers is $N = 30$k, τ is the imaginary time step, ΔE deviation of the expectation value from its exact value 1.5 and σ is the standard deviation of 20 blocks of data. Each block consists of 50 iterations. A new energy estimate was calculated after each block.

τ	ΔE	σ
1	−0.0526	0.0008
0.3	−0.0197	0.0016
0.1	−0.0096	0.0034
0.03	−0.0063	0.0049
0.01	−0.0041	0.0085
0.001	0.0137	0.0235

Table 4
Incoherent RTPI combined with DMC. The walker distribution $N = 30$k is sampled by DMC with ($\tau = 0.01$) and RTPI step length is $\Delta t = 0.1$. Evaluated expectation values and DMC total energy are given with their standard deviations. Notations are the same as in the previous Tables. DMC is calculated from 20 blocks of data with 50 iterations per block. RTPI step is run once for every other block.

	ΔE	σ_E	ΔV	σ_V	ϵ^2
RTPI	0.0033	0.0060	0.0022	0.0039	0.005
DMC	−0.0041	0.0085			

evaluate expectation values for observables other than the total energy, even as simple as the potential energy. This is due to the availability of the wave function in form of walker distribution, only. Thus, in evaluation of the expectation value matrix elements the walker distribution implicitly contributes as the bra wave function, but ket is not available.

For direct sampling of matrix elements another representation of the wave function, the ket vector, is needed. For this purpose the incoherent RTPI on DMC walkers can be used. Then, also the overlap integral and potential energy become straightforward to sample for

$$\langle V \rangle = \frac{\langle \psi \mid V \mid \psi \rangle}{\langle \psi \mid \psi \rangle}. \tag{32}$$

Similarly, expectation values for any local multiplicative operators become available. Also, another total energy estimate is obtained from sampling the phase evolution in real time.

The incoherent RTPI can be used to evaluate, not only the ground state, but also the excited states with the positive and negative amplitudes, and thus, it provides means for locating the nodal surfaces. This suggests combining the two approaches for evaluation of excited states, or in general, states with nodes in the spirit of released nodes idea; RTPI would be used in finding the nodes and evaluating another wave function, as well as another total energy, while DMC is used to sample the paths for RTPI. This has potential for increasing the usefulness and capabilities of the simple DMC approach.

For practical use the number of RTPI steps can be kept much less than the DMC steps. In case nodal information is not needed, only one RTPI step at the end may be sufficient. Evaluation of statistical precision calls for more than that, of course.

In Table 4 we show the data evaluated with the combined approach. The underlying DMC has been run with $\tau = 0.01$, see Table 3 and RTPI on top of that with $\Delta t = 0.1$ with the optimal choice of other parameters, see above. RTPI step has been run once for every other block of 50 DMC steps.

We find that DMC sampling of walkers from the distribution derived from the potential function leads to smoother spatial distribution than that of guided by the wave function amplitude from RTPI. This can be clearly seen by comparing the distributions in Figs. 9 and 12, and also, the amplitudes in Figs. 10 and 13. This also yields better energetics which can be seen by comparing the values

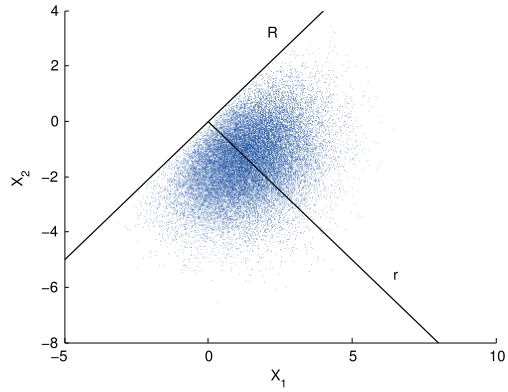

Fig. 12. DMC simulation snapshot of walker distribution in a plane of coordinates of electrons (x_1, x_2) and separated coordinates (r, R), in atomic units. Parameters $\tau = 0.001$ and $N = 30{,}000$ were used.

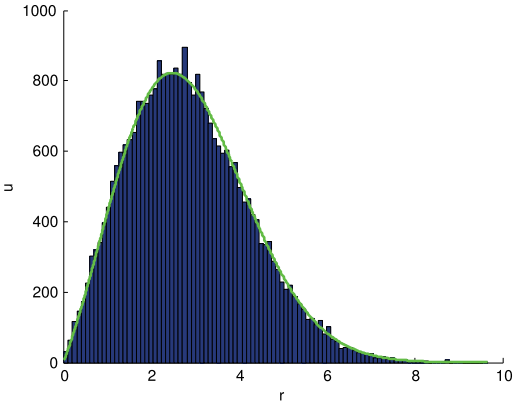

Fig. 13. Snapshot histogram of walker distribution in DMC simulation with $\tau = 0.001$ and $N = 30{,}000$. $\mid x_b - x_a \mid$ projection. Green line is the analytical solution fitted to the data. u is the number of walkers in each bin and r is in atomic units. (For interpretation of the references to color in this figure legend, the reader is referred to the web version of this article.)

from Tables 1 and 4. In the latter one there are less stray walkers at very low density region. We assume that the reason for this is in the different nature of the guiding distribution: for DMC it is stable well-defined potential, while for the Metropolis algorithm in RTPI it is the calculated amplitude presented in the Monte Carlo grid. This problem is always present at the region of low walker density.

Thus, if more stability is needed and larger number of walkers becomes too expensive, it may be necessary to use cumulative distribution of the amplitude from several previous RTPI steps. According to our preliminary testing, same type of problem may arise in locating the nodal surfaces accurately enough. Use of the cumulative distributions calls for numerical algorithms for efficient interpolation and updating the collected data.

Based on the experience, so far, the combination of the simple Diffusion Monte Carlo and incoherent Real Time Path Integral methods form a novel approach for electronic structure calculations that is capable of extending usefulness of the former. However, its significance remains to be tested in practice.

5. Conclusions

We have introduced a new approach based on the incoherent real time path integrals (iRTPI) for ground and excited state electronic structure calculations. It includes correlations between electrons exactly, within the numerical accuracy, which can be made better than the systematic error from the kernel simply by using Monte Carlo technique. Here, we use Hooke's atom, a two-electron system with very strong correlation, as our test case, which we solve with both iRTPI and diffusion Monte Carlo (DMC) for comparison. The high accuracy and stability of iRTPI is demonstrated, and the improved Trotter kernel is shown to be useful with large enough number of Monte Carlo walkers. In addition, useful numerical parameters for the present case have been determined for stable and self-consistent simulations.

In its present form the computational cost of iRTPI is significantly higher than that of DMC. However, one of the advantages of iRTPI is that it provides one with the wave function explicitly, and thus, the evaluation of local multiplicative expectation values becomes straightforward. Moreover, it is also capable of locating excited states, and thus, the related nodal surfaces, the technical details of which were not considered here. In addition, incoherent dynamics can be turned to coherent dynamics, in case quantum dynamics is relevant.

We also showed that another novel approach obtained by combining the iRTPI and DMC methods allows a more straightforward means for evaluation of various observables within the robust framework of DMC. Due the capability of iRTPI for locating the nodal surfaces, it will be interesting to further test this combination method in a released node fashion of DMC. This would mean a trial wave function free DMC also for fermions.

Perturbation theory was shown to be useful for analytical solutions in case of strong confinements, which may become more challenging for numerical methods and available approximate solutions. On the other hand, for weak confinements, *e.g.* in quantum dots, the presented numerical iRTPI method is expected to be robust.

Acknowledgments

For computational resources we like to thank the Techila Technologies facilities and TCSC at Tampere University of Technology, and also, services of the Finnish IT Center for Science (CSC).

References

[1] R.P. Feynman, A.R. Hibbs, Quantum Mechanics and Path Integrals, McGraw-Hill, New York, 1965.
[2] R.P. Feynman, Rev. Modern Phys. 20 (1948) 367.
[3] N. Makri, Comput. Phys. Commun. 63, 389–414; N. Makri; Chem. Phys. Lett. 193, (1992) 435.
[4] Ilkka Ruokosenmäki, Tapio T. Rantala, Commun. Comput. Phys. 18 (2015) 91.
[5] D.M. Ceperley, Rev. Modern Phys. 67 (1995) 279.
[6] I. Kylänpää, (Ph.D. Thesis), Tampere University of Technology, 2011.
[7] I. Kylänpää, T.T. Rantala, J. Chem. Phys. 133 (2010) 044312;
I. Kylänpää, T.T. Rantala, J. Chem. Phys. 135 (2011) 104310;
I. Kylänpää, T.T. Rantala, Phys. Rev. A 80 (2009) 024504.
[8] Militzer, D.M. Ceperley, Phys. Rev. B 63 (2001) 066404.
[9] B.L. Hammond, W.A. Lester Jr., P.J. Reynolds, Monte Carlo Methods in Ab initio Quantum Chemistry, World Scientific, 1994.
[10] M. Taut, Phys. Rev. A 48 (1993) 5.
[11] U. Oseguera, M. de Llano, J. Math. Phys. 34 (1993) 4575.
[12] Taksu Cheon, T. Shigehara, Phys. Rev. Lett. 82 (1999) 12.
[13] M. Girardeau, J. Math. Phys. 1 (1960) 516.
[14] A.G. Volosniev, D.V. Fedorov, A.S. Jensen, M. Valiente, N.T. Zinner, Nature Commun. 5 (2014) 5300.
[15] C.J. Umrigar, M.P. Nightingale, K.J. Runge, J. Chem. Phys. 99 (1993) 2865.
[16] D.M. Ceperley, J. Stat. Phys. 63 (1991) 1237.
[17] Norm M. Tubman, Ilkka Kylänpää, Sharon Hammes-Schiffer, David M. Ceperley, Phys. Rev. A 90 (2014) 042507.
[18] T.D. Kieu, C.J. Griffin, Phys. Rev. E 49 (1994) 3855–3859.
[19] L.S. Schulman, Techniques and Applications of Path Integration, Wiley, New York, 1981.
[20] N. Metropolis, A.W. Rosenbluth, M.N. Rosenbluth, H. Teller, E. Teller, J. Chem. Phys. 21 (1953) 1087.
[21] V.S. Filinov, Nucl. Phys. B 271 (1986) 717–725.
[22] N. Makri, J. Math. Phys. 36 (1995) 2430–2456.
[23] Pierre François Loos, Peter M.W. Gill, J. Chem. Phys. 131 (2009) 241101.
[24] M. Taut, Phys. Rev. B 63 (2001) 115319.
[25] T. Sako, G.H.F Diercksen, J. Phys.: Condens. Matter. 15 (2003) 5487–5509.
[26] Orion Ciftja, Phys. Scr. 88 (2013) 058302.
[27] Lin-Wang Wang, arXiv:cond-mat/9805031v3.
[28] H. Sprekeler, G. Kielich, A. Wacker, E. Schöll, Phys. Rev. B 69 (2004) 125328.
[29] Ronald J. White, W. Byers Brown, J. Chem. Phys. 53 (1970) 3869.
[30] O.V. Kibis, Phys. Lett. A 166 (1992) 393–394.
[31] P.M.W. Gill, D.P. O'Neilla, J. Chem. Phys. 122 (2005) 094110.
[32] Garnett W. Bryant, Phys. Rev. Lett. 59 (10) (1987) 1140.
[33] Debbie Futai Tuan, J. Chem. Phys. 50 (1969) 2740.
[34] Pinchus M. Laufer, J.B. Krieger, Phys. Rev. A 33 (3) (1986) 1480.
[35] N.R. Kestner, O. Sinanoglu, Phys. Rev. 128 (1962) 2687.
[36] John M. Benson, W. Byers Brown, J. Chem. Phys. 53 (1970) 3880.
[37] Jerzy Cioslowski, Katarzyna Pernal, J. Chem. Phys. 113 (2000) 8434.
[38] Darragh P. O'Neill, Peter M.W. Gill, Phys. Rev. A 68 (2003) 022505.
[39] S. Kais, D.R. Herschbach, N.C. Handy, C.W. Murray, G.J. Laming, J. Chem. Phys. 99 (1993) 417.
[40] S. Kais, D.R. Herschbach, R.D. Levine, J. Chem. Phys. 91 (1989) 7791.

PUBLICATION

III

Eigenstates and Dynamics of Hooke's Atom: Exact Results and Path Integral Simulations

H. Gholizadehkalkhoran, I. Ruokosenmäki and T. T. Rantala

Journal of Mathematical Physics 59.(2018)
DOI: 10.1063/1.5028503

Eigenstates and dynamics of Hooke's atom: Exact results and path integral simulations

Hossein Gholizadehkalkhoran, Ilkka Ruokosenmäki, and Tapio T. Rantala

Citation: Journal of Mathematical Physics **59**, 052104 (2018); doi: 10.1063/1.5028503
View online: https://doi.org/10.1063/1.5028503
View Table of Contents: http://aip.scitation.org/toc/jmp/59/5
Published by the American Institute of Physics

JOURNAL OF MATHEMATICAL PHYSICS **59**, 052104 (2018)

Eigenstates and dynamics of Hooke's atom: Exact results and path integral simulations

Hossein Gholizadehkalkhoran, Ilkka Ruokosenmäki, and Tapio T. Rantala
Physics, Tampere University of Technology, P.O. Box 692, FI-33101 Tampere, Finland

(Received 11 March 2018; accepted 24 April 2018; published online 11 May 2018)

The system of two interacting electrons in one-dimensional harmonic potential or Hooke's atom is considered, again. On one hand, it appears as a model for quantum dots in a strong confinement regime, and on the other hand, it provides us with a hard test bench for new methods with the "space splitting" arising from the one-dimensional Coulomb potential. Here, we complete the numerous previous studies of the ground state of Hooke's atom by including the excited states and dynamics, not considered earlier. With the perturbation theory, we reach essentially exact eigenstate energies and wave functions for the strong confinement regime as novel results. We also consider external perturbation induced quantum dynamics in a simple separable case. Finally, we test our novel numerical approach based on real-time path integrals (RTPIs) in reproducing the above. The RTPI turns out to be a straightforward approach with exact account of electronic correlations for solving the eigenstates and dynamics without the conventional restrictions of electronic structure methods. *Published by AIP Publishing.* https://doi.org/10.1063/1.5028503

I. INTRODUCTION

The problem of two electrons confined in a harmonic potential, sc. Hooke's atom, has been investigated by several authors.[1–8] There are analytical solutions of the ground and excited states, but only for some specific confinement parameters or oscillator frequencies.[1] There are also some approximate and numerical approaches to solve the problem, but all of these are focused on the ground state energy and wave function of the three-dimensional system.[8–13]

Solution of the problem can be reduced to those of center-of-mass (CM) and internal dynamics, and the latter one, further to radial and angular components. The radial component is the solution at the positive and negative parts of one-dimensional space, and thus, it turns out to form the solutions of one-dimensional Hooke's atom—analytically for the above-mentioned specific set of confinement parameters. These two parts can be combined to form symmetric and antisymmetric spatial wave functions as singlet and triplet (or bosonic and fermionic) states, respectively.

However, the one-dimensional Coulomb potential is not trivial to consider, and therefore, it has been a case of interest since 1959.[14] It has been argued in many previous studies[14–19] that only the odd wave functions are valid solutions of the Schrödinger equation. More recent studies on one dimensional strongly interacting confined quantum systems[21–26] and previous studies on relativistic and non-relativistic one dimensional Coulomb potential[14–20,27,28] motivate us to revisit the problem and demonstrate how to find solutions for all eigenstates and all confinement parameters both analytically and numerically.

Oseguera and de Llano[29] have proven that for the attractive one-dimensional Coulomb potential the singularity acts as an impenetrable barrier and space is divided into two independent domains. This is called the space splitting effect. Therefore, solutions for the positive and negative values of the relative coordinates of a two-particle system are completely independent. In one-dimension, the attractive delta function interaction and Coulomb interaction both cause the space splitting, too.[29]

Due to the space splitting, the relative coordinate wave function of two particles should vanish at the origin. Extension of the problem to repulsive Coulomb potential is simple. It is enough to replace $-e^2 \rightarrow e^2$, and again, it can be shown similar to the attractive Coulomb interaction that the amplitude

of reflection coefficient for repulsive Coulomb interaction equals to one and the singularity acts as an impenetrable barrier.[29]

In this study, we complete the numerous earlier studies by presenting solutions from the perturbation theory (PT) for all confinement parameters, and also, for both the ground state and excited states dynamics. We assess the accuracy of PT solutions as a function of confinement and order of PT. Our analytical PT results give better match with the exact numerical solutions in a strong confinement region as compared with interpolation formula in Ref. 1.

Furthermore, with a novel numerical approach based on Feynman path integral formalism in real time (RTPI),[30] we find wave functions, energetics, and dynamics of such a strongly correlated system to confirm the PT results and trends. We also assess the robustness of RTPI for excited states and dynamics, where it is applied for the first time.

In Sec. II, we introduce PT and RTPI for the one-dimensional confined charged particles. In Sec. III, we give the PT and RTPI solutions to Hooke's atom and assess the quality and accuracy by comparing with exact solutions for both eigenstates and quantum dynamics in an external time-dependent electric field.

II. MODEL AND METHODS

A. Separation of variables

The Hamiltonian of two electrons in a 3D harmonic well is

$$H = \frac{-\hbar^2}{2m_e}\nabla_1^2 + \frac{-\hbar^2}{2m_e}\nabla_2^2 + \frac{1}{2}m_e\omega^2 x_1^2 + \frac{1}{2}m_e\omega^2 x_2^2 + \frac{e^2}{|x_1 - x_2|}, \tag{1}$$

where x_1 and x_2 are the three coordinates of electrons 1 and 2, respectively. The relative and center of mass (CM) motion of the two electrons can be separated by defining new variables

$$r = x_1 - x_2$$

and

$$R = \frac{x_1 + x_2}{2}.$$

Now, the Hamiltonian separates as

$$H = H(r) + H(\ell) + H(R),$$

where $H(\ell) = \ell(\ell + 1)\hbar^2/2\mu r^2$ is the rotational part. For the rotational ground state of the relative motion ($\ell = 0$), one can rewrite the above Hamiltonian as follows:

$$\begin{aligned} H &= \frac{-\hbar^2}{2\mu}\frac{d^2}{dr^2} + \frac{1}{2}\mu\omega^2 r^2 + \frac{e^2}{|r|} + \frac{-\hbar^2}{2M}\nabla_R^2 + \frac{1}{2}M\omega^2 R^2 \\ &= H(r) + H(R), \end{aligned} \tag{2}$$

where $\mu = m_e/2$ and $M = 2m_e$ are the reduced and the total mass of electrons, respectively. If separating the wave function and total energy as $\psi(r, R) = \frac{u(r)}{r}\Phi(R)$ and $E_{tot} = E + E_{CM}$, then the CM motion is simple harmonic oscillation in all three dimensions

$$\frac{-\hbar^2}{2M}\frac{d^2}{dR^2}\Phi + \frac{1}{2}M\omega^2 R^2\Phi = E_{CM}\Phi, \tag{3}$$

where $E_{CM} = (N + 1/2)\hbar\omega$ with non-negative integers N. Relative motion of the electrons is harmonic oscillation with the Coulomb interaction as a perturbation in the rotational ground state ($\ell = 0$),

$$-\frac{\hbar^2}{2\mu}u''(r) + (\frac{1}{2}\mu\omega^2 r^2 + \frac{e^2}{|r|})u(r) = Eu(r). \tag{4}$$

Equations (3) and (4) define the dynamics of 1D Hooke's atom without external fields. The solutions are bound states with quantized energies and those of the CM are states of a simple harmonic oscillator.

B. Perturbation theory

In this section, we review the PT and its applicability in one dimensional confined quantum systems with Coulomb potential as the interparticle interaction.

1. Reference states and boundary conditions

Equation (4) remains as the one dimensional Schrödinger equation to be solved. It would be natural to consider the Coulomb repulsion as perturbation and choose the harmonic oscillator as the reference system. However, in one-dimensional PT because of the space spitting effect, we are looking for solutions of relative motion with the boundary condition and symmetry like those of one-dimensional hydrogen atom at the origin[14–19]

$$u(0) = 0. \tag{5}$$

This means that the odd numbered eigenstates of harmonic oscillator (4), only, are acceptable. Then, the exactly solvable problem with the same boundary condition as one dimensional Coulomb potential is[31]

$$-\frac{\hbar^2}{2\mu}\zeta_n''(r) + \frac{1}{2}\mu\omega^2 r^2 \zeta_n(r) = \epsilon_n \zeta_n(r), \tag{6}$$

where ζ_n are the eigenstates of one dimensional harmonic potential. The exact solutions are

$$\zeta_n(r) := \frac{\left(\frac{1}{\sqrt[4]{\pi}}\sqrt{\xi}\right)\exp\left(\frac{-1}{2}\xi^2 r^2\right)H_n(\xi r)}{\sqrt{2^n n!}},$$
$$\epsilon_n = (n + \frac{1}{2})\hbar\omega,$$
$$\xi = \sqrt{\frac{\mu\omega}{\hbar}},$$
$$n = 1, 3, 5, \ldots$$

where H_n are the Hermite polynomials and only odd quantum numbers apply.

The integral solution of Eq. (4) can be written as[31]

$$u(r) = -\langle G(r, r')|\delta v(r')|u(r')\rangle, \tag{7}$$

$$\delta v(r') = \frac{e^2}{|r'|}, \tag{8}$$

where $G(r, r')$ is Green's function of Eq. (6) with the same boundary conditions as $u(r)$, i.e., Eq. (5). Using the eigenfunction expansion of Green's function, we have[31]

$$u_n = \zeta_n + \sum_{p\neq n}\frac{\langle\zeta_p|\delta v|u\rangle}{E_n - \epsilon_p}\zeta_p, \tag{9}$$

$$E_n = \epsilon_n + \langle\zeta_n|\delta v|u_n\rangle. \tag{10}$$

This is normal PT theory with odd numbered eigenstates. The validity condition ($\langle\zeta_n|\delta v|u_n\rangle \ll |E_n - E_{n\pm1}|$) should also hold.[32] We will discuss this in Sec. III.

C. Path integral approach

Recently, we have presented a novel real-time path integral (RTPI) approach to the electronic structure calculations and coherent quantum dynamics. It was first tested in the case of a single electron quantum dot.[28] Combined with Monte Carlo sampling of paths, RTPI was demonstrated to be a robust first-principles method and relatively simple to use, but computationally heavy.

Later, it was shown that in the case of Hooke's atom RTPI is capable of incorporating the electronic correlations exactly within numerical accuracy.[31] Now, we demonstrate finding not only the ground state but lowest excited states, and also, dynamics as a response to external electric fields. We analyze the role of relevant approximations, the Monte Carlo method, and numerical parameters.

Thus, the RTPI is a general numerical method for testing the perturbation theoretical predictions, where analytical data are not available. Simultaneously, we can test the numerical performance and accuracy of RTPI for finding more complex many-particle wave functions and quantum phenomena, which are out of reach with the conventional first-principles methods.

The first and second excited states are calculated with the incoherent propagation path integral Monte Carlo[30,33] simulations. The used parameters in atomic units are time step ($t = 0.1$), number of walkers ($N = 300\,000$), and the walker size ϵ ($\epsilon^2 = 0.005$). The purpose of the last parameter is to reduce the oscillations of the kinetic propagator. This is done by representing a single walker as a Gaussian function with variance ϵ^2 instead of Dirac delta function.[33]

Here, it should be noted that the RTPI simulations are carried out in single-particle coordinates x_1 and x_2, thus testing the performance of description of the electron correlations.

III. ONE DIMENSIONAL HOOKE'S ATOM

In this section, we discuss the solutions of one dimensional Hooke's atom within PT and RTPI. First we consider lowest stationary states, and then, dynamics in the presence of external time dependent electric field.

A. Stationary eigenstates

1. Ground state

Taut has introduced some exact solutions of 3D Hooke's atom for certain confinement parameters.[1] For the relative motion, this means solutions to the following Schrödinger equation [Eq. (9) in Ref. 1]:

$$-\frac{u''(r)}{2} + \frac{1}{2}\omega^2 r^2 u(r) + \frac{1}{2}\frac{1}{r}u(r) = E_n u(r). \tag{11}$$

This is equivalent to the Schrödinger equation (4) for a particle with reduced mass ($\mu = 1$) and $\frac{1}{\sqrt{2}}$ electric charge. However, the approach involves finding solutions of two simultaneous equations, which restricts the answers to some specific values of ω and states.

Out of those we choose $\omega = 0.5$, because the analytical exact solution of the ground state is available for this value and it is also the largest one in the set of specified values of ω. In the first order PT, the energy levels as a function of n and ω can be written as

$$E_n = \left(2n + \frac{3}{2}\right)\hbar\omega + \frac{e^2 2^{-2n-1}\xi}{\sqrt{\pi}(2n+1)!}\int_{-\infty}^{\infty}\frac{e^{-(\xi x)^2}H_{2n+1}(\xi x)^2}{|x|}\,dx. \tag{12}$$

Where n is non- negative integers. The first term in Eq. (12) represents the simple harmonic oscillator energy levels with odd quantum number. Because of odd Hermite polynomials in the integrand, we are not worried about the singularity at origin. Thus, the first few energy levels are

$$E_0 = 2e^2\sqrt{\frac{\mu\omega}{\pi\hbar}} + \frac{3\omega\hbar}{2},$$
$$E_1 = \frac{5e^2}{3}\sqrt{\frac{\mu\omega}{\pi\hbar}} + \frac{7\omega\hbar}{2},$$
$$E_2 = \frac{89e^2}{60}\sqrt{\frac{\mu\omega}{\pi\hbar}} + \frac{11\omega\hbar}{2},$$
$$E_3 = \frac{381e^2}{280}\sqrt{\frac{\mu\omega}{\pi\hbar}} + \frac{15\omega\hbar}{2}.$$

In Ref. 1, the interpolation method of eigenenergies is also presented. However, the fitting has been done for the confinement parameters in a narrow region, only. The maximum value of ω for the ground state is 0.5, and by increasing the number of states, the corresponding maximum ω decreases. Therefore, the extrapolation results for the ground state are accurate in region $\omega \leq 0.5$, for the first

excited state in region $\omega \leq 0.38$, and for higher states this region becomes narrower (cf. Table I in Ref. 1).

Rather than analytical exact solutions, there are two approximations in Ref. 1: the weak and the strong confinement approximations. As discussed in Ref. 33, for the largest confinement parameter ($\omega = 0.5$), the PT gives more accurate results compared to the weak and strong approximations.

A comparison between the analytical exact and perturbative solutions for $\omega \leq 0.5$ is shown in Fig. 1. The difference between these two decreases as n and ω increase, so the maximum difference appears for the ground state. For small values of ω, the PT is less accurate, because the validity condition for PT ($V_{nn} \ll |E_n - E_{n\pm1}|$) is violated. We can use the average value of kinetic energy as a limit for the validity of PT. In the first order perturbative approximation, the average kinetic energy of relative motion for the ground state becomes negative for $\omega < \frac{4e^4\mu}{9\pi\hbar^3}$, which sets a minimum acceptable ω for the ground state in PT.

The ground state wave function and its properties have been discussed in detail in Ref. 33 already.

2. First two excited states

For the excited states with $\omega > 0.5$, the PT gives accurate results even in the first order. The accuracy of the PT results has been checked (up to fourth order) comparing the numerical exact solutions for the one-dimensional Hooke's atom.

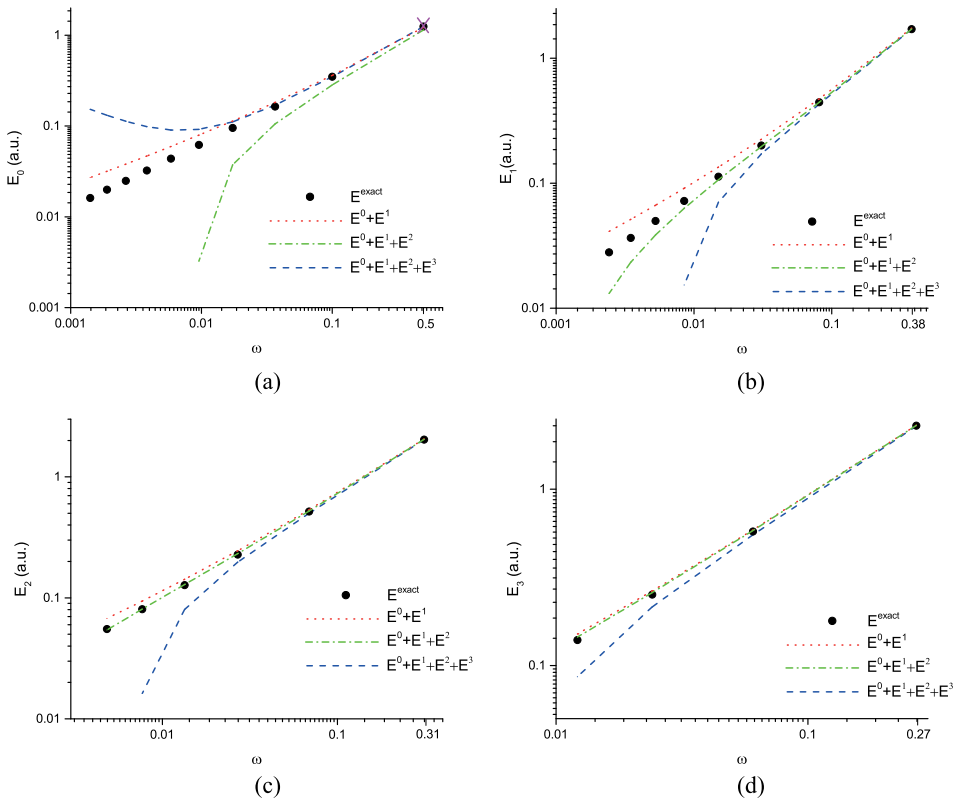

FIG. 1. Comparison of PT and analytical exact total energies (solid black circles) results in Ref. 1 of Hooke's atom in atomic units (hartree). The first-, second-, and third-order corrected energies are shown by the dotted (red), dotted-dashed (green), and dashed (blue) lines, respectively, and all axes are in logarithmic scale. (a) Ground state energy, $n = 0$ as a function of ω in logarithmic scales. The pink cross shows the RTPI result.[33] (b) First excited state, $n = 1$. (c) Second excited state, $n = 2$. (d) Third excited state, $n = 3$.

Figure 2 shows the relative errors between the first order PT and the numerical exact solution eigenenergies for the $\omega \geq 0.5$. As seen, even in the first order PT the relative errors reduce rapidly for excited states. The relative error for the ground state is around 5% and for states with $n \geq 3$, the relative errors are less than 1%.

We can compare the PT results for the first excited state of the relative motion with the analytical exact solution for $\omega = \frac{2}{5.26\,137}$. This ω has been chosen, because the analytical exact solution for the first excited state is available.[1] The analytical exact solution wave function for this frequency is[1]

$$u_{1,\text{exact}} = Nr\exp(-\frac{\omega}{2}r^2)\Big(r^3 - 36(r+4)r^2\omega + 12r^2 + 72r + 144\Big), \tag{13}$$

where N is the normalization constant.

Comparison between the exact solution and PT solutions is given in Fig. 3. As expected, the first order PT has larger deviation from the exact solution, compared with the second and third order PT. Figure 3(b) shows the relative error between different order PT wave functions and exact solution.

Table I shows the results for the expectation values of Coulomb potential (V_c), relative motion harmonic potential ($V_{H,r}$), and relative motion kinetic energy (T_r). The total energy is the $E_{CM,0} + E_0$. The expectation values have been calculated directly from normalised wave functions. The RTPI energetics is in good match with the exact energies (and PT, where the analytical exact results are not available), but there is a systematic error where the electrons are close to each other ($r \to 0$) or when their separation is large. The former is due to the improved Trotter kernel approximation[28] with smaller error near the singular potential with finite time step. The latter is mostly caused by the small density of the Monte Carlo grid in that region and that error can be made smaller by increasing the number of walkers.[30,33]

The first two excited states are combinations of the CM and relative motion ground states and first excited states. The first (second) excited state is a combination of the ground state of relative motion (CM) and excited state of CM (relative motion).

For the excited states, the results are reported for the $\omega = \frac{1}{2}$, because the analytical exact solution for the ground state is available for this frequency,[1] and the results can also be compared with the the work on RTPI.[33] Using the Virial theorem for one dimensional harmonic oscillator, we have[32]

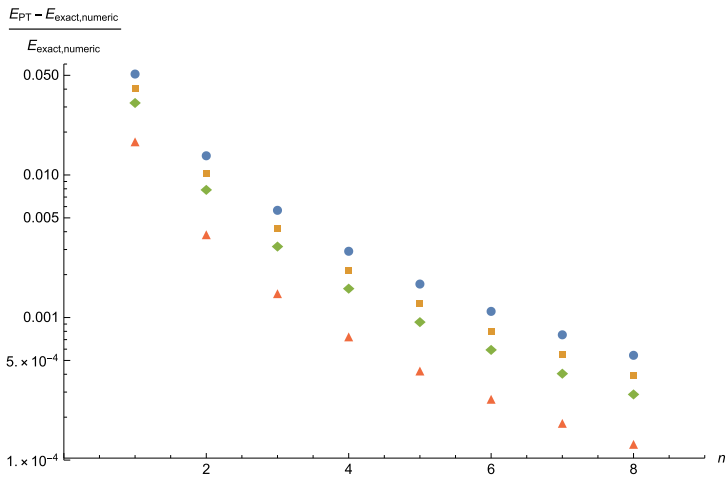

FIG. 2. The relative errors $(E_{PT} - E_{\text{exact-numeric}})/E_{\text{exact-numeric}}$ for the eigenenergies $n = 1, \ldots, 8$ of Hooke's atom [$\omega = 0.5$ (blue circles), 0.7 (brown squares), 0.9 (green lozenges), and 2.0 (red triangles)]. The PT results in this figure are of the first order.

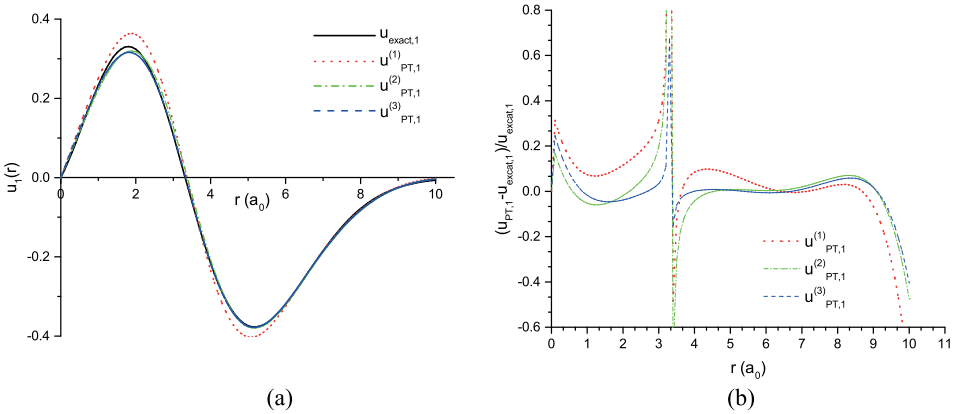

FIG. 3. (a) Comparison between the analytical exact solution (solid black line) and different order PT results for the first excited state wave function of relative motion ($\omega = \frac{2}{5.261\,37}$). $u^{(n)}_{PT,1}$ represents the nth-order corrections in PT. The first, second, and third order corrections are, respectively, shown by the dotted (red), dotted-dashed (green), and dashed (blue) lines. The relative error increases around the node and tail of the exact solution, where the wave function tends to zero. The horizontal axes represent relative distance between electrons in atomic units, i.e., bohr radius. (a) Analytical exact and different order PT wave functions. (b) Relative error between PT and analytical exact wave function.

$$\langle T_{CM}\rangle = \langle V_{H,CM}\rangle = (n+\frac{1}{2})\frac{\hbar\omega}{2}, \tag{14}$$

where T_{CM} is kinetic energy of center of mass motion and $V_{H,CM} = \frac{1}{2}M\omega^2R^2$ is the CM harmonic potential. Here, for $n = 1$, this gives 3/8 = 0.375. Table II shows the RTPI, PT, and analytical exact values (where available) for kinetic and potential energies of Hooke's atom. As one can see that the results are in agreement with exact solution results.

TABLE I. Expectation values of kinetic and potential energies of the first excited state in PT ($\omega = \frac{2}{5.261\,37}$) calculated directly from normalized wave functions. Comparison between the exact and PT wave functions is given in Fig. 3.

	Exact value	1st order PT	2nd order PT	3rd order PT
V_c	0.3521	0.3638	0.3452	0.3508
$V_{H,r}$	0.7671	0.7276	0.7832	0.7807
T_r	0.5912	0.6217	0.5845	0.5807
Total energy	1.9006	1.9032	1.9030	1.9024

TABLE II. The first excited state ($\omega = 0.5$) and its expectation values. The first excited state is the combination of first excited state of CM and ground state of relative motion.

	Exact value	RTPI	1st order PT	2nd order PT	3rd order PT
V_c	0.4474	0.4530(4)[a]	0.4354	0.4443	0.4466
$V_{H,r}$	0.5131	0.5117(1)[a]	0.5161	0.5218	0.5181
T_r	0.2894	0.2870(9)[b]	0.3028	0.2847	0.2861
$V_{H,CM}$	0.375	0.3722(1)[a]	0.375	0.375	0.375
T_{CM}	0.375	0.3765(15)[b]	0.375	0.375	0.375
Potential energy	1.3355	1.3369(3)[b]	1.3265	1.3412	1.3397
Total energy	2	1.9969(6)[c]	2.0043	2.0010	2.0009

[a]Potential energy = $V_c + V_{H,r} + V_{H,CM}$ and its components are calculated as RTPI output.
[b]The expectation values of T_r and T_{CM} are calculated directly from normalized wave functions.
[c]Total energy has been calculated (independent from potential and kinetic energies) directly from the wave function's phase in RTPI.

TABLE III. The second excited state and its properties as Table II (cf. Fig. 4). The second excited state is combination of the CM ground state and first excited state of relative motion. Analytical exact values for this state are not available. The accuracy of the PT has been checked for the closest confinement parameter in Fig. 3(a) and Table I.

	Exact value	RTPI	1st order PT	2nd order PT	3rd order PT
V_c	...	0.4234(9)[a]	0.4233	0.4074	0.4119
$V_{H,r}$	...	0.9811(9)[a]	0.9530	1.0074	1.0043
T_r	...	0.786(4)[b]	0.8159	0.7771	0.7753
$V_{H,CM}$	0.125	0.1620(3)[a]	0.125	0.125	0.125
T_{CM}	0.125	0.0986(7)[b]	0.125	0.125	0.125
Potential energy	...	1.5665(6)[b]	1.5013	1.5399	1.5413
Total energy	...	2.4331(2)[c]	2.4423	2.4420	2.4417

[a]Potential energy = $V_c + V_{H,r} + V_{H,CM}$ and its components are calculated as RTPI output.
[b]The expectation values of T_r and T_{CM} are calculated directly from normalized wave functions.
[c]Total energy has been calculated (independent from potential and kinetic energies) directly from the wave function's phase in RTPI.

The energetics of the second excited state is shown in Table III. Clearly, for the second excited state, the average of T_r (relative motion kinetic energy), T_{CM}, and $V_{H,CM}$ from RTPI simulation is not well-fitted to the exact and PT results. This can be explained by the shape of the wave function. As one can see from Fig. 4, the RTPI predicts wider wave function comparing to the exact and PT. A wider wave function has smaller kinetic energy, and for the harmonic confinement, it gives larger potential energy. However, the total value of the eigenenergy and potential energy is in agreement with data from PT. Therefore, the different contributions balance each other in such way that the total quantities approach the correct values.

B. Dynamics in the presence of external transient field

Time evolution of the stationary states has been successfully simulated using RTPI in Ref. 33 already. As expected, there appears as change in the phase of the wave function only. To test the time evolution of Hooke's atom, a short time pulse of spatially constant electric field (linear in space and Gaussian in time) has been considered as a perturbation. We have chosen the external potential as

$$U(x,t) = \frac{U_0}{\sqrt{\pi\alpha}} x \exp\left(-\frac{(t-t_0)^2}{\alpha}\right), \tag{15}$$

where $U_0 = 1$, $\alpha = 0.1$, and $t_0 = 1$ (in atomic units).

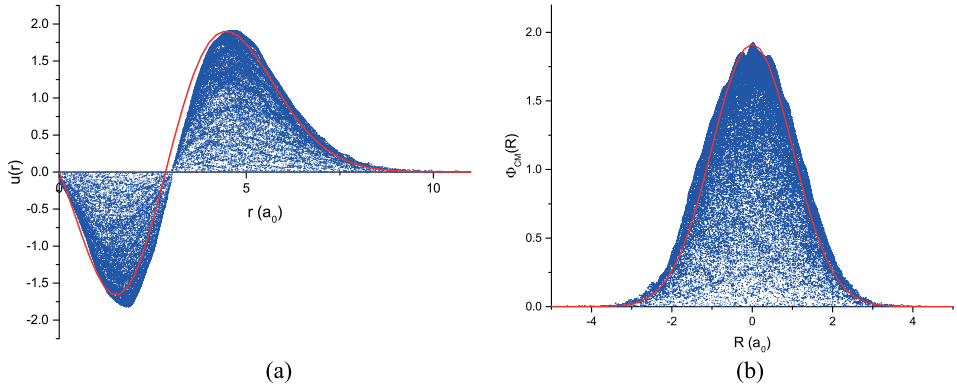

FIG. 4. A snapshot of the wave function from the converged RTPI simulation with $\Delta t = 0.1$, $N = 300\,000$, and $\omega = 0.5$ (blue walkers). Red line is an envelope curve from the 3rd order PT [cf. Fig. 3(a), $\omega \simeq 0.38$] in (a) and exact solution from Eq. (3) in (b) fitted to the data. All the figures are in atomic units. (a) The first excited state of Internal motion. (b) Ground sate of CM motion.

In the presence of this external electric field, the Hamiltonian of the system becomes as

$$\begin{aligned} H &= \frac{-\hbar^2}{2m_e}\nabla_1^2 + \frac{-\hbar^2}{2m_e}\nabla_2^2 + \frac{1}{2}m_e\omega^2 x_1^2 + \frac{1}{2}m_e\omega^2 x_2^2 + \frac{e^2}{|x_1 - x_2|} + U(x_1,t) + U(x_2,t) \\ &= H(r) + H(R) + 2U(R,t) \\ &= H(r) + H(R) + f(t)R, \end{aligned}$$

where $f(t) = \frac{2}{\sqrt{\pi\alpha}}\exp(-\frac{(t-t_0)^2}{\alpha})$.

1. Exact solution

As expected the spatially constant electric field does not change the internal motion and its effects appear only in CM motion. Therefore, in this subsection, we just discuss the CM motion. However, the RTPI solves the unseparated total wave function in single-particle coordinates again, and its results are presented in Subsection III B 2.

The Heisenberg equation of motion simplified into two coupled partial differential equations (PDE) can be written as

$$\begin{aligned} \frac{d}{dt}\langle R\rangle &= \frac{\langle P_{CM}\rangle}{M}, \\ \frac{d}{dt}\langle P_{CM}\rangle &= -(M\omega^2\langle R\rangle + f(t)), \end{aligned} \tag{16}$$

where P_{CM} is the center of mass momentum. To find the average potential energy, we need $\langle R^2\rangle$, which is found from the following coupled PDEs:

$$\begin{aligned} \frac{d}{dt}\langle R^2\rangle &= \frac{2}{M}\left(\frac{\langle P_{CM}^2\rangle}{M} - M\omega^2\langle R^2\rangle - f(t)\langle R\rangle\right), \\ \frac{d}{dt}\langle P_{CM}^2\rangle &= -2M\omega^2\left(\frac{\langle P_{CM}^2\rangle}{M} - M\omega^2\langle R^2\rangle - f(t)\langle R\rangle\right) - 2\frac{d}{dt}\langle f(t)P_{CM}\rangle. \end{aligned} \tag{17}$$

Solution for $\langle R\rangle$ and $\langle P_{CM}\rangle$, give us the average of the potential energies as a function of time. Figure 5 shows the average of the total potential energy as a function of time.

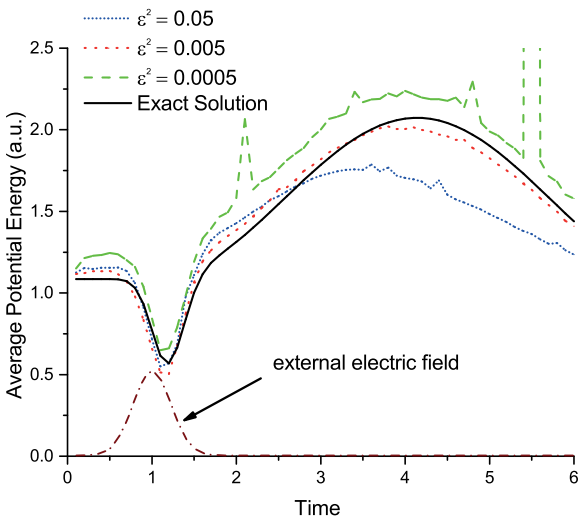

FIG. 5. Potential energy in atomic units from one MC simulation $\Delta t = 0.1$ and $N = 100\,000$ with different walker size ϵ in atomic units. Blue short dotted line $\epsilon^2 = 0.05$, red dotted line $\epsilon^2 = 0.005$, and green dashed line $\epsilon^2 = 0.0005$. The black solid line represents the exact solution.

2. Coherent RTPI simulation

In the time domain simulations, the ground state is affected by Gaussian shape pulse discussed above. As can be seen from the potential energies in Fig. 5, the walkers' size ϵ affects the results much more than in incoherent propagation. Too large ϵ cuts out higher energy states and results in incorrect energies (blue line) and too small ϵ increases in the incidental numerical error from the kinetic energy part of the propagator (green line). That is expected as it cuts out higher energy states, which are not present in the simulation of lower eigenstates but contribute to the real time evolution. For the real-time dynamics, ϵ must be chosen smaller than that for the optimal incoherent propagation.[30,33] There is a delay in the system response to such an ultrafast transient process. It is due to the inertia of electrons. After the external pulse, the total energy is conserved and the electrons remain in harmonic oscillation.

Figure 6 shows the different interaction contributions in the potential energy. As expected, the Coulomb interaction remains unchanged during the time evolution, and the effects of the external electric field just appear in a short time interval.

3. Fourier transformation and time evolution

After the external pulse, the Hamiltonian of the system returns to its initial time independent form, but the wave function remains as a superposition of eigenstates of the unperturbed system,

$$\Psi(r, R, t) = \sum c_i \psi_i(r, R) e^{-t\frac{E_i t}{\hbar}},$$

where c_i depends on the matrix elements of the external potential. Therefore, the Fourier transform of Ψ is a sum of Dirac delta functions located at E_i. In practice, one can perform the Fourier transform by collecting finite samples of the wave function at different times and coordinates. Here the PT is used to find the time evolution for illustration of the approach. In the absence of analytical solutions, RTPI can be used to find the wave function time evolution.

Figure 7 shows the Fast Fourier Transformation (FFT) of the one dimensional Hooke's atom after applying the $U(x, t) + U(x^2, t)$ as the external potential. We choose a nonlinear perturbation $x + x^2$ because it has non-zero matrix elements for the first few excited states. The sampling rate is 100 (atomic units) and total integration time is 46 (atomic units). From Fig. 7, the eigenenergies are located at $\{1.5, 2.0, 2.43, 2.5, 2.93, 3.45\}$. Here we used $\Psi(1, 1, t)$ as the input in FFT.

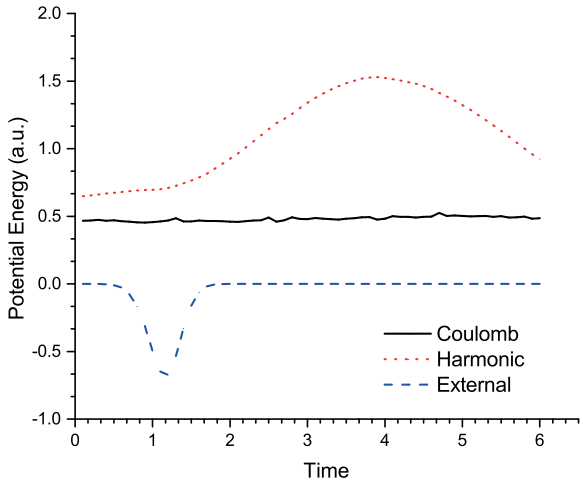

FIG. 6. Contributions to the potential energy in atomic units from Coulombic (black solid line), harmonic (red dotted line), and external potential (blue dashed line) effects from one MC simulation with $N = 100\,000$ and $\epsilon^2 = 0.005$.

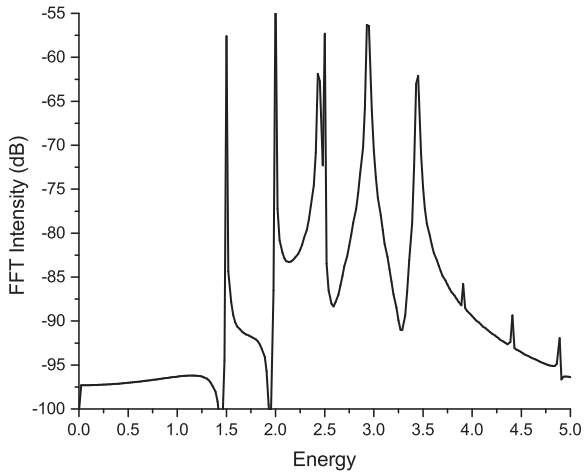

FIG. 7. Fast Fourier Transformation (FFT) of time dependent wave function of the one dimensional Hooke's atom. Peaks are located at 1.5, 2.0, 2.43, 2.5, 2.93, and 3.45. The small peaks at the end of energy axis come from numerical error.

IV. CONCLUSIONS

Hooke's atom has served as a well-defined model system, but also, as a challenging problem for decades.[1–20] In addition to analytical approaches,[1–8] numerical calculations have been published,[1–14] and the specific challenges have arisen from the one-dimensional case and Coulomb space splitting, in particular.[15–27] All of these studies, however, have considered the ground state, only.

In this study, we have been able to complete these numerous studies by including the excited states and dynamics induced by an external potential. We have shown how perturbation theory (PT) provides an accurate approach in the strong confinement regime, $\omega > 0.5$, and in particular, the real-time path integral (RTPI) approach with Monte Carlo simulation is a general and robust simulation tool[28,31] for confined quantum systems. It should be mentioned here that similar studies could be carried out for other atoms with exact analytical solutions.[34–36]

We have demonstrated that PT is accurate enough, even for higher excited states. This means that PT is probably suitable for studying the properties of the strongly one-dimensionally confined many body or few-body quantum systems.[21–26] Unlike earlier analytical results, as described in Sec. III, PT is applicable for all confinement parameters and eigenstates.

With the RTPI, the improved Trotter kernel is shown to be useful with a large enough number of Monte Carlo walkers, in cases where exact propagators are not available. We find that the accuracy and stability of RTPI are tunable with the number of Monte Carlo walkers and the real time step size. Regarding ground states, the computational cost of RTPI is significantly higher than that of Diffusion Monte Carlo. However, one of the advantages of RTPI is that it provides one with the wave function explicitly, and thus, the evaluation of local multiplicative expectation values becomes straightforward. Moreover, as RTPI is capable of locating the nodal surfaces of excited states, it can be used to find the nodal surfaces in a diffusion Monte Carlo simulation of the excited states.

ACKNOWLEDGMENTS

The authors thanks the Tampere University of Technology for support.

[1] M. Taut, Phys. Rev. A **48**(5), 3561 (1993).
[2] U. Merkt, J. Huser, and M. Wagner, Phys. Rev. B **43**, 7320 (1991).
[3] M. Taut, Phys. Rev. B **63**, 115319 (2001).
[4] O. Ciftja, Phys. Scr. **88**, 058302 (2013).
[5] H. Sprekeler, G. Kießlich, A. Wacker, and E. Scholl, Phys. Rev. B **69**, 125328 (2004).

[6] R. J. White and W. Byers Brown, J. Chem. Phys. **53**, 3869 (1970).
[7] G. W. Bryant, Phys. Rev. Lett. **59**(10), 1140 (1987).
[8] N. R. Kestner and O. Sinanoglu, Phys. Rev. **128**, 2687 (1962).
[9] D. Futai Tuan, J. Chem. Phys. **50**, 2740 (1969).
[10] P. M. Laufer and J. B. Krieger, Phys. Rev. A **33**(3), 1480 (1986).
[11] J. M. Benson and W. Byers Brown, J. Chem. Phys. **53**, 3880 (1970).
[12] J. Cioslowski and K. Pernal, J. Chem. Phys. **113**, 8434 (2000).
[13] D. P. O'Neill and P. M. W. Gill, Phys. Rev. A **68**, 022505 (2003).
[14] R. Loudon, Am. J. Phys. **27**, 649 (1959).
[15] G. Palma and U. Raff, Can. J. Phys. **84**, 787–800 (2006).
[16] D. P. O'Neill and P. M. W. Gill, J. Chem. Phys. **122**, 094110 (2005).
[17] L. K. Haines and D. H. Roberts, Am. J. Phys. **37**, 1145 (1969).
[18] A. N. Gordeyev and S. C. Chhajlany, J. Phys. A: Math. Gen. **30**, 6893 (1997).
[19] H. N. Nunez-Yepez, A. L. Salas-Brito, and D. A. Solis, Phys. Rev. A **83**, 064101 (2011); **89**, 049908(E) (2014).
[20] H. N. Spector and J. Lee, Am. J. Phys. **53**, 248 (1985).
[21] A. G. Volosniev, D. V. Fedorov, A. S. Jensen, M. Valiente, and N. T. Zinner, Nat. Commun. **5**, 5300 (2014).
[22] X.-W. Guan *et al.*, Phys. Rev. Lett. **111**, 130401 (2013).
[23] Xi-W. Guan *et al.*, Rev. Mod. Phys. **85**, 1633 (2013).
[24] Y.-a. Liao *et al.*, Nature **467**, 567 (2010).
[25] T. Kinoshita, T. Wenger, and D. S. Weiss, Science **305**, 1125 (2004).
[26] B. Paredes *et al.*, Nature **429**, 277 (2004).
[27] W. Fischer, H. Leschke, and P. Müller, J. Phys. A: Math. Theor. **40**, 1011 (2007).
[28] C. A. Downing and M. E. Portnoi, Phys. Rev. A **90**, 052116 (2014).
[29] U. Oseguera and M. de Llano, J. Math. Phys. **34**, 4575 (1993).
[30] I. Ruokosenmäki and T. T. Rantala, Commun. Comput. Phys. **18**, 91 (2015).
[31] P. McCord Morse and H. Feshbach, *Methods of Theoretical Physics* (McGraw-Hill, 1953), Vol. 2.
[32] L. D. Landau and E. M. Lifshitz, *Quantum Mechanics: Non-Relativistic Theory* (Elsevier, 1981).
[33] I. Ruokosenmäki *et al.*, Comput. Phys. Commun. **210**, 45 (2017).
[34] M. Moshinsky, Am. J. Phys. **36**, 52 (1968).
[35] R. Crandall, R. Whitnell, and R. Bettega, Am. J. Phys. **52**, 438 (1984).
[36] C. A. Downing, Phys. Rev. A **95**, 022105 (2017).

PUBLICATION
IV

Real-Time Diffusion Monte Carlo Method

I. Ruokosenmäki and T. T. Rantala

Communications in Computational Physics 25.(2019), 347–360
DOI: 10.4208/cicp.OA-2018-0048

Commun. Comput. Phys.
doi: 10.4208/cicp.OA-2018-0048

Vol. **25**, No. 2, pp. 347-360
February 2019

Real-Time Diffusion Monte Carlo Method

Ilkka Ruokosenmäki[1,*] and Tapio T. Rantala[1]

[1] *Laboratory of Physics, Tampere University of Technology, Finland.*

Received 19 February 2018; Accepted (in revised version) 14 May 2018

Abstract. Direct sampling of multi-dimensional systems with quantum Monte Carlo methods allows exact account of many-body effects or particle correlations. The most straightforward approach to solve the Schrödinger equation, Diffusion Monte Carlo, has been used in several benchmark cases for other methods to pursue. Its robustness is based on direct sampling of a positive probability density for diffusion in imaginary time. It has been argued that the corresponding real time diffusion can not be realised, because the corresponding oscillating complex valued distribution can not be used to drive diffusion. Here, we demonstrate that this can be done by turning the distribution piecewise positive and normalisable, and also, by using four types of walkers. This study is a proof of concept demonstration using the well-known and transparent case: one-dimensional harmonic oscillator. Furthermore, we show that our novel method can be used to find not only the ground state but also excited states and even the time evolution of a given wave function. Considering fermionic systems, this method may turn out to be feasible for finding the wave function nodes for other approaches.

AMS subject classifications: 81-08

Key words: Path integral, quantum dynamics, first-principles, Monte Carlo, real-time.

1 Introduction

Quantum Monte Carlo (QMC) methods form a collection of robust approaches to study quantum many-particle systems [1]. With QMC the central benefit is that one can deal with multi-dimensional systems, where standard grid based methods become computationally too heavy. With Path Integral and Green's function approaches the many-body effects or correlations can be taken into account without introducing approximations and evaluated within numerical accuracy, which is limited by the computational resources, only. Furthermore, if starting from the first-principles, also the systematic errors are avoidable. Thus, for the field of electronic structure calculations, with QMC one can

*Corresponding author. *Email addresses:* ilkka.ruokosenmaki@tut.fi (I. Ruokosenmäki), Tapio.T.Rantala@iki.fi (Tapio. T. Rantala)

benchmark the energetics and structure of atoms and molecules with desired accuracy. It is even straightforward in cases where the wave function is everywhere positive or can be considered as piecewise positive between given nodes.

Diffusion Monte Carlo (DMC) or Green's function Monte Carlo is a typical representative of QMC. In several cases it has been demonstrated to be a simple but accurate approach to find the ground state [1,2]. In particular, both bosonic [3] and fermionic [4,5] systems have been successfully considered. A recent example is benchmarking the hydrogen molecule and its simple reaction conformations with increasing accuracy [6].

With DMC the Schrödinger equation in imaginary time turns to a diffusion equation, whose "imaginary time evolution" or iteration converges to the ground state. Transformation of the Schrödinger equation to the corresponding integral equation shows how diffusion can be simulated with random walkers guided by the interactions of quantum particles. The walker distribution, which is everywhere positive converges to the ground state wave function. This is the simple idea of DMC simulation, where it is essential that the product of the wave function and diffusion probability is everywhere positive. The latter one is the kernel of the integral equation [6–9].

Due to the everywhere positive "diffusion distribution" interpretation as the wave function, simulation of excited states and indistinguishable fermions becomes problematic with DMC [4,10]. Nodes of the wave function should be known, *e.g.* by symmetry, or approximated with good enough accuracy to make it piecewise positive. Though there are practical approximate ways around the problem, mostly with approximate nodes, this remains as an impediment with DMC.

Based on the probability interpretation of the kernel and wave function, and diffusion nature of the random walk, it has been argued that the simple and useful principles of DMC, above, can not be used to solve the Schrödinger equation with real time path integrals [11, 12]. In this study we show that this is not true and we present a practical solution to this problem, which is related to the sc. "numerical sign problem" of real-time path integrals [12]. Furthermore, we demonstrate that our new real-time path integral approach is capable of finding, not only the ground state, but also excited states, and also, it can be used to simulate proper real time quantum dynamics – not to be mixed with diffusion.

This study is a proof-of-concept demonstration of a novel "real-time DMC". Therefore, we have chosen a transparent test case, the well-known one-dimensional harmonic oscillator (ODHO), where the method and its performance are clearly seen. We also benefit from the exact propagator of the harmonic oscillator while testing the real-time diffusion.

2 Diffusion Monte Carlo and its real time counterpart

2.1 Positive probability density

The well-known imaginary time ($\tau = it$) integral equation of the conventional Diffusion Monte Carlo (DMC or τDMC) for the many-body wave function ψ is

$$\psi(x_b,\tau_b)=\int_a G(x_b,\tau_b;x_a,\tau_a)\psi(x_a,\tau_a)\mathrm{d}x_a, \tag{2.1}$$

where the kernel G is the Green's function of the system, the position space representation of the imaginary time evolution operator. The Eq. (2.1) is written in one-dimensional space of x, here and in what follows, but extension to more dimensions is trivial. For a time step $\tau=\tau_b-\tau_a$, and using the Trotter expansion one gets

$$\begin{aligned} &G\approx G_{\mathrm{diff}}G_{\mathrm{B}},\\ &G_{\mathrm{diff}}=C\exp\left[-(x_b-x_a)^2/2\tau\right],\\ &G_{\mathrm{B}}=\exp\left[-\left(\frac{1}{2}(V(x_b)+V(x_a))-E_T\right)\tau\right], \end{aligned} \tag{2.2}$$

where $C=(2\pi\tau)^{-3/2}$ and E_T is the trial energy, iterated to the ground state total energy at self-consistency, $\psi(x_b)=\psi(x_a)$. The Green's function and the stationary solution of Eq. (2.1) becomes exact as $\tau\to 0$.

Now, the kernel G is everywhere real and positive, and therefore, it can be considered as a normalizable probability density in Monte Carlo evaluation of the ground state wave function $\psi(x)$ as the stationary walker density [2]. The power of τDMC arises from the independence of Monte Carlo walkers in "diffusion", and also, the locality of G_{diff}, which increases the accuracy of G_{B}.

The imaginary time integral equation (2.1) can be derived from the more fundamental real time equation [7] of the same form

$$\psi(x_b,t_b)=\int_a K(x_b,t_b;x_a,t_a)\psi(x_a,t_a)\mathrm{d}x_a, \tag{2.3}$$

where the kernel K is the path integral over the time step $t=t_b-t_a$, $(t_a<t_b)$,

$$K(x_b,t_b;x_a,t_a)=\int_{x_a}^{x_b}\exp(\mathrm{i}S[x_b,x_a])\mathcal{D}x(t). \tag{2.4}$$

Here $S[x_b,x_a]=S[x](x_b,x_a)=\int_{t_a}^{t_b}L_x dt$ is the action along the path $x(t)$ from $a=(x_a,t_a)$ to $b=(x_b,t_b)$ and L_x is the corresponding Lagrangian [7]. Now, finding the Monte Carlo solutions for ψ from Eqs. (2.1) and (2.3) greatly differ.

The τDMC diffusion like procedure can not be used directly to solve Eq. (2.3) for ψ, because the kernel K, as a path integral, is a complex valued functional of interfering paths coupling all of the walkers. Thus, K can not be interpreted as a probability [11,12], and furthermore, it is delocalised with complex exponential tails oscillating in whole space, the more the shorter the time step t.

Here, we present a novel idea solving this problem and formulate a "real-time diffusion Monte Carlo" (tDMC or RTDMC) procedure, which retains the advantage of "diffusion of independent walkers". Furthermore, the tDMC enables evaluation of excited

states and even real time quantum dynamics, out of reach with the τDMC. We have these advanced features in our direct real-time path integral (RTPI) approach [8, 9], already, but there, all of the paths coupling the walkers $\{x_{ai}\}_{i=1}^{N_a}$ and $\{x_{bj}\}_{j=1}^{N_b}$ need to be considered. With increasing number of walkers it leads to quadratic growth ($\propto N^2$, assuming $N_a = N_b = N$) of computational efforts with RTPI. With tDMC, however, the growth of efforts is close to linear ($\propto N$), only.

First, we separate the integrand in Eq. (2.3) to terms, which can be considered as "positive probabilities", and second, we accomplish normalization by restricting the space of integration. We separate similarly both the kernel $K \propto \exp(\mathrm{i}\phi)$ [7] and the wave function $\psi(a)$ at the right hand side of (2.3) to four parts as

$$\begin{aligned} K(b,a) &= C\exp(\mathrm{i}\phi) = C[\cos(\phi)+\mathrm{i}\sin(\phi)] = C\left[\cos(\phi)+\mathrm{i}\cos(\frac{\pi}{2}-\phi)\right] \\ &= C\left[\cos^2(\frac{\phi}{2})-\sin^2(\frac{\phi}{2})+\mathrm{i}\left(\cos^2\left(\frac{\frac{\pi}{2}-\phi}{2}\right)-\sin^2\left(\frac{\frac{\pi}{2}-\phi}{2}\right)\right)\right] \\ &= K_+(b,a)-K_-(b,a)+\mathrm{i}K_{+\mathrm{i}}(b,a)-\mathrm{i}K_{-\mathrm{i}}(b,a) \end{aligned} \tag{2.5}$$

and

$$\psi(a) = \psi_+(a)-\psi_-(a)+\mathrm{i}\psi_{+\mathrm{i}}(a)-\mathrm{i}\psi_{-\mathrm{i}}(a). \tag{2.6}$$

This splits the integrand into 16 terms. Here C and ϕ are some functions of a and b, that can be chosen so that C is real and positive. Rearrangement of these terms allows splitting the left hand side of (2.3) with the same principle as

$$\begin{aligned} \psi_+(b) &= \int_a K_+\psi_+ dx_a + \int_a K_-\psi_- dx_a + \int_a K_{+i}\psi_{-\mathrm{i}} dx_a + \int_a K_{-i}\psi_{+\mathrm{i}} dx_a, \\ \psi_-(b) &= \int_a K_+\psi_- dx_a + \int_a K_-\psi_+ dx_a + \int_a K_{+i}\psi_{+\mathrm{i}} dx_a + \int_a K_{-i}\psi_{-\mathrm{i}} dx_a, \\ \psi_{+\mathrm{i}}(b) &= \int_a K_+\psi_{+\mathrm{i}} dx_a + \int_a K_-\psi_{-\mathrm{i}} dx_a + \int_a K_{+i}\psi_+ dx_a + \int_a K_{-i}\psi_- dx_a, \\ \psi_{-\mathrm{i}}(b) &= \int_a K_+\psi_{-\mathrm{i}} dx_a + \int_a K_-\psi_{+\mathrm{i}} dx_a + \int_a K_{+i}\psi_- dx_a + \int_a K_{-i}\psi_+ dx_a, \end{aligned} \tag{2.7}$$

each of which is everywhere real and positive. Here, all of the K_{sub} and ψ_{sub} on the right-hand side stand for $K_{\mathrm{sub}}(b,a)$ and $\psi_{\mathrm{sub}}(a)$, respectively, where $a=(x_a,t_a)$, $b=(x_b,t_b)$ and sub = $\{+,-,+i,-i\}$. Thus, the complete wave function at the end of the time step $t = t_b - t_a$ can be written as

$$\psi(b) = \psi_+(b)-\psi_-(b)+\mathrm{i}\psi_{+\mathrm{i}}(b)-\mathrm{i}\psi_{-\mathrm{i}}(b). \tag{2.8}$$

Thus, our approach is reminiscent of an old τDMC method of Arnow *et al.* [4], where positive and negative walkers were used for the respective parts of the wave function. The main differences are the following. Here, we have four types of walkers and each walker generates all other types of walkers. Therefore, all parts of Eqs. (2.7) are correlated

and unlike in τDMC [4] they do not separately converge to the ground state, but instead, we are able to simulate time evolution of a complex time-dependent wave function, as discussed below.

In Eqs. (2.7), we have a fully delocalised piecewise everywhere positive probability density to sample, which first needs to be normalised. In case of a wave function localized in a finite domain we know that the contributions to $\psi(b)$ in Eq. (2.8) cancel outside the domain and close to the domain boundaries inside. Then, we can normalise the partial probabilities of Eq. (2.5) in a so chosen domain and run diffusion localised in the domain. Next, let us discuss the kernel and related approximations.

2.2 Kernel

The kernel in closed form is known for a few special systems only [7, 14]. The harmonic oscillator ($V(x)=\frac{1}{2}m\omega^2$) is one of those with the kernel

$$K(x_b,t_b;x_a,t_a)=\exp(-i\theta)\left(\frac{m\omega}{2\pi\hbar|\sin(\omega t)|}\right)^{1/2} \times\exp\left\{\frac{im\omega}{2\hbar\sin(\omega t)}\left[(x_b^2+x_a^2)\cos(\omega t)-2x_bx_a\right]\right\}, \tag{2.9}$$

where $t=t_b-t_a$ and $\theta=\frac{\pi}{4}(1+2\text{trunc}(\omega t/\pi))$. Here, "trunc$(x)$" denotes the truncation function, the largest integer less than or equal to x.

In general, for a given potential $V(x)$ we need to approximate kernels and the most usual approximation is sc. "short time approximation" or Trotter kernel [11, 13]

$$K(x_b,t_b;x_a,t_a)\approx\left[\frac{1}{2\pi\mathrm{i}t}\right]^{N/2}\exp\left[\frac{\mathrm{i}}{2t}(x_b-x_a)^2-\frac{\mathrm{i}t}{2}(V(x_a)+V(x_b))\right], \tag{2.10}$$

which becomes exact as $t\to 0$, cf. Eq. (2.2).

Both of the kernels (2.9) or (2.10) can be written in the piecewise positive form by using the recipe given in Eq. (2.5). For the Trotter kernel we define notations: average Lagrangian $\bar{L}=\left[\frac{1}{2t}(x_b-x_a)^2\right]-\left[\frac{t}{2}(V(x_a)+V(x_b))\right]$, $C=\left[\frac{1}{2\pi t}\right]^{1/2}$ and $D=\frac{C\sqrt{2}}{2}$. Then, we write

$$\begin{aligned}
K(b,a)&=C(-\mathrm{i})^{1/2}\exp(\mathrm{i}(\bar{L}))=C\exp\left(\mathrm{i}\left(\bar{L}-\frac{\pi}{4}\right)\right)\\
&=\frac{C\sqrt{2}}{2}\left[\cos\left(\bar{L}-\frac{\pi}{4}\right)+\mathrm{i}\sin\left(\bar{L}-\frac{\pi}{4}\right)\right]=D\left[\cos\left(\bar{L}-\frac{\pi}{4}\right)+\mathrm{i}\cos\left(\frac{3\pi}{4}-\bar{L}\right)\right]\\
&=D\left[\cos^2\left(\frac{\bar{L}-\frac{\pi}{4}}{2}\right)-\sin^2\left(\frac{\bar{L}-\frac{\pi}{4}}{2}\right)+\mathrm{i}\left(\cos^2\left(\frac{\frac{3\pi}{4}-\bar{L}}{2}\right)-\sin^2\left(\frac{\frac{3\pi}{4}-\bar{L}}{2}\right)\right)\right]\\
&\equiv D\left[K_+(b,a)-K_-(b,a)+\mathrm{i}K_{+\mathrm{i}}(b,a)-\mathrm{i}K_{-\mathrm{i}}(b,a)\right].
\end{aligned} \tag{2.11}$$

In case of the harmonic oscillator it should be noted, that while the accuracy of short time approximation increases with decreasing time step, the exact kernel allows any length of time step. However, both of these kernels diverge for $t=0$ and the exact one also periodically for $t_n=n\pi/\omega$.

2.3 Real-time diffusion

While the imaginary time diffusion is a very local phenomenon, the more the shorter the time step τ, whereas, the real-time diffusion is fully delocalized in form of oscillatory $\sin^2$ and $\cos^2$ functions, the wave length depending on the average Lagrangian in the time step t. Thus, it is sufficient to consider and normalize these distributions in the chosen domain, only, and correctly with respect to each other. Diffusion out of the box can be ignored, because it is known that the different contributions in Eqs. (2.8) cancel at long distances.

The four parts of the initial wave function $\psi(a)$ in Eq. (2.6) are presented with corresponding four sets of walkers, whose total number is N_a. Neither real contributions $\psi_+(a)$ and $\psi_-(a)$ nor the imaginary contributions $\psi_{+i}(a)$ and $\psi_{-i}(a)$ should pairwise overlap as the complex wave function should be single valued. This is not absolutely necessary to carry on calculations, as we show later. Now, the real-time diffusion of these walkers according to the Eq. (2.7) results in four strongly delocalised and pairwise overlapping contributions, real $\psi_+(b)$ and $\psi_-(b)$, and imaginary $\psi_{+i}(b)$ and $\psi_{-i}(b)$. Then, the real and imaginary parts of the wave function are simply the two sums of their positive and negative contributions. These are found by cancellation or pairwise annihilation of nearby walkers until the nodal surfaces between the positive and negative amplitudes appear.

There is a large cancellation of walkers also in the box, *e.g.*, the wave function must vanish close to the domain boundaries, and similar cancellation turns out to dominate everywhere in the domain. In fact, it is only a small fraction of walkers, which eventually remain presenting the wave function. Due to the massive cancellation of diffusing walkers all initial walkers need to be massively duplicated in each time step to maintain the total number of walkers.

A one-timestep real time diffusion is demonstrated in Fig. 1. The initial state is ODHO ground state gaussian real wave function, *i.e.*, $\psi(a)=\psi_+(a)$. The real components $\psi_+(b)$ and $\psi_-(b)$ after propagation with the exact kernel (2.9) over a short time step t are shown. We see that most of the walkers will cancel out, leaving behind the initial real gaussian shape, but slightly scaled down. Similarly, the $\psi_{+i}(b)$ and $\psi_{-i}(b)$ after cancellation result in a small negative gaussian shape for the imaginary part, as expected, not shown in Fig. 1. This corresponds to rotation of the wave function from the real axis downwards with a small angle, which is interpreted as multiplication with the phase factor $\mathrm{e}^{-iEt/\hbar}$.

Here we use a simple one-dimensional cancellation algorithm. We define a *walker touch parameter* δ, and when positive and negative walkers appear closer than δ, they annihilate each other. Finding an efficient cancellation algorithm turns out to be a key fac-

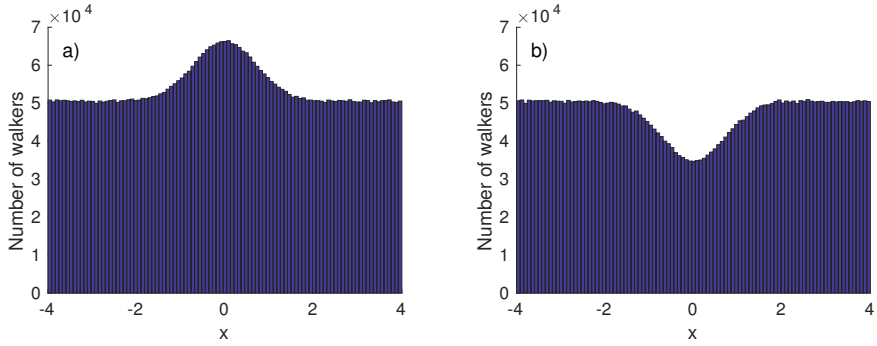

Figure 1: Distribution of a) positive and b) negative walkers ($\psi_+(b)$ and $\psi_-(b)$) after one time step $t=0.1$ from gaussian real wave function $\psi_+(a)$ and $N(x_a)\approx 10^7$ walkers. Histogram bin width is 0.08.

tor in the present method with large number of walkers and oscillatory nature of tDMC propagators it may become a key issue in multidimensional spaces. Continuation without walker annihilation leads to waste of efforts, as can be predicted from Fig. 1, and finally, losing the remaining meaningful wave function into noise. This is one manifestation of the "sign problem", which still is an area of ongoing research [6, 10, 15].

3 Coherent propagation

First, we consider straightforward simulation of quantum dynamics by using the above developed tDMC. We call this *coherent propagation*, because the phase factor of the wave function is properly treated. Next, we consider *incoherent propagation* and demonstrate its use for finding the stationary eigenstates of the system instead of running full quantum dynamics.

3.1 Quantum dynamics from real time diffusion

Because this study is a "proof of the concept tDMC", we continue with the simple, well-known and transparent ODHO as the test bench. Furthermore, for ODHO we have the exact propagator available, and thus, the issues related with the real time diffusion and approximate propagators can be investigated separately.

Hence, we run dynamics of a particle in the potential $V(x)=\frac{1}{2}m\omega^2x^2$ with $\omega=2$. This may be related to an electron in a "harmonic quantum dot" or in an atom. Thus, it is practical to use related atomic units, where $m=\hbar=a_0=1$, where a_0 is the Bohr radius and the unit of time is $(ma_0^2)/\hbar\approx 24$ as. Now, $\omega=2$ corresponds to relatively strong confinement.

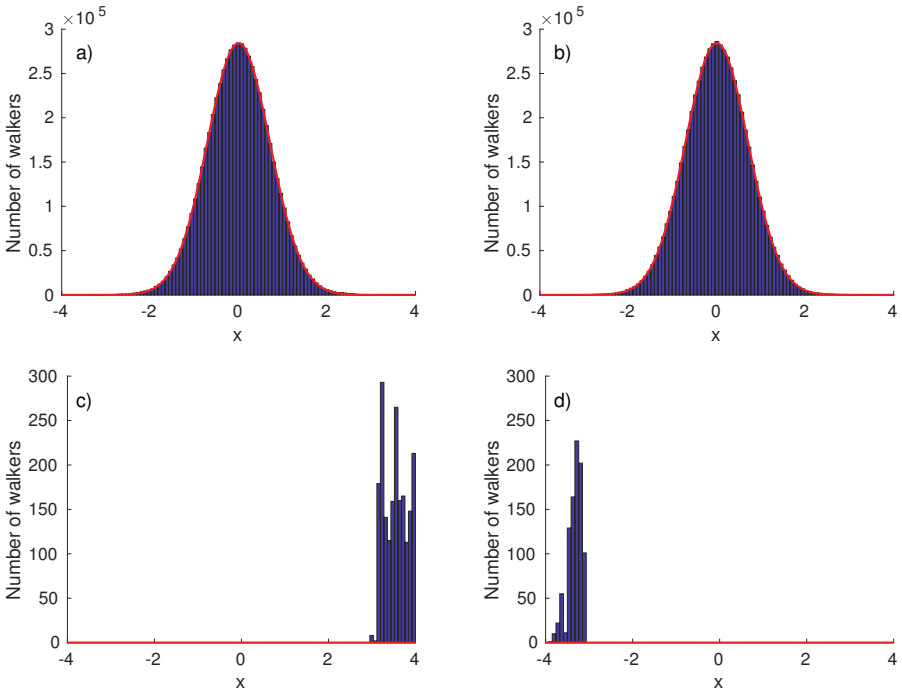

Figure 2: Distribution of walkers after the first time step, $T=\pi/4$, from the positive real ground state $\psi_+(a)$ of ODHO, followed by cancellation. All four components of the wave function are presented: a) positive real ($N\approx 6.27\times 10^7$), b) negative imaginary ($N\approx 6.26\times 10^7$), c) negative real ($N\approx 2.0\times 10^3$) and d) positive imaginary ($N\approx 0.9\times 10^3$) walkers. Note the different scaling on the vertical axes of the latter two. Red solid line is the properly normalized exact wave function and same normalization is used for all components. Notations are the same as in Fig. 1.

For the stationary ground state dynamics ($E=1$), in each time step we expect to see the rotation of the phase factor $\exp(-iEt/\hbar)=\exp(-it)$, only, without any change in the absolute value of the wave function. Thus, the dynamics is expected to be simple oscillation of the real and imaginary parts of the ground state wave function in a phase difference of $\pi/2$. The initial phase is chosen to be zero at $T_0=0$, *i.e.*, $\psi(0)=\psi_+(a)$ as before. We start with $N(a)=10^7$ and run the simulation with the exact kernel (2.9), time steps $t=\pi/4$ and duplicating walkers in x_a enough so that after the cancellation $N(b)\geq N(0)$. Fig. 2 shows the distribution of remaining walkers after the first time step, $T=\pi/4$.

As expected, we find the same copy of the starting gaussian as the positive real and imaginary parts and small remnants of incomplete cancellation in both opposite sign parts, as a numerical error. Here, with the walker touch parameter $\delta=0.01$, the remaining

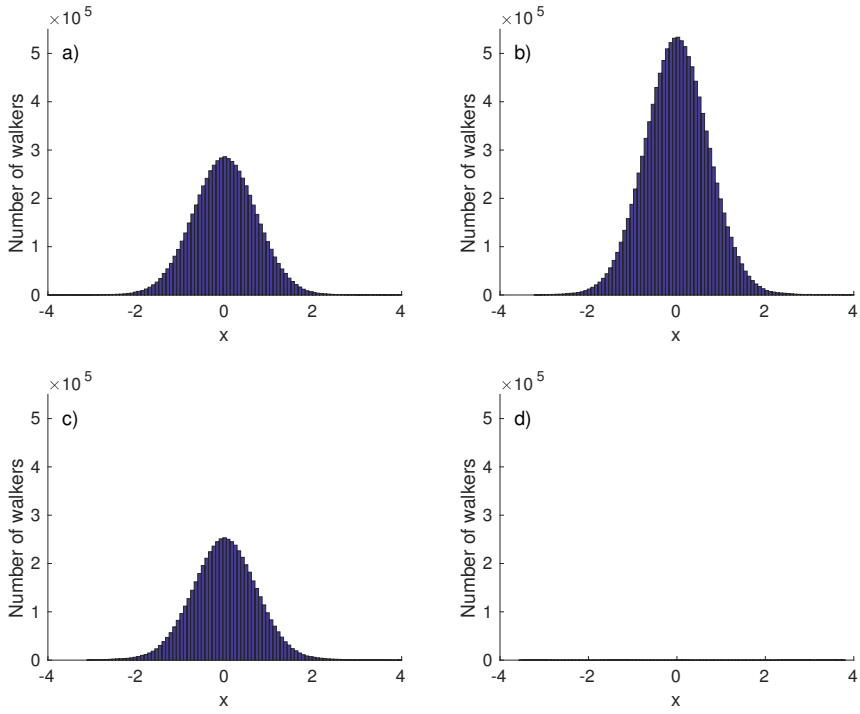

Figure 3: Distribution of negative imaginary walkers at a) $T=\pi/4$, b) $T=2\pi/4$, c) $T=3\pi/4$ and d) $T=4\pi/4$ in the dynamics started in Fig. (2). Notations are the same as in Fig. 2.

opposite sign walkers are less than the proper walkers with a factor smaller than 10^{-4}. Thus, the cancellation is almost perfect.

In Fig. 3 we show the negative imaginary part of the wave function from further simulation, at times $T=\pi/4$, $2\pi/4$, $3\pi/4$, and $4\pi/4$. Clearly, the evolution is correct and at $T=\pi$ the wave function is purely real and negative with zero imaginary contribution.

3.2 Evaluation of observables and eigenenergies

Evaluation of transient expectation values of local operators, like multiplicative potential energy faces the same problem as with the τDMC, the wave function is given by the walker density, only. Application of operators on the wave function or even finding the square of the wave function $\psi^*\psi$ numerically is not straightforward. In our earlier studies we have demonstrated, that for τDMC one can easily evaluate the complex valued wave function of the system at each τDMC walker by using our direct real time path integral

(RTPI) approach [8]. The RTPI time step is heavy to calculate, and therefore, could be restricted only to a few τDMC iteration steps, where needed.

Now, the RTPI can be used together with tDMC similarly as with τDMC in cases, where the wave function is purely real or imaginary. This becomes relevant and useful with eigenstates and incoherent dynamics, in the next section.

With the eigenstates we should be able to monitor the phase factor of the wave function to find the corresponding eigenenergies. Now, we cannot evaluate the local energy for each walker as can be done with RTPI [8]. However, we can evaluate the change in the ratio of the number of real and imaginary walkers to approximate the average collective change in the phase factor. Thus, for the eigenenergy we write

$$E=-\frac{\theta\hbar}{t}=-\tan^{-1}\left(\frac{\psi_{\mathrm{Im}}}{\psi_{\mathrm{Re}}}\right)\frac{\hbar}{t}\approx\tan^{-1}\left(\frac{N(x_{\mp i})}{N(x_{\pm})}\right)\frac{\hbar}{t}. \tag{3.1}$$

For this to be accurate the time step should be short enough that the phase angle θ is small, but also, the ratio $N(x_{\mp i})/N(x_{\pm})$ should be close to one so that the noise effect is minimised. Furthermore, one should keep track of the quadrants of the complex plane and corresponding changes of sign, where relevant.

If the wave function is not an eigenstate but a superposition, for a short time step and small angle we can approximate

$$-\frac{\theta\hbar}{t}=-\tan^{-1}\left(\frac{\sum_i c_i\sin(\theta_i)}{\sum_i c_i\cos(\theta_i)}\right)\frac{\hbar}{t}\approx-\tan^{-1}\left(\frac{\sum_i c_i\theta_i}{\sum_i c_i}\right)\frac{\hbar}{t}\approx\frac{\sum_i c_i E_i}{\sum_i c_i}=E, \tag{3.2}$$

where the sum goes over the eigenstates with contributions c_i.

4 Incoherent propagation

Earlier, we have developed the RTPI for coherent quantum dynamics and another RTPI version with incoherent dynamics for finding the eigenstates and energies of a system [8]. The incoherent dynamics is kind of quantum Zeno propagation, where the wave function is kept real. In numerical simulation this can be accomplished by collapsing the complex wave function to a real one after each short time step. In practise, the complex wave function is projected onto the real values by dropping off the imaginary part [8].

4.1 Finding excited eigenstates

The τDMC simulation converges to the lowest eigenstate (ground state) by adjusting the potential zero reference parameter E_T in Eq. (2.2) to the lowest eigenvalue. The convergence is usually unstable and needs continuous regulation with E_T. Recently, we have shown that the incoherent propagation of real time path integral dynamics RTPI drives the system to an eigenstate, which is closest to the zero reference of the potential energy [8]. Furthermore, the convergence is stable and does not need careful adjustment of potential zero reference.

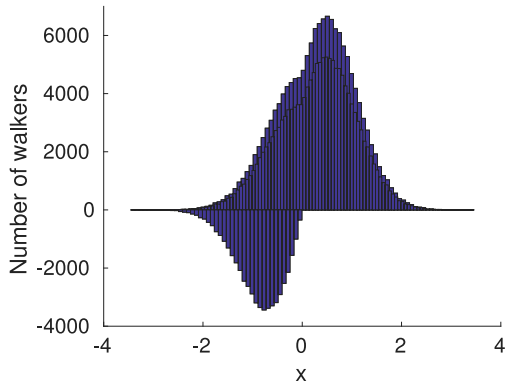

Figure 4: Positive ($N=150\times10^3$) and negative walkers ($N=50\times10^3$) of the superposition of 1st excited and the ground state ($N=100\times10^3$ each). Other notations are the same as in above figures.

Here too, we can insert the zero reference parameter E_T into the Eq. (2.10) and use it to choose the energy, for which we want to find the closest excited state. Also, we can scan the parameter E_T to find all eigenstates within a given range.

Fig. 4 shows a superposition of walkers of the real ground state and those of the real first excited state. We see that the representation of the superposition is not unique, but calls for cancellation of positive and negative walkers. However, we demonstrate robustness of the incoherent tDMC by starting with this initial wave function and run 100 time steps of length $t=0.1$ with 10^6 walkers. The zero reference is set as $E_T=0$.

We monitor the eigenenergy from Eq. (3.1) in Fig. 5. The exact value $E=1$ is expected. It can be seen that the convergence has been achieved in about 60 time steps to about $E=1.1$. Thus, there is some systematic error left, which we trace coming from the short time step. With a too short time step false positive imaginary walkers appear, although all correct imaginary contribution should be negative. This seems to relate also with the size of the domain, 8 atomic units. Now, increasing the time step to $t=0.8$ after 100 steps improves the energy estimate as clearly seen in the last ten time steps. Then, the energy estimate from simulation is 0.9974 ± 0.0030 (2 SEM).

Finally, we search for the first excited state by using the incoherent propagation and starting from the same initial superposition state shown in Fig. 4. Now, the potential zero reference is set as $E_T=2.5$ and we expect to find the eigenenergy of 3.

By using a time step $t=\pi/12$ the first excited state is found as shown in Fig. 6 and the eigenenergy becomes as 3.0199 ± 0.0076 (2 SEM). Fig. 6 shows the distribution of walkers after 100 timesteps to the convergence. As the figure shows, the node of the wave function is clear and sharp. By fitting to the histogram we get 0.0191, which is close to the exact value of 0.

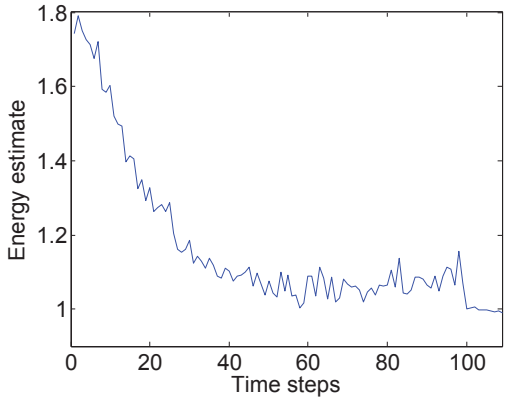

Figure 5: Estimated energy that demonstrates convergence starting from the superposition of the 1st excited state and ground state in incoherent tDMC ending to the ground state. The exact ground state eigenenergy is one, $E=1$. $N\approx 10^6$, and $t=0.1$ for the first 100 time steps and then $t=0.8$.

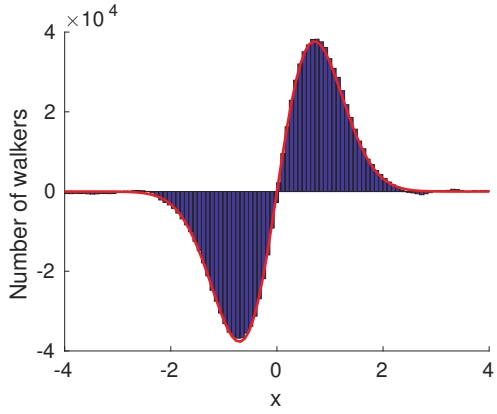

Figure 6: Distribution of positive ($N\approx 0.57\times 10^6$) and negative ($N\approx 0.56\times 10^6$) real walkers after the system has converged to its 1st excited state. Red solid line is the properly normalized exact wave function.

This approach may be one of the practical ways to locate nodal surfaces for other QMC methods like τDMC, and thus, give help in finding the practical solutions to the fermion sign problem.

5 Conclusions

We have demonstrated how the real-time path integral kernel $K(x_b,t_b;x_a,t_a)$, Eq. (2.4), can be used to evaluate the time evolution of a wave function with an entirely new way: driving delocalised "diffusion" of Monte Carlo walkers. Therefore, we call our new approach as real-time DMC or tDMC. There is a transparent analogy with the conventional imaginary time DMC or τDMC, where a local kernel $G(x_b,\tau_b;x_a,\tau_a)$, Eq. (2.2), drives ordinary like diffusion of walkers in imaginary time. However, it should be noted that tDMC is based on the real time path integral formalism, but τDMC is not!

It had been suspected that the real time counterpart of τDMC can not be realised, because the oscillating complex valued K delocalised in space is not capable of driving real time diffusion similarly as the everywhere positive and normalizable G drives imaginary time diffusion. It was known, of course, that the real time kernel can be used to evaluate the time-dependent wave function by using the Eq. (2.3) directly, which couples all walkers within a time step making the numerical calculations heavy. For that and some other practical reasons we were the first to realise the Real Time Path Integral (RTPI) approach for such light particles as electrons [8, 9].

Thus, our tDMC is a truly novel QMC method. It incorporates the essential features of τDMC, and similarly, it can be used to find the system ground state energy and wave function with accuracy depending on the computational capacity. In addition, with tDMC one can find also the excited states and the wave function nodes. The latter may turn out to be useful in practical solutions of the fermion sign problem, if combined with other approaches like the conventional τDMC.

The tDMC can be run for incoherent dynamics or coherent dynamics, the same way as the RTPI. The former is used to find the eigenstates, while the latter, for evaluation of the time evolution of a wave function. Comparison of tDMC and RTPI in running quantum dynamics is interesting. In RTPI the walker distribution is (or follows) the wave function, *i.e.*, it is essentially localised in the wave function. This may restrict the wave function response to fast transient effects or tunneling to a region, where walkers do not exist. The tDMC with the fully delocalised diffusion, instead, fills the whole considered space with excess walkers in each time step before cancelling of walkers takes place. Thus, the propagation is fully delocalised in the whole space in the spirit of path integrals, though the actual wave function may remain relatively localised. Thus, the time evolution immediately responds to any distant changes in the external potential and allows start of tunneling into a region, where the wave function is essentially zero.

As we consider this first study as a "proof of concept" for tDMC, we chose a transparent and well-known one-dimensional harmonic oscillator as the test bench for the demonstration. Now, the tDMC remains to be tested with many-particle systems, where the challenge will be the walker cancellation procedure in multi-dimensional space. With further developments, we expect the tDMC supplement the RTPI approaches [8, 9], the QMC methods without the Fermion sign problem.

Acknowledgments

For computational resources we thank Techila Technologies and TCSC for their facilities at Tampere University of Technology, and also, services of the Finnish IT Center for Science (CSC).

References

[1] J. M. Thijssen; Computational Physics (Cambridge University, 2nd ed., 2007).
[2] B. L. Hammond, W. A. Lester Jr., P. J. Reynolds; Monte Carlo Methods in Ab initio Quantum Chemistry (World Scientific, 1994).
[3] Kalos et al. Phys. Rev. **A 9**, 2178 (1974); and D. M. Ceperley, Rev. Mod. Phys. **67**, 279 (1995).
[4] D. M. Arnow, M. H. Kalos, M. A. Lee and K. E. Schmidt; J. Chem. Phys. **77**, 5562 (1982).
[5] D. M. Ceperley; Path Integral Monte Carlo Methods for Fermions (Ed. K. Binder and G. Ciccotti, Editrice Compositori, Bologna Italy 1996).
[6] J. B. Anderson, J. Chem. Phys. **144**, 166101 (2016); K.E. Riley and J. B. Anderson, J. Chem. Phys. **118**, 3437–3438 (2003); and J. B. Anderson, C. A. Traynor and B. M. Boghosian; J. Chem. Phys. **95**, 7418–7425 (1991).
[7] R. P. Feynman and A. R. Hibbs; Quantum Mechanics and Path Integrals (McGraw-Hill, New York, 1965); and R. P. Feynman, Rev. Mod. Phys. **20**, 367 (1948).
[8] I. Ruokosenmäki and T. T. Rantala; Comm. in Comput. Phys., **18**, 91 (2015).
[9] I. Ruokosenmäki, H. Gholizade, I. Kylänpää and T. T. Rantala; Comput. Phys. Comm., **210**, 45-53 (2017).
[10] M. H. Kalos and F. Pederiva; Phys. Rev. Lett. **85**, 3547 (2000).
[11] N. Makri; Comp. Phys. Comm. **63**, 389–414; and N. Makri; Chem. Phys. Lett. **193**, 435 (1992).
[12] T. D. Kieu, C. J. Griffin; Phys. Rev. **E 49**, 3855–3859 (1994).
[13] L. S. Schulman; Techniques and Applications of Path Integration (Wiley, New York, 1981).
[14] N. S. Thornber and E. F. Taylor; Am. JPhys. **66**, 1022–1024 (1998).
[15] A. Alexandru, G. Başar, P. F. Bedaque, S. Vartak and N. C. Warrington; Phys, Rev. Lett. **117**, 081602 (2016).